รายงานวิจัยฉบับสมบูรณ์

โครงการ

การพัฒนาตัวเร่งปฏิกิริยาแพลเลเดียมบนตัวรองรับขนาดนาโนสำหรับปฏิกิริยาไฮโดรจิเนชัน

โดย

ผศ.ดร. จูงใจ ปั้นประณต และคณะ

มิถุนายน 2553

สัญญาเลขที่ RMU5080030

รายงานวิจัยฉบับสมบูรณ์

โครงการ

การพัฒนาตัวเร่งปฏิกิริยาแพลเลเดียมบนตัวรองรับขนาดนาโนสำหรับปฏิกิริยาไฮโดรจิเนชัน

ผศ.ดร. จูงใจ ปั้นประณต

ภาควิชาวิศวกรรมเคมี คณะวิศวกรรมศาสตร์

จุฬาลงกรณ์มหาวิทยาลัย

สนับสนุนโดยสำนักงานคณะกรรมการอุดมศึกษาและสำนักงานกองทุนสนับสนุนการวิจัย

Abstract

Nanocrystalline SiO_2, Al_2O_3, TiO_2, and $ZnAl_2O_4$ have been synthesized by different methods, namely sol-gel, solvothermal, and flame spray pyrolysis and employed as supports for Pd catalysts. The catalyst performance in selective hydrogenation of alkyne to alkene was correlated with physicochemical properties of the catalysts such as the nature of supports, the metal particle size, and the degree of metal-support interaction. Higher metal dispersion and improved catalyst performance was obtained using these nanometer-sized supports.

Keywords nanocrystalline materials; hydrogenation; Pd catalyst

บทคัดย่อ

งานวิจัยนี้ทำการสังเคราะห์ผลึกขนาดนาโนเมตรของซิลิกาอะลูมินาไทเทเนียมไดออกไซด์และซิงค์อะลูมิเนตโดยวิธีการต่าง ๆ ได้แก่วิธีโซล-เจลวิธีโซลโวเทอร์มอลและวิธีเฟลมสเปรย์ไพโรไลซิสและศึกษาการนำไปประยุกต์ใช้เป็นตัวรองรับตัวเร่งปฏิกิริยาแพลเลเดียมสำหรับปฏิกิริยาไฮโดรจิเนชันแบบเลือกเกิดของสารอัลไคน์เป็นอัลคีนพบว่าประสิทธิภาพในการเร่งปฏิกิริยาในปฏิกิริยาดังกล่าวมีความสัมพันธ์กับสมบัติเชิงกายภาพและเคมีของตัวเร่งปฏิกิริยาได้แก่ชนิดของตัวรองรับขนาดอนุภาคของโลหะและอันตรกิริยาระหว่างโลหะและตัวรองรับโดยสามารถเตรียมตัวเร่งปฏิกิริยาที่มีประสิทธิภาพสูงบนตัวรองรับที่มีขนาดผลึกระดับนาโนเมตรเหล่านี้

คำสำคัญ ผลึกขนาดนาโนเมตร ตัวเร่งปฏิกิริยาแพลเลเดียม ไฮโดรจิเนชัน

Executive Summary

ปฏิกิริยาไฮโดรจิเนชันเป็นปฏิกิริยาที่มีการใช้งานอย่างแพร่หลายในอุตสาหกรรมเคมี อุตสาหกรรมการกลั่นน้ำมันและอุตสาหกรรมปิโตรเคมีเช่นการผลิตสารไซโคลเฮกเซนซึ่งเป็นสารตั้งต้นที่ใช้ในการผลิตไนลอนโดยปฏิกิริยาไฮโดรจิเนชันของเบนซีนการกำจัดสารปนเปื้อนจำพวกอะโรมาติกส์ซึ่งเป็นพิษในอุตสาหกรรมการกลั่นน้ำมันดิบการกำจัดอะเซทิลีนออกจากสายป้อนเอทิลีนในอุตสาหกรรมการผลิตพอลิเอทิลีนนอกจากนี้ปฏิกิริยาไฮโดรจิเนชันยังเป็นปฏิกิริยาที่สำคัญในการสังเคราะห์สารอินทรีย์ต่างๆเช่นสารเคมีที่มีมูลค่าเพิ่มสูงที่มักใช้เป็นสารตั้งต้นในการผลิตยามอนอเมอร์สำหรับสังเคราะห์พอลิเมอร์ ไขมันและน้ำมันสังเคราะห์ เป็นต้นตัวเร่งปฏิกิริยาที่ว่องไวสำหรับปฏิกิริยาไฮโดรจิเนชันได้แก่โลหะมีตระกูลต่างๆเช่นแพลเลเดียม (Pd) แพลตินัม (Pt) โรเดียม (Rh) และรูเทเนียม (Ru) โดยที่แพลเลเดียมจะให้ความว่องไวและค่าการเลือกเกิดเป็นผลิตภัณฑ์จำพวกอัลคีนสูงกว่าโลหะชนิดอื่นๆเพื่อเพิ่มความว่องไวและความเสถียรของตัวเร่งปฏิกิริยาตัวเร่งปฏิกิริยาแพลเลเดียมมักเตรียมบนตัวรองรับที่เป็นโลหะออกไซด์ที่มีพื้นที่ผิวสูงเช่นคาร์บอนซิลิกาอะลูมินาไทเทเนียมไดออกไซด์และซีโอไลท์ทั้งนี้ตัวรองรับต่างชนิดกันพบว่าส่งผลต่อทั้งความว่องไวการเลือกเกิดของผลิตภัณฑ์และการเสื่อมสภาพของตัวเร่งปฏิกิริยา

ปัจจุบันได้มีการสังเคราะห์โลหะออกไซด์ที่มีผลึกขนาดนาโนเมตรโดยวิธีต่างๆเช่นวิธีโซล-เจลวิธีโซลโวเทอร์มอลวิธีเฟลม-สเปรย์ไพโรไลซิสพบว่าโลหะออกไซด์ที่มีขนาดนาโนเมตรมีสมบัติและคุณลักษณะที่แตกต่างไปจากโลหะออกไซด์แบบดั้งเดิมที่มีผลึกขนาดใหญ่เช่นไทเทเนียมไดออกไซด์ที่มีผลึกขนาดเล็กในระดับนาโนให้ความว่องไวในการเร่งปฏิกิริยาด้วยแสงสูงกว่าตัวเร่งปฏิกิริยาขนาดใหญ่ ในงานวิจัยนี้ศึกษาการประยุกต์ใช้โลหะออกไซด์ขนาดนาโนเมตรเป็นตัวรองรับตัวเร่งปฏิกิริยาโดยมุ่งเน้นการพัฒนาตัวเร่งปฏิกิริยาแพลเลเดียมบนตัวรองรับโลหะออกไซด์ขนาดนาโนเมตรต่างๆอาทิซิลิกาอะลูมินาไทเทเนียมไดออกไซด์และซิงค์อะลูมิเนตที่สังเคราะห์โดยวิธีการต่างๆได้แก่วิธีโซล-เจลวิธีโซลโวเทอร์มอลและวิธีเฟลมสเปรย์ไพโรไลซิสสำหรับใช้ในปฏิกิริยาไฮโดรจิเนชันของสารอัลไคน์เป็นอัลคีนพบว่าประสิทธิภาพในการเร่งปฏิกิริยาในปฏิกิริยาดังกล่าวมีความสัมพันธ์กับสมบัติเชิงกายภาพและเคมีของตัวเร่งปฏิกิริยาได้แก่ชนิดของตัวรองรับขนาดอนุภาคของโลหะและอันตรกิริยาระหว่างโลหะและตัวรองรับโดยสามารถเตรียมตัวเร่งปฏิกิริยาที่มีประสิทธิภาพสูงบนตัวรองรับที่มีขนาดผลึกระดับนาโนเมตรเหล่านี้

1. วัตถุประสงค์ของงานวิจัย

เพื่อพัฒนาตัวเร่งปฏิกิริยาแพลเลเดียมที่มีประสิทธิภาพสูงบนตัวรองรับโลหะออกไซด์ขนาดนาโนเมตรต่างๆเช่นซิลิกาอะลูมินาและไทเทเนียมไดออกไซด์ สำหรับใช้ในปฏิกิริยาไฮโดรจิเนชัน

2. ระเบียบวิธีวิจัย

2.1 รวบรวมงานวิจัยที่เกี่ยวข้อง (literature review)

2.2 สังเคราะห์โลหะออกไซด์ที่มีผลึกขนาดนาโนเมตร

2.3 สังเคราะห์ตัวเร่งปฏิกิริยาแพลเลเดียมบนตัวรองรับขนาดนาโนที่เตรียมขึ้น

2.4 ทดสอบคุณลักษณะและสมบัติทางกายภาพและเคมี (physical and chemical properties) ของตัวเร่งปฏิกิริยาที่เตรียมได้

2.5 ทดสอบประสิทธิภาพสำหรับปฏิกิริยาไฮโดรจิเนชันของสารอินทรีย์ต่างๆเช่นอะเซทิลีน (วัฏภาคแก๊ส) ฟินิลอะเซทิลีน (วัฏภาคของเหลว) 1-เฮปไทด์ (วัฏภาคของเหลว)

2.6 ทดสอบการเสื่อมสภาพของตัวเร่งปฏิกิริยาหลังการทำปฏิกิริยา

2.7 วิเคราะห์ข้อมูล จัดทำรายงาน นำเสนอผลงานเพื่อตีพิมพ์ในวารสาร

3. รายชื่อและสังกัดของผู้ร่วมวิจัย ผู้ช่วยวิจัย นักศึกษา ที่ร่วมวิจัยในโครงการ

ผู้ร่วมวิจัย

1. ผศ.ดร. โอกร เมฆาสุวรรณดำรง
ภาควิชาวิศวกรรมเคมี มหาวิทยาลัยศิลปากร จ. นครปฐม

ผู้ช่วยวิจัย (นิสิต)

1. น.ส. สิริมา สมบูรณ์ธนกิจ
ภาควิชาวิศวกรรมเคมี คณะวิศวกรรมศาสตร์ จุฬาลงกรณ์มหาวิทยาลัย
2. น.ส. พัชราภรณ์ วีระชวนะศักดิ์
ภาควิชาวิศวกรรมเคมี คณะวิศวกรรมศาสตร์ จุฬาลงกรณ์มหาวิทยาลัย
3. นาย นิติกร ว่องวรนนท์
ภาควิชาวิศวกรรมเคมี คณะวิศวกรรมศาสตร์ จุฬาลงกรณ์มหาวิทยาลัย
4. นาย ทรงพล โพธาขวัญประชา
ภาควิชาวิศวกรรมเคมี คณะวิศวกรรมศาสตร์ จุฬาลงกรณ์มหาวิทยาลัย
5. น.ส. สุธนา จินายน
ภาควิชาวิศวกรรมเคมี คณะวิศวกรรมศาสตร์ จุฬาลงกรณ์มหาวิทยาลัย
6. น.ส. ตติยา แสงคำ

4. เนื้อหางานวิจัย

ในส่วนของเนื้อหางานวิจัยนี้ได้แบ่งเป็น 5 ส่วนดังนี้ (1) การสังเคราะห์ผลึกโลหะออกไซด์ขนาดนาโนเมตร(2)การเตรียมตัวเร่งปฏิกิริยาแพลเลเดียมบนโลหะออกไซด์ขนาดนาโนเมตรที่สังเคราะห์ขึ้นโดยเทคนิคการเคลือบฝังแบบเปียก(3)การวิเคราะห์คุณลักษณะและสมบัติทางกายภาพและเคมีของตัวเร่งปฏิกิริยาโดยเครื่องมือวิเคราะห์ต่างๆ (4) การทดสอบความว่องไวในการเร่งปฏิกิริยาของตัวเร่งปฏิกิริยาในปฏิกิริยาไฮโดรจิเนชันของสารประกอบจำพวกอัลไคน์และ(5)ผลการทดลองและอภิปรายผล

4.1 การสังเคราะห์ผลึกโลหะออกไซด์ขนาดนาโนเมตร

4.1.1 การสังเคราะห์ผลึกโลหะออกไซด์ขนาดนาโนเมตรโดยวิธีโซลเจล

ตัวอย่างการสังเคราะห์ SiO_2 โดยวิธีโซลเจล

Silica was prepared by the sol-gel technique using the sol composition of 40 ml of tetraethylorthosilicate (TEOS), 10.5 ml of ethanol, 12.5 ml of de-ionized water, and 1 ml of hydrochloric acid (HCl). The mixtures were stirred vigorously for 1 h. Then the gel was calcined at 500^{o}C for 6 h in order to remove any organic.

4.1.2 การสังเคราะห์ผลึกโลหะออกไซด์ขนาดนาโนเมตรโดยวิธีโซลโวเทอร์มอล

ตัวอย่างการสังเคราะห์ $ZnAl_2O_4$ โดยวิธีโซลโวเทอร์มอล

Zinc aluminate spinel ($ZnAl_2O_4$) was prepared by the solvothermal technique using aluminium isopropoxide (Aldrich) and zinc (II) acetylacetonate (Merck) (Zn/Al molar ratio = 0.5) as reactants suspended in toluene (Carlo Erba Reagenti). First, the mixture of aluminium isopropoxide, 15.0 g and appropriate amount of zinc (II) acetylacetonate (Zn/Al molar ratio = 0.5) was prepared in 100 cm^3 toluene in a 1.5 dm^3 autoclave reactor. The suspension was heated to 300^{o}C at the rate of 2.5^{o}C/min and held at that temperature for 2 h. The resulting products were washed with methanol and dried in air and then calcined in a furnace at various temperatures (500, 700, 900, or 1150^{o}C) for 1 h.

4.1.3 การสังเคราะห์ผลึกโลหะออกไซด์ขนาดนาโนเมตรโดยวิธีเฟลมสเปรย์ไพโรไลซิส

ตัวอย่างการสังเคราะห์ TiO_2 โดยวิธีเฟลมสเปรย์ไพโรไลซิส

Synthesis of TiO_2 was carried out using a spray flame reactor [see Figure 1]. Titanium (IV) tert-butoxide (TNB; Aldrich) was chosen as raw materials for preparation of a liquid-phase precursor. The precursors were prepared by dissolving the appropriate amounts of substance in xylene (MERCK; 99.8 vol.%)/acetonitrile (Fluka; 99.5 vol.%) mixtures (70/30 vol%). During particle synthesis, 5 ml/min of liquid precursor are fed to the flame by a syringe pump and disperse with 5 l/min oxygen forming fine spray

droplets. The pressure drop at the capillary tip was maintained at 1.5 bar by adjusting the orifice gap area at the nozzle. The spray was ignited by supporting flamelets feed with oxygen (3 l/min) and methane (1.5 l/min) which were positioned in a ring around the nozzle outlet. A sintered metal plate ring (8 mm wide, starting at a radius of 8 mm) provided additional 25 l/min of oxygen as sheath for the supporting flame. The product particles were collected on a glass fiber filter (Whatman GF/D, 15 cm in diameter) with the aid of a vacuum pump.

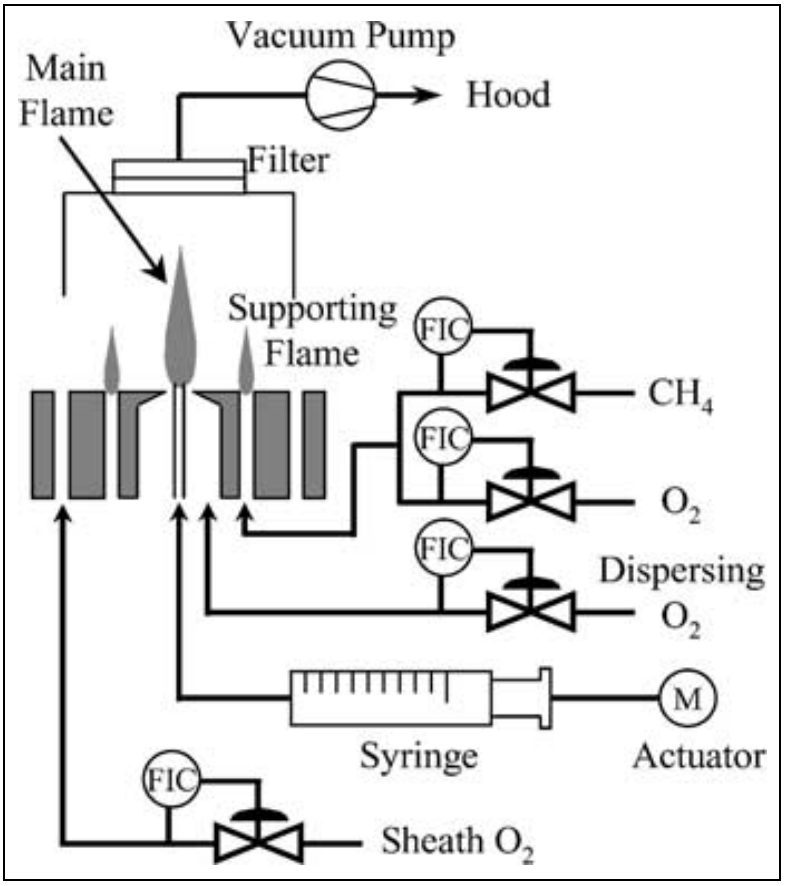

Figure 1 Schematic of the FSP process for nanomaterials synthesis

4.2 การเตรียมตัวเร่งปฏิกิริยาแพลเลเดียมบนโลหะออกไซด์ขนาดนาโนเมตรที่สังเคราะห์ขึ้นโดยเทคนิคการเคลือบฝังแบบเปียก (Incipient Wetness Impregnation method)

Supported Pd catalysts were prepared by the incipient wetness impregnation method using $Pd(NO_3)_2$ (Aldrich) as the palladium precursor. The support was

impregnated to incipient wetness with an aqueous solution containing sufficient palladium to result in 1 wt% Pd catalysts. The catalyst samples were dried in an oven at 100◦C overnight and calcined in air at 400◦C for 6 h prior to characterization.

4.3การวิเคราะห์คุณลักษณะและสมบัติทางกายภาพและเคมีของตัวเร่งปฏิกิริยาโดยเครื่องมือวิเคราะห์ต่าง ๆได้แก่

4.3.1 N_2 physisorption

ปริมาณพื้นที่ผิวปริมาตรรูพรุนและขนาดของรูพรุนโดยเฉลี่ยทำการตรวจวัดโดยเครื่อง Micromeritics ASAP 2020 ที่ศูนย์เชี่ยวชาญเฉพาะทางด้านคาตาไลซิสและวิศวกรรมปฏิกิริยาที่ใช้ตัวเร่งปฏิกิริยา ภาควิชาวิศวกรรมเคมี คณะวิศวกรรมศาสตร์ จุฬาลงกรณ์มหาวิทยาลัย

4.3.2 X-ray diffraction (XRD)

รูปแบบของ XRD ของตัวเร่งปฏิกิริยาวัดโดยเครื่อง SIEMENS D5000 X-ray diffractometer ที่มี CuK_α radiation และ Ni Filter ที่ศูนย์เชี่ยวชาญเฉพาะทางด้านคาตาไลซิสและวิศวกรรมปฏิกิริยาที่ใช้ตัวเร่งปฏิกิริยาภาควิชาวิศวกรรมเคมีคณะวิศวกรรมศาสตร์ จุฬาลงกรณ์มหาวิทยาลัย

4.3.3 Scanning electron microscopy (SEM)

ลักษณะพื้นผิวของตัวเร่งปฏิกิริยาทดสอบโดยเครื่อง JEOL JSM-35CF scanning electron microscope (SEM) ที่ดำเนินการที่ 20 kV ที่ศูนย์เครื่องมือวิเคราะห์แห่งจุฬาลงกรณ์มหาวิทยาลัย

4.3.4 Transmission electron microscopy (TEM)

ขนาดผลึกของแพลเลเดียมออกไซด์และการกระจายตัวของแพลเลเดียมวิเคราะห์โดยเครื่อง JEOL-JEM 2010 transmission electron microscopeที่ดำเนินการที่ 80-200 kV ที่ National Metal and Materials Technology Center (MTEC)

4.3.5 CO-pulse chemisorption

ปริมาณแพลเลเดียมที่ว่องไวสามารถวัดได้โดยเทคนิคCO-chemisorption โดยประมาณ 0.2 กรัมของตัวเร่งปฏิกิริยาจะถูกบรรจุในเครื่องปฏิกรณ์ที่อยู่ในเตาอบหลังจากรีดิวซ์ในบรรยากาศไฮโดรเจนที่อุณหภูมิห้องและไล่แก๊สที่เหลือด้วยฮีเลียมแล้วแก๊ส

คาร์บอนมอนออกไซด์จะถูกฉีดเข้าไปบนตัวเร่งปฏิกิริยาเพื่อให้เกิดการดูดซับปริมาณแก๊สที่ดูดซับวัดได้โดยเครื่องthermal conductivity detector (TCD) ทำการทดสอบที่ศูนย์เชี่ยวชาญเฉพาะทางด้านคาตาไลซิสและวิศวกรรมปฏิกิริยาที่ใช้ตัวเร่งปฏิกิริยาภาควิชาวิศวกรรมเคมีคณะวิศวกรรมศาสตร์ จุฬาลงกรณ์มหาวิทยาลัย

4.3.6 X-ray photoelectron spectroscopy (XPS)

The XPS measurement was carried out using an AMICUS photoelectron spectrometer equipped with an Mg K_α X-ray as a primary excitation and KRATOS VISION2 software. XPS elemental spectra were acquired with 0.1 eV energy step at a pass energy of 75 kV. All the binding energies were referenced to the C 1s peak at 285 eV of the surface adventitious carbon.

4.3.7 Electron spin resonance (ESR)

Electron spin resonance spectroscopy (ESR) was conducted using a JEOL JESRE2X electron spin resonance spectrometer. The intensity of ESR was calculated using a computer software program ES-PRIT ESR DATA SYSTEM version 1.6.

4.3.8 Inductively coupled plasma-optical emission spectroscope (ICP-OES)

The bulk composition of catalyst quantitatively is determined by ICP-OES method using Optima 2100 DV. Often special procedures are needed to dissolve catalysts in preparation for analysis, particularly refractory materials such as certain noble metals and ceramics.

4.4 วิธีการทดสอบความว่องไวในการเร่งปฏิกิริยาของตัวเร่งปฏิกิริยาในปฏิกิริยาไฮโดรจิเนชันของสารประกอบจำพวกอัลไคน์เช่นอะเซทิลีนฟีนิลอะเซทิลีนและเฮปไทน์ในเครื่องปฏิกรณ์แบบเบดนิ่งหรือแบบหม้ออัดความดัน

Liquid-phase partial hydrogenation of 1-heptyne was carried out in a 50 cm^3 stainless steel autoclave. Approximately 0.02 g of supported Pd catalyst was placed in the reactor with 10 cm^3 of 2 vol% of 1-heptyne in toluene. Afterward the reactor was filled with hydrogen at 1 bar pressure. Stirring was switched on to start the reaction, and reaction was carried out for 5 min. The products were analyzed by gas chromatography with a flame ionization detector.

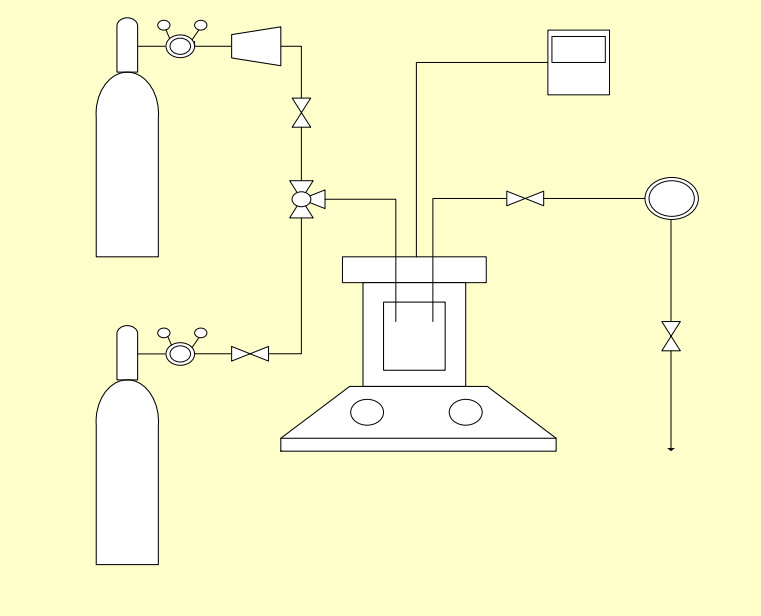

CO2

Figure 2 A schematic diagram of the liquid-phase hydrogenation system

Selective acetylene hydrogenation was performed in a quartz tube reactor (ID 9 mm). Prior to the start of each run, the catalyst was reduced in H_2 at 500^{o}C for 2 h. Then the reactor was purged with argon and cooled down to the reaction temperature, 40°C. Feed gas composed of 1.46% C_2H_2, 1.71% H_2, 15.47% C_2H_6 and balanced C_2H_4 (Rayong Olefin Co., Ltd) and a GHSV of 5400 h^{-1} were used. The composition of product and feed stream were analyzed by a Shimadzu GC 8A equipped with TCD and FID detectors (molecular sieve-5A and carbosieve S2 columns, respectively). Acetylene conversion as used herein is defined as moles of acetylene converted with respect to acetylene in feed. Ethylene selectivity is defined as the percentage of acetylene hydrogenated to ethylene over totally hydrogenated acetylene. The ethylene being hydrogenated to ethane (ethylene loss) is the difference between all the hydrogen consumed and all the acetylene which has been totally hydrogenated.

H2

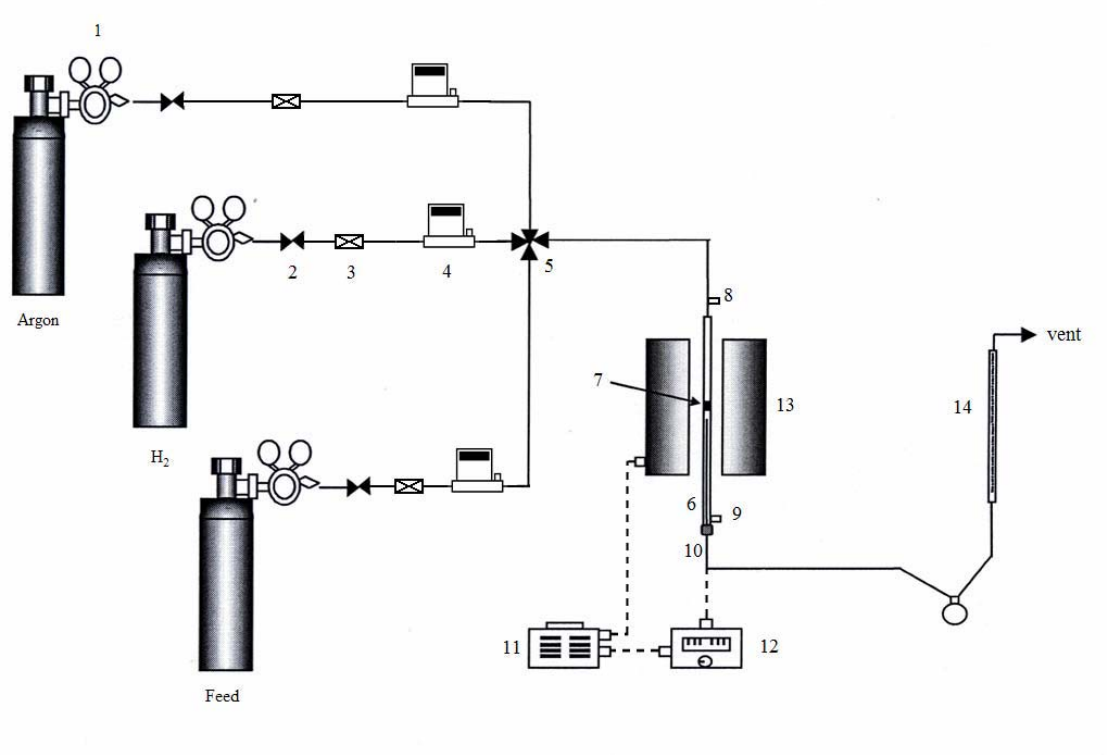

1. pressure regulator
2. on-off valve
3. filter
4. mass flow controller
5. 4-ways fitting
6. reactor
7. catalyst bed
8. sampling point (feed)
9. sampling point (product)
10. thermocouple
11. variable voltage transformer
12. temperature controller
13. electric furnace
14. bubble flow meter

Figure 3 Flow diagram of the selective hydrogenation of acetylene

4.5 ผลการทดลองและอภิปรายผล

4.5.1 Selective hydrogenation of acetylene in excess ethylene on micron-sized and nanocrystalline TiO_2 supported Pd catalysts

The use of pure anatase TiO_2 (either micron- or nano-sized) as supports for Pd catalysts produced high ethylene selectivities during selective acetylene hydrogenation in excess ethylene. In contrast, the use of pure rutile TiO_2 supported ones resulted in ethylene loss due to over-hydrogenation of ethylene to ethane. The differences in ethylene selectivity of the various Pd/TiO_2 were due mainly to the presence/absence of the Ti^{3+} defective sites on the TiO_2 support, rather than the difference in the crystallite sizes of the TiO_2 support.

Table 1.1 Properties of the various TiO_2 supports

Sample	BET S.A.[a] (m^2/g)	crystallite size[b] (nm)	Atomic concentration[c] (%) Ti/O
TiO_2-com-A	64.4	n.d.	0.287
TiO_2-com-R	18.3	n.d.	0.250
TiO_2-sol gel	39.3	10	0.232
TiO_2-solvothermal	26.8	17	0.220

Table 1.2 Characteristics of the various TiO_2-supported Pd catalysts

Catalyst	BET S.A.[a] (m^2/g)	CO pulse chemisorption[b] ($x10^{-18}$ molecule CO/g cat.)	Pd dispersion[c] (%)	d_P[d] Pd^0 (nm)	%atomic concentration[e] Ti/O	Pd/Ti
Pd/TiO_2-com-A	44.5	2.23	3.93	28.5	0.253	0.084
Pd/TiO_2-com-R	17.2	1.55	2.73	41.0	0.240	0.168
Pd/TiO_2-sol gel	33.8	1.19	2.10	53.3	0.282	0.011
Pd/TiO_2-solvothermal	26.0	0.49	0.86	130.2	0.274	0.006

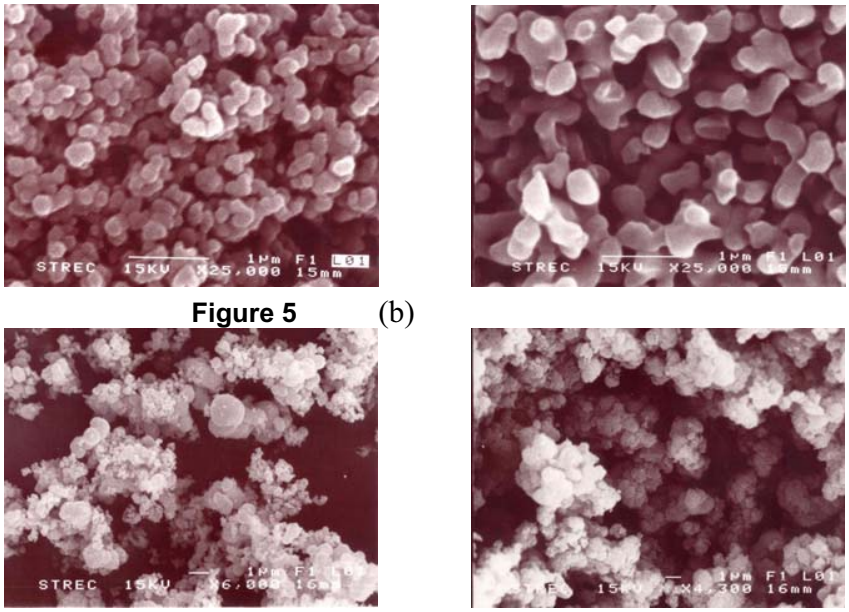

Figure 5 (b)

© (d)

Figure 1.1 SEM micrographs of (a) TiO_2-com-A (b) TiO_2-com-R (c) TiO_2-sol-gel and (d) TiO_2-solvothermal

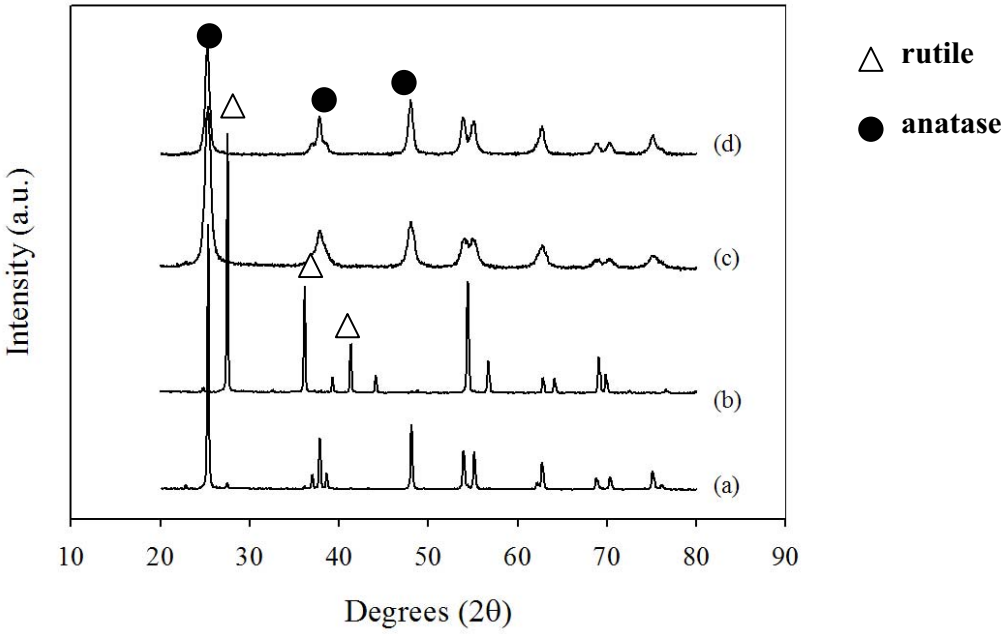

Figure 1.2 XRD results of (a) TiO_2-com-A (b) TiO_2-com-R (c) TiO_2-sol-gel and (d) TiO_2-solvothermal

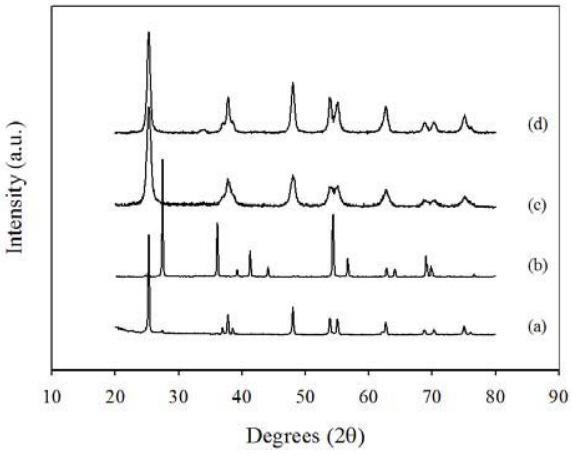

Figure 1.4 XRD results of (a) Pd/TiO_2-com-A (b) Pd/TiO_2-com-R (c) Pd/TiO_2-sol-gel and (d) Pd/TiO_2-solvothermal

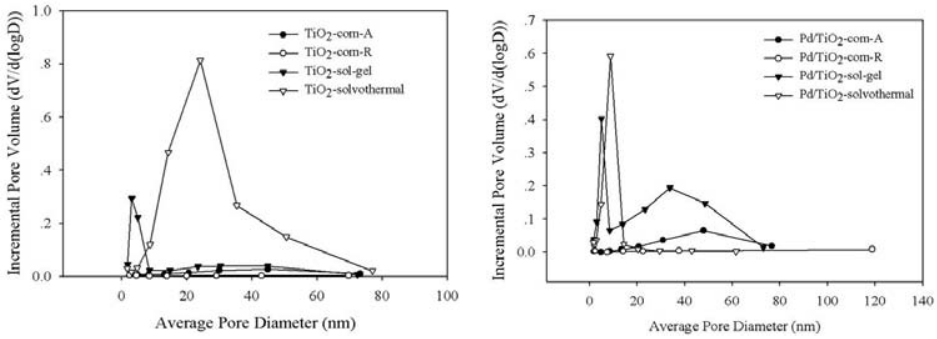

Figure 1.5 Pore size distribution results of the various Pd/TiO_2 catalysts

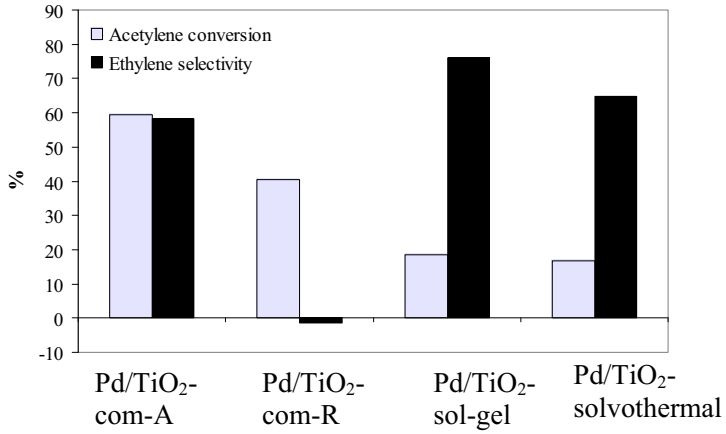

Figure 1.6 Catalyst performances in selective acetylene hydrogenation

4.5.2 Characteristics and Catalytic Properties of Pd/SiO_2 Synthesized by One-Step Flame Spray Pyrolysis in Liquid-Phase Hydrogenation of 1-Heptyne

Pd/SiO_2 catalysts with 0.5-10 wt% Pd loadings were prepared by one-step flame spray pyrolysis (FSP) and characterized by N_2 physisorption, X-ray diffraction (XRD), transmission electron microscopy (TEM), CO chemisorption, and X-ray photoelectron spectroscopy (XPS). The average cluster/particles size of Pd as revealed by TEM were ca. 0.5 to 3 nm. The turnover frequencies (TOFs) of the flame-made catalysts decreased from 66.2 to 4.3 s^{-1} as Pd loading increased from 0.5 to 10 wt%, suggesting that the catalytic activity was dependent on Pd particle/cluster size. However, there were no appreciable influences on 1-heptene selectivity. The flame-made Pd/SiO_2 showed better properties than the conventional prepared catalysts. Their advantages are not only the presence of large pores that facilitates diffusion of the reactants and products, but also the high catalytic activity of as-synthesized catalysts so that further pretreatment is not necessary.

Table 2.1 Physicochemical Properties of Flame-Made SiO_2 and Pd/SiO_2 Catalysts

Catalyst	BET Surface Areas[a]	Pore Volume[a]	CO chemisorption results[b]			XPS results Pd $3d_{5/2}$		Atomic ratio[e]
			CO uptake ($x10^{-18}$ molecule CO/g cat.)	%Pd dispersion[c]	$d_P Pd^{0,d}$ (nm)	B.E. (eV)	FWHM	Pd/Si
	(m^2/g)	(cm^3/g)						
SiO_2	196	0.48	n/a[f]	n/a	n/a	n/a	n/a	n/a
0.5%Pd/SiO_2	246	0.43	1.0	3.42	33	n/a	n/a	0.0011
0.5%Pd/SiO_2_R[g]	-	-	1.1	3.53	32	-	-	-
1%Pd/SiO_2	251	0.46	1.9	3.40	33	n/a	n/a	0.0014
2%Pd/SiO_2	260	0.49	3.3	2.88	39	n/a	n/a	0.0018
5%Pd/SiO_2	306	0.59	13.4	4.71	24	337.4	2.389	0.0139
10%Pd/SiO_2	299	0.69	25.8	4.55	25	337.4	3.189	0.0404
1% Pd/SiO_2-com	234	1.02	3.3	5.81	19	-	-	0.0033

[a] Error of measurement was ± 10%.
[b] Error of measurement was ± 5% as determined directly.
[c] Based on the total palladium loaded and an assumption of CO/Pd = 1.
[d] Based on d = (1.12/D) nm [25], where D = fractional metal dispersion.
[e] Based on XPS results.
[f] n/a = not available.
[g] R = after reduced for 2 h in H_2 at room temperature.

Table 2.2 Catalytic Properties for Liquid-Phase 1-Heptyne Selective Hydrogenation[a]

Catalyst	Conversion (%)	1-Heptene Selec. (%)	TOF[b] (s^{-1})
0.5%Pd/SiO_2	42	93	66.2
1%Pd/SiO_2	43	92	34.1
	100[C]	62[C]	-
2%Pd/SiO_2	54	94	25.3
5%Pd/SiO_2	75	95	8.6
10%Pd/SiO_2	73	94	4.3
1% Pd/SiO_2-com	20	100	7.7
	100[C]	13[C]	-

[a] Reaction conditions were 105 kPa, 30°C, 5 min, and catalyst/substrate molar ratio = 1/1,600

[b] TOF = mole product/mole Pd metal/s. Based on the amount of active Pd atoms Measured by CO chemisorption.

[c] Reaction conditions were 105 kPa, 30°C, 40 min, and catalyst/substrate molar ratio = 1/500

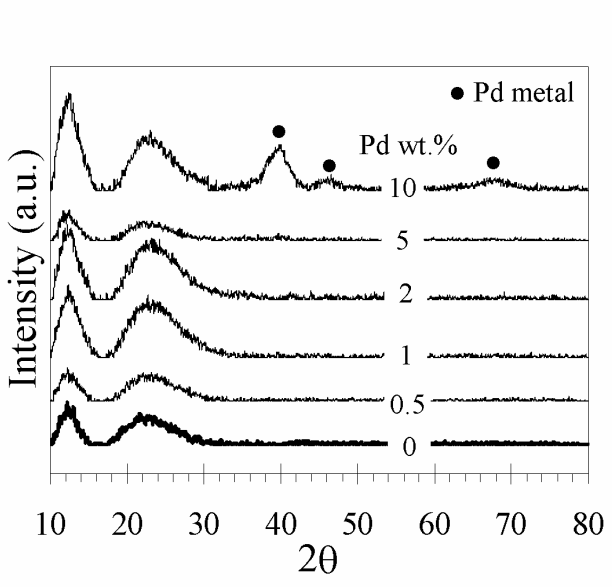

Figure 2.1 XRD patterns of the flame-made Pd/SiO_2 catalysts (as synthesized)

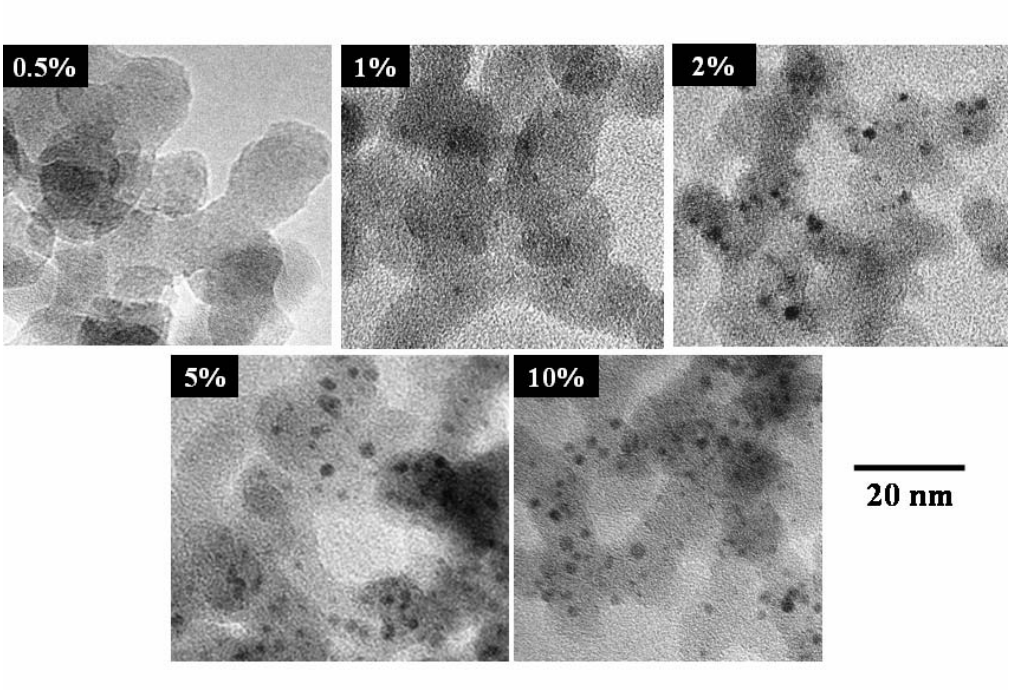

Figure 2.2 TEM micrographs of (a) the as-synthesized and (b) the spent flame-made Pd/SiO_2 catalysts (after reaction)

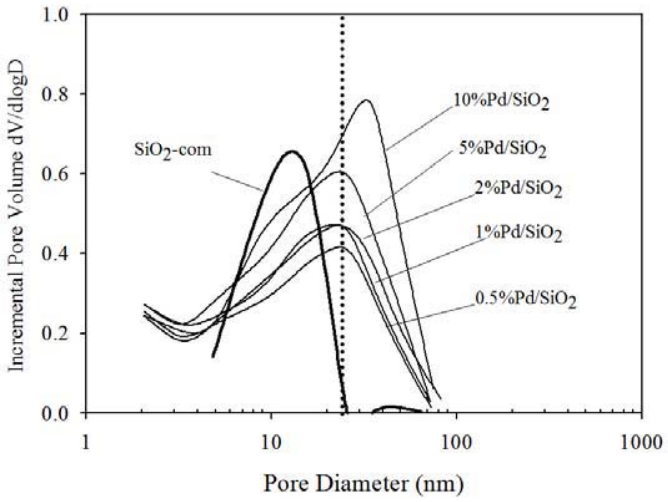

Figure 2.3 Pore size distribution of the flame-made Pd/SiO_2 catalysts with 0.5-10 wt% Pd loading

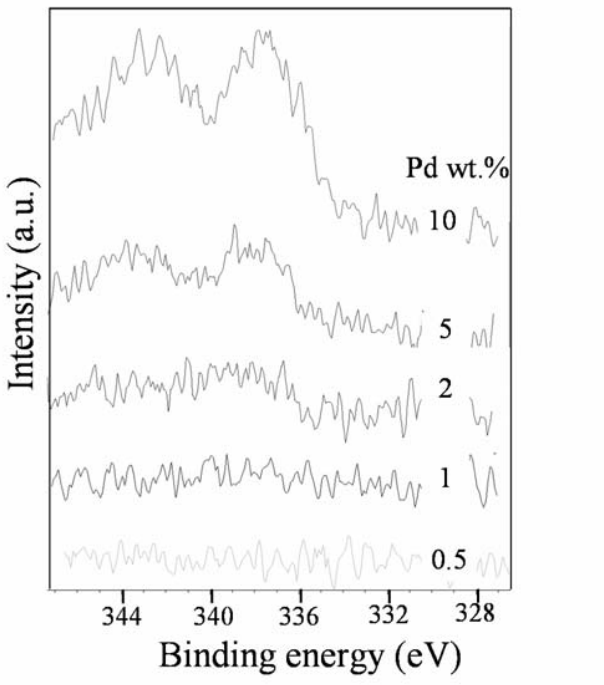

Figure 2.4 XPS results for Pd $3d_{5/2}$ of the flame-made Pd/SiO_2 catalysts

4.5.3 Performance of Pd Catalysts Supported on Nanocrystalline α-Al_2O_3 and Ni-Modified α-Al_2O_3 in Selective Hydrogenation of Acetylene

Nanocrystalline α-Al_2O_3 and Ni-modified α-Al_2O_3 have been prepared by sol-gel and solvothermal methods and employed as supports for Pd catalysts. Regardless of the preparation method used, $NiAl_2O_4$ spinel was formed on the Ni-modified α-Al_2O_3 after calcination at 1150°C. However, an additional of NiO peaks was also observed by X-ray diffraction for the solvothermal-made Ni-modified α-Al_2O_3 powder. Catalytic performances of the Pd catalysts supported on these nanocrystalline α-Al_2O_3 and Ni-modified α-Al_2O_3 in selective hydrogenation of acetylene were found to be superior to those of the commercial α-Al_2O_3 supported one. Ethylene selectivities were improved in the order: Pd/Ni-modified α-Al_2O_3-sol-gel > Pd/Ni-modified α-Al_2O_3-solvothermal ≈ Pd/α-Al_2O_3-sol–gel > Pd/α-Al_2O_3-solvothermal >> Pd/ α-Al_2O_3-commerical. As revealed by NH_3 temperature program desorption studies, incorporation of Ni atoms in α-Al_2O_3 resulted in a significant decrease of acid sites on the alumina supports. Moreover, XPS revealed a shift of Pd 3d binding energy for Pd catalyst supported on Ni-modified α-Al_2O_3-sol-gel where only $NiAl_2O_4$ was formed, suggesting that the electronic properties of Pd may be modified.

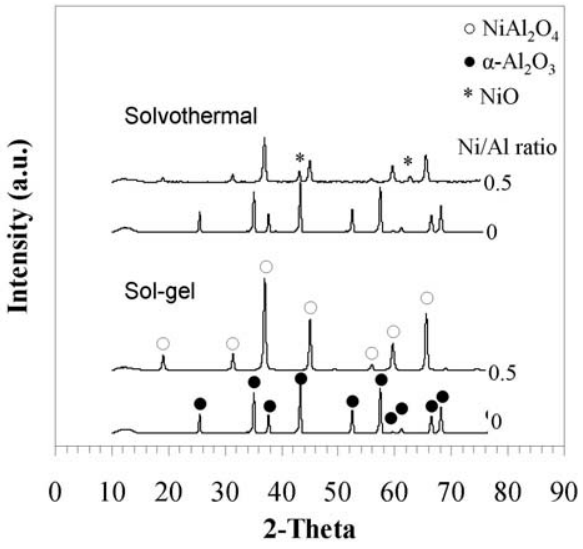

Figure 3.1 XRD patterns of the various Pd catalysts supported on nanocrystalline α-Al_2O_3 and Ni-modified α-Al_2O_3 prepared by sol-gel and solvothermal methods.

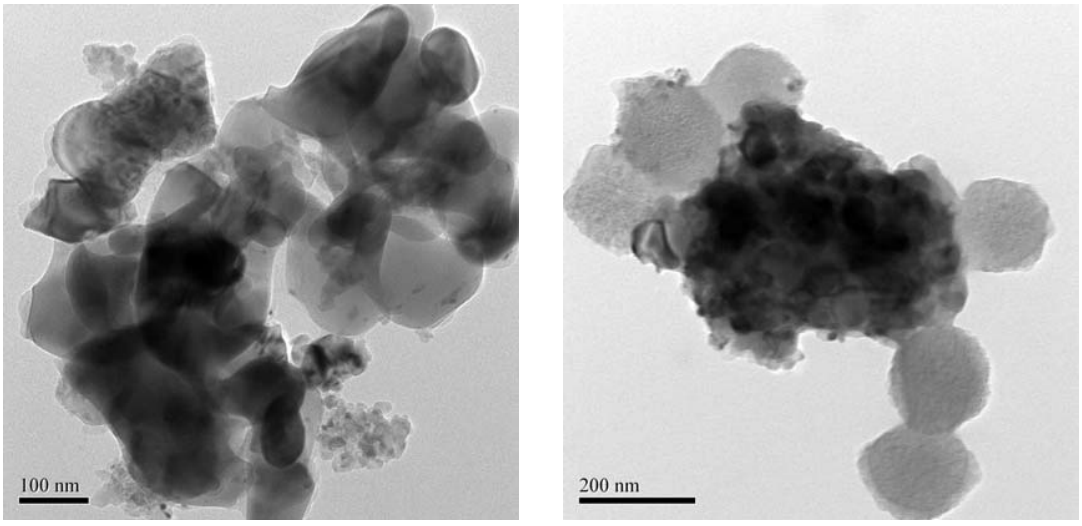

(a) **(b)**

Figure 3.2 TEM micrographs of (a) Pd/α-Al_2O_3-solvothermal, and (b) Pd/Ni-modified α-Al_2O_3-solvothermal.

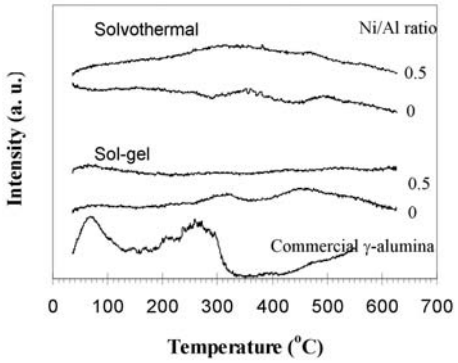

Figure 3.3 NH_3 temperature program desorption profiles for the sol-gel and solvothermal-made α-Al_2O_3 and the Ni-modified α-Al_2O_3 supports.

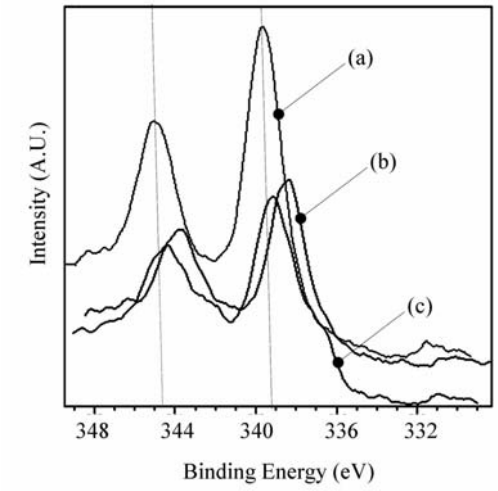

Figure 3.4 XPS results of Pd 3d for (a) Pd/α-Al_2O_3-sol-gel (b) Pd/Ni-modified α-Al_2O_3-sol-gel and (c) Pd/Ni-modified α-Al_2O_3-solvothermal.

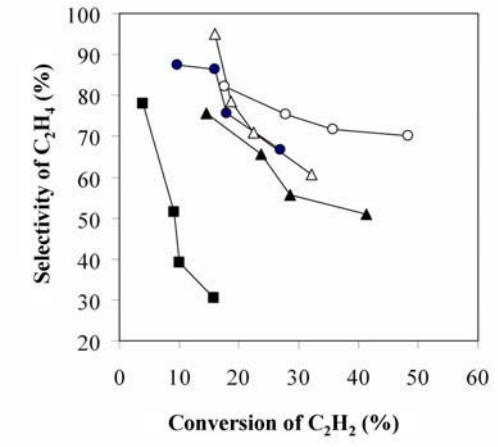

Figure 3.5 Performance of sol-gel (circle; ○) and solvothermal (triangle; Δ) made Pd/α-Al_2O_3 (filled symbols), Pd/commercial α-Al_2O_3 (filled square; ■) and Pd/Ni-modified α-Al_2O_3 (open symbols) catalysts in selective acetylene hydrogenation.

4.5.4 A Comparative Study of Strong Metal-Support Interaction and Catalytic Behaviors of Pd Catalysts Supported on Micron- and Nano-sized TiO_2 in Liquid-Phase Selective Hydrogenation of Phenylacetylene

The strong metal-support interaction and catalytic behaviors of Pd catalysts supported on micron- (0.1 μm) and nano-sized (14 nm) TiO_2 were investigated in the liquid-phase selective hydrogenation of phenylacetylene to styrene. It was found that when supported on the nano-sized TiO_2, the Pd/TiO_2 catalyst that reduced by H_2 at 500°C exhibited strong metal-support interaction (SMSI) and much improved catalyst performance in liquid-phase selective hydrogenation of phenylacetylene. However, as revealed by CO pulse chemisorption, X-ray photoelectron spectroscopy (XPS), transmission electron microscopy (TEM), and CO-temperature program desorption results, the SMSI effect was not detected for the micron-sized TiO_2 supported ones. It is suggested during high temperature reduction, the inner Ti^{3+} in large crystallite size TiO_2 was more difficult to diffuse to the Pd surface than the surface Ti^{3+} in the smaller crystallite size ones. Sintering of Pd^0 metal was observed instead.

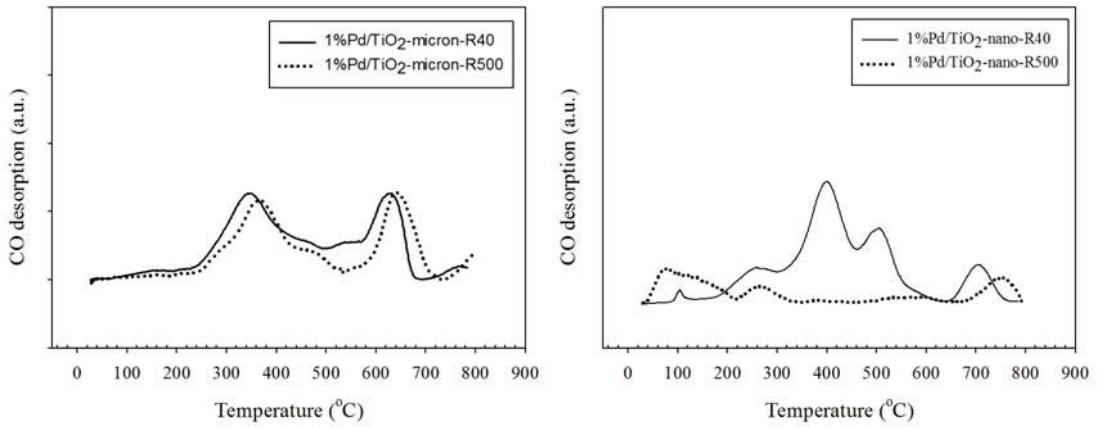

Figure 4.1 CO-temperature programmed desorption profiles of 1%Pd/TiO_2-micron and 1%Pd/TiO_2-nano reduced at 40 and 500°C

3.5.5 Effect of strong metal-support interaction on the catalytic performance of Pd/TiO_2 in the liquid-phase semihydrogenation of phenylacetylene

Liquid-phase semihydrogenation of phenylacetylene under mild conditions has been investigated on a series of solvothermal-derived nano-TiO_2 supported Pd catalysts with various TiO_2 crystallite sizes in the range of 9-23 nm. As revealed by CO chemisorption and transmission electron microscopy, all the catalysts exhibited strong metal-support interaction (SMSI) when reduced at 500°C. The catalysts with SMSI show remarkably high catalytic performance in terms of both hydrogenation activities (turnover frequencies (TOFs) 9.1-21.4 s^{-1}) and moderate-high selectivities to styrene (86-90%) at complete conversion of phenylacetylene. Without SMSI effect (the catalysts reduced at 40°C), styrene selectivity and catalytic activity depended largely on the Pd particle size in which small Pd particles (formed on small crystallite size TiO_2 supports) exhibited lower phenylacetylene conversion and poor styrene

selectivity. Moreover, the TOF values of the non-SMSI catalysts were similar to those reported in the literature for other supported Pd catalysts in liquid-phase semihydrogenation of phenylacetylene under mild conditions (TOFs 1.3-2.8 s^{-1}).

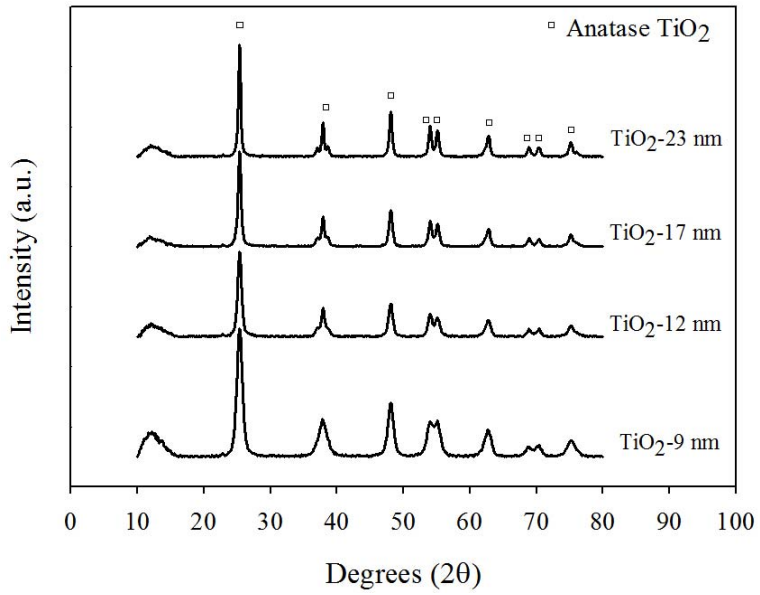

Figure 5.1 XRD patterns of the solvothermal-derived TiO_2 with different crystallite sizes

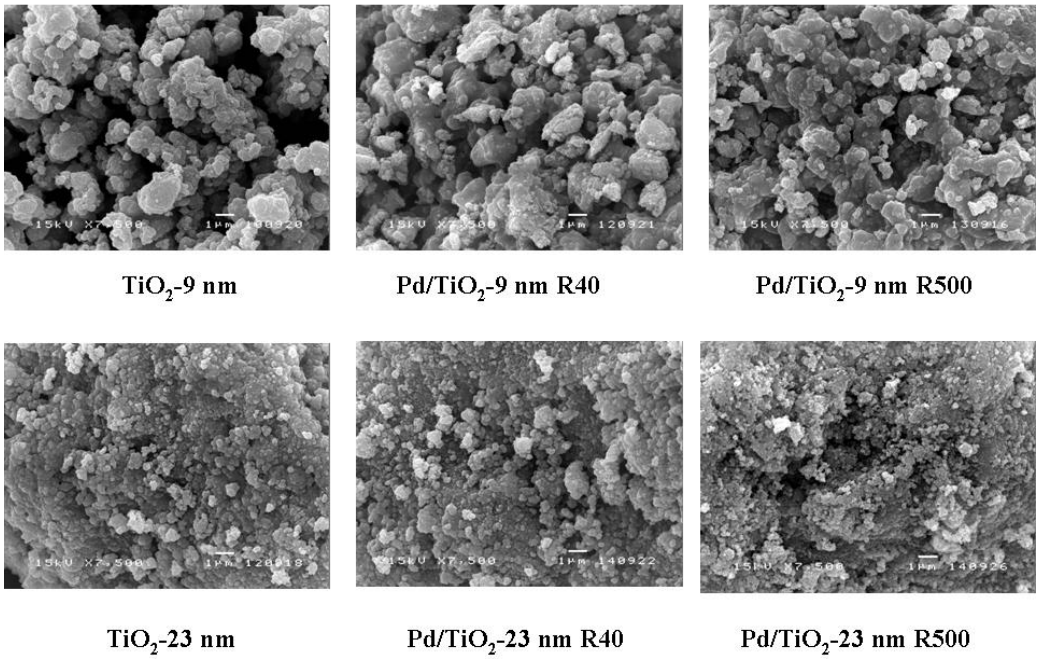

Figure 5.2 SEM micrographs of calcined and reduced Pd/TiO_2 catalysts. Reduction temperature = 40°C (R40), 500°C (R500)

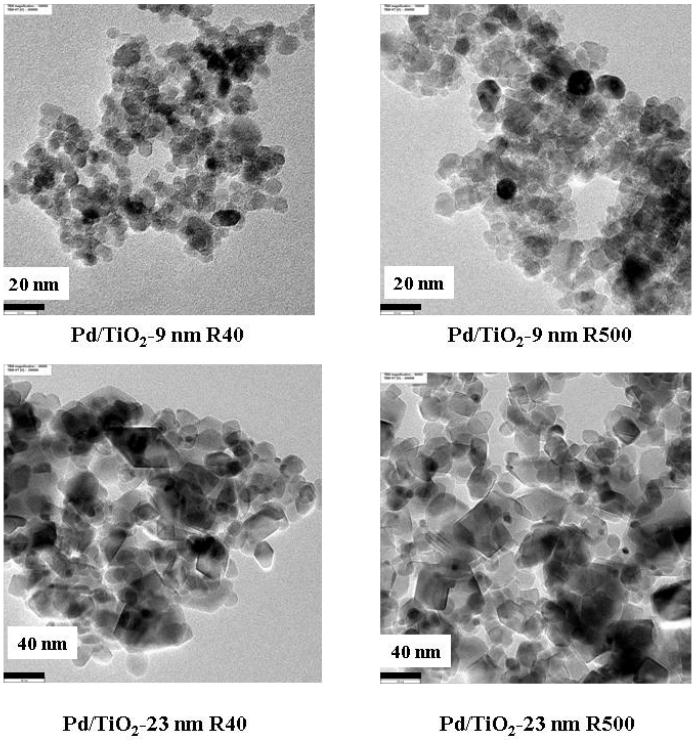

Figure 5.3 TEM micrographs of Pd/TiO_2-9 nm and Pd/TiO_2-23 nm reduced at 40°C (R40) and 500°C (R500)

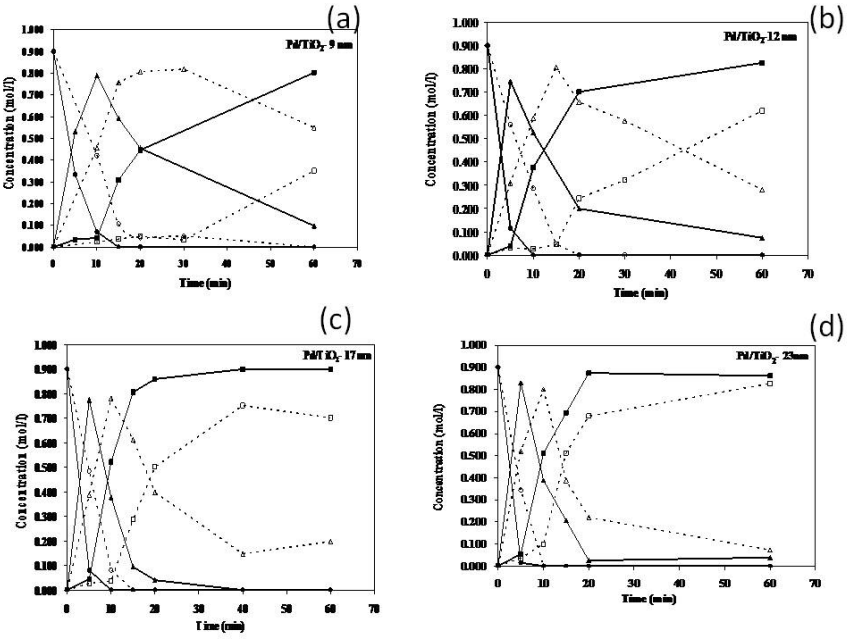

Figure 5.4 Liquid-phase semihydrogenation of phenylacetylene over the Pd/TiO_2 catalysts: = phenylacetylene = styrene = ethylbenzene, solid symbols = Pd/TiO_2 catalysts reduced at 40°C and open symbols = Pd/TiO_2 catalysts reduced at 500°C (a) Pd/TiO_2-9 nm (b) Pd/TiO_2-12 nm (c) Pd/TiO_2-17 nm (d) Pd/TiO_2-23 nm (reaction conditions were H_2 pressure = 5 bar and 30°C).

4.5.6 Selective Hydrogenation of Acetylene over Pd Catalysts Supported on Nanocrystalline α-Al_2O_3 and Zn-Modified α-Al_2O_3

The catalytic performance of Pd catalysts supported on nanocrystalline α-Al_2O_3 and Zn-modified α-Al_2O_3 prepared by sol-gel and solvothermal methods was studied in the selective hydrogenation of acetylene. Acidity of the nanocrystalline α-Al_2O_3 was significantly decreased by incorporation of Zn atoms in the α-Al_2O_3. Both of acetylene conversions and ethylene selectivities were improved in the order: Pd/Zn-modified α-Al_2O_3-sol-gel > Pd/Zn-modified α-Al_2O_3-solvothermal > Pd/α-Al_2O_3-sol–gel ≈ Pd/α-Al_2O_3-solvothermal >> Pd/α-Al_2O_3-commerical. As revealed by thermal gravimetric and differential temperature analysis (TG-DTA), Pd catalysts on the nanocrystalline Zn-modified α-Al_2O_3 also showed less deactivation by coke formation.

Table 6.1 Characteristics of the various Pd/α-Al_2O_3 and Pd/Zn-modified α-Al_2O_3 catalysts.

	Crystallite size (nm)		BET surface area	Pore Vol.	Avg. Pore Diameter	Pd active sites ($x10^{-17}$ molecule CO	Pd dispersion	d_P Pd^0
Sample	α–Al_2O_3	$ZnAl_2O_4$	(m^2/g)	(cm^3/g)	(nm)	/g cat.)	(%)	(nm)
Pd/Al_2O_3 SG	31.0	n.d.[a]	1.6	0.011	20.4	11.3	8.8	13
Pd/Zn-Al_2O_3 SG	40.4	28	1.9	0.020	11.8	4.9	3.9	29
Pd/Al_2O_3 SV	69.5	n.d.	14.9	0.075	13.6	32.9	20.8	5
Pd/Zn-Al_2O_3 SV	32.8	14.9	10.7	0.100	22.4	22.8	16.6	7

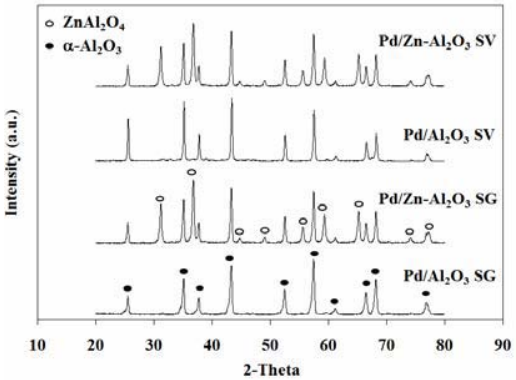

Figure 6.1 XRD patterns of the Pd/α-Al_2O_3 and Pd/Zn-modified α-Al_2O_3 supports prepared by sol-gel (SG) and solvothermal (SV) methods.

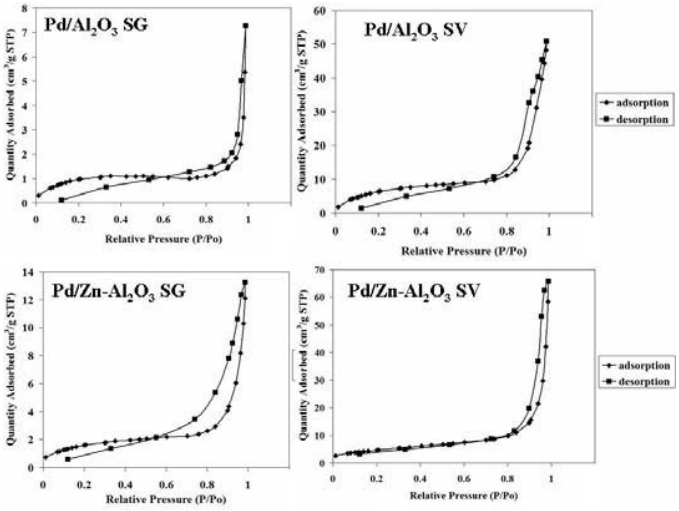

Figure 6.2 N_2 adsorption-desorption isotherms of the Pd/α-Al_2O_3 and Pd/Zn-modified α-Al_2O_3 supports prepared by sol-gel (SG) and solvothermal (SV) methods

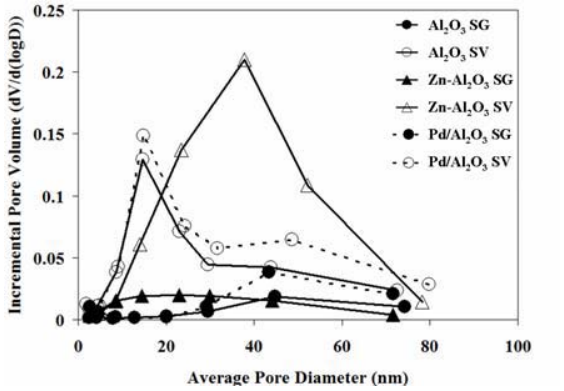

Figure 6.3 Pore size distributions of the α-Al_2O_3, Zn-modified α-Al_2O_3, and Pd/α-Al_2O_3

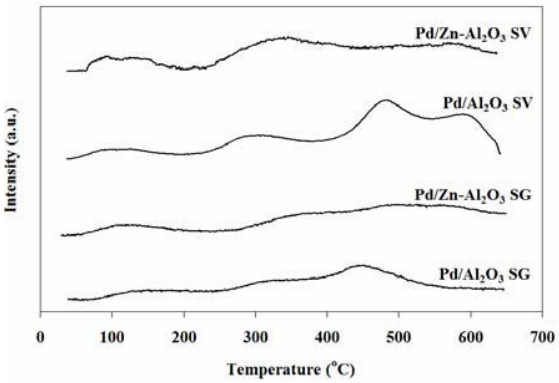

Figure 6.4 NH_3 temperature program desorption profiles for the Pd/α-Al_2O_3 and Pd/Zn-modified α-Al_2O_3 supports prepared by sol-gel (SG) and solvothermal (SV) methods.

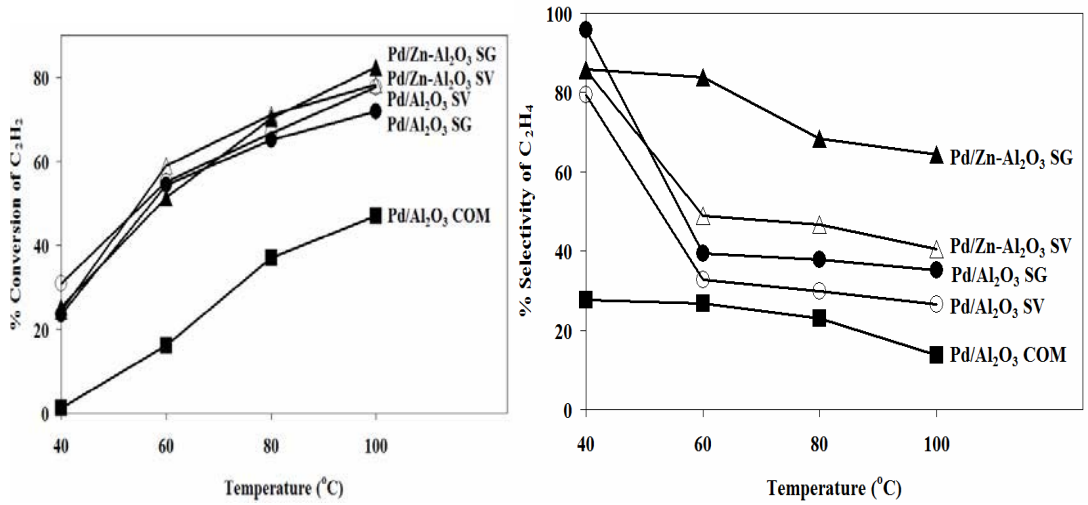

Figure 6.6 Temperature dependence of the catalytic performance of Pd/α-Al_2O_3 and Pd/Zn-modified α-Al_2O_3 catalysts; (A) in terms of % conversion of C_2H_2 (B) in terms of % selectivity of C_2H_4.

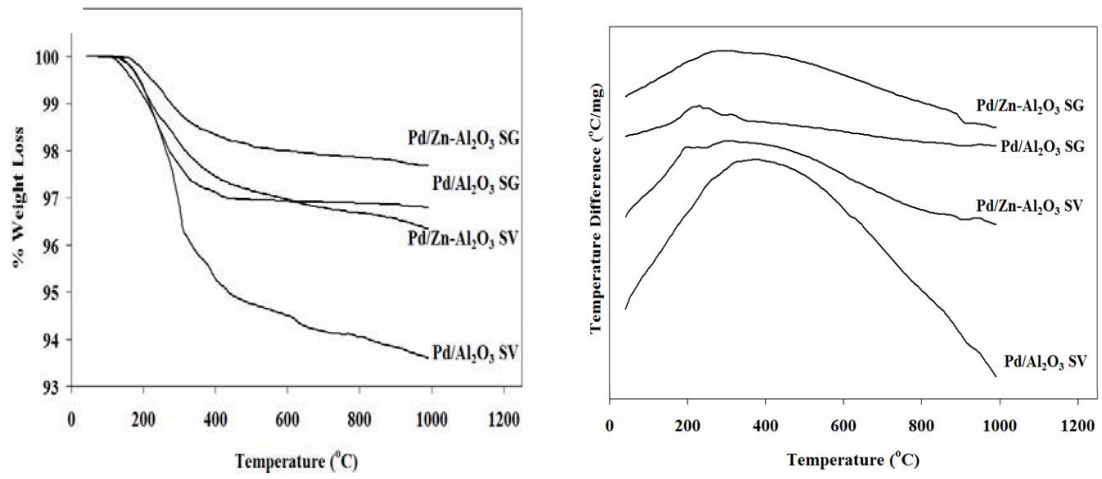

Figure 6.7 Thermal gravimetric and differential temperature analysis (TG/DTA) of Pd/α-Al_2O_3 and Pd/Zn-modified α-Al_2O_3 catalysts after reaction; (A) in terms of temperature (ºC) and weight loss (%), (B) in terms of temperature (ºC) and temperature difference (ºC/mg).

4.5.7 Improvement of Pd/Al_2O_3 Catalyst Performance in Selective Acetylene Hydrogenation using Mixed-Phases Al_2O_3 Support

The catalytic performances of Pd catalysts supported on γ-Al_2O_3, α-Al_2O_3, and mixed phases Al_2O_3 were investigated in the selective hydrogenation of acetylene in ethylene feed stream. It was found that the use of mixed phases Al_2O_3 with approximately 64% of α-phase resulted in significant improvements in both acetylene conversion and ethylene selectivity. The presence of small amount of transition-phase in the alumina supports brought about higher BET surface area and Pd dispersion as well as improvement of reduction ability of the Pd/Al_2O_3 catalysts. On the other hand, significant amount of α-Al_2O_3 is necessary for high ethylene selectivity due to the lower amount of ethylene adsorbed.

Table 7.1 The physical properties of alumina with various phase compositions.

Samples	α-Phase (%)	BET Surface Area (m^2/g)	Crystallite Size (nm)[a]		Pore Volume[b] (cm^3/g)	Average Pore Diameter[b] (Å)
			γ-phase	α-phase		
Al-α100	100	12.3	n.d.	44.5	0.03	90.1
Al-α64	64	36.1	28.3	45.8	0.14	129.6
Al-α47	47	45.4	17.8	48.9	0.20	151.9
Al-α14	14	67.3	11.8	46.0	0.30	143.8
Al-α0	0	244.1	3.7	n.d.	0.66	78.9

Table 7.2 Physiochemical properties of Pd supported on alumina with various phase compositions.

Samples	Pd Active Sites[a] ($\times 10^{-18}$ CO molecule/g-cat)	%Pd Dispersion[b]	d_p[c] (Pd^0) (nm)	Pd $3d_{5/2}$[d]		Atomic Concentration[d] Pd/Al
				B.E. (eV)	FWHM	
Pd/Al-α100	7.4	12.5	8.9	336.9	1.8	0.034
Pd/Al-α64	11.0	18.5	6.1	336.9	2.0	0.027
Pd/Al-α47	25.4	42.9	2.6	336.4	2.4	0.020
Pd/Al-α14	31.7	53.5	2.1	336.4	2.3	0.011
Pd/Al-α0	35.1	59.2	1.9	336.4	2.2	0.001

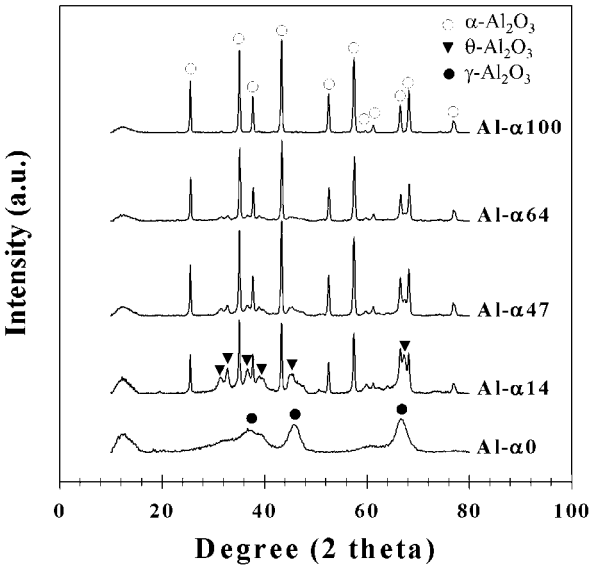

Figure 7.1 The XRD patterns of the Al_2O_3 supports containing various % of α-phase

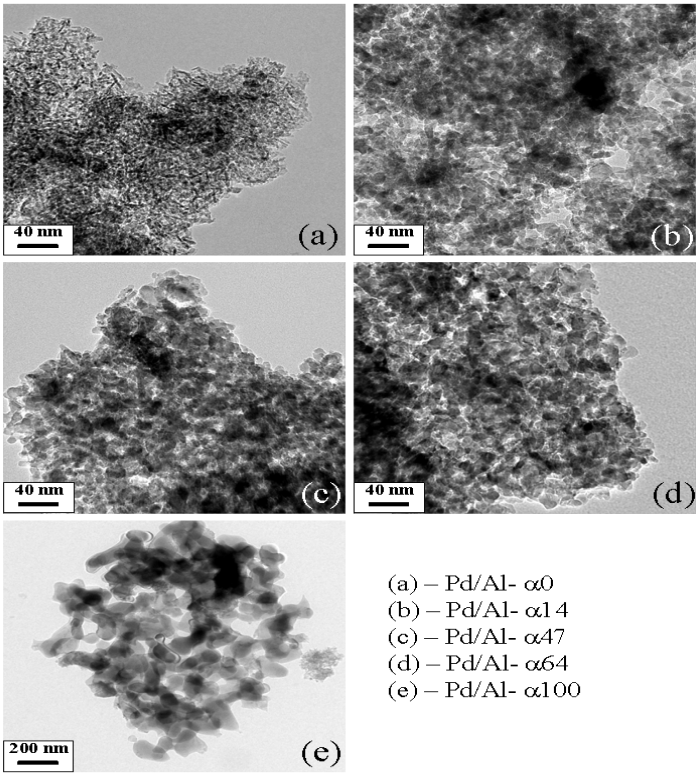

Figure 7.2 Transmission electron micrographs of the Pd/Al_2O_3 catalysts

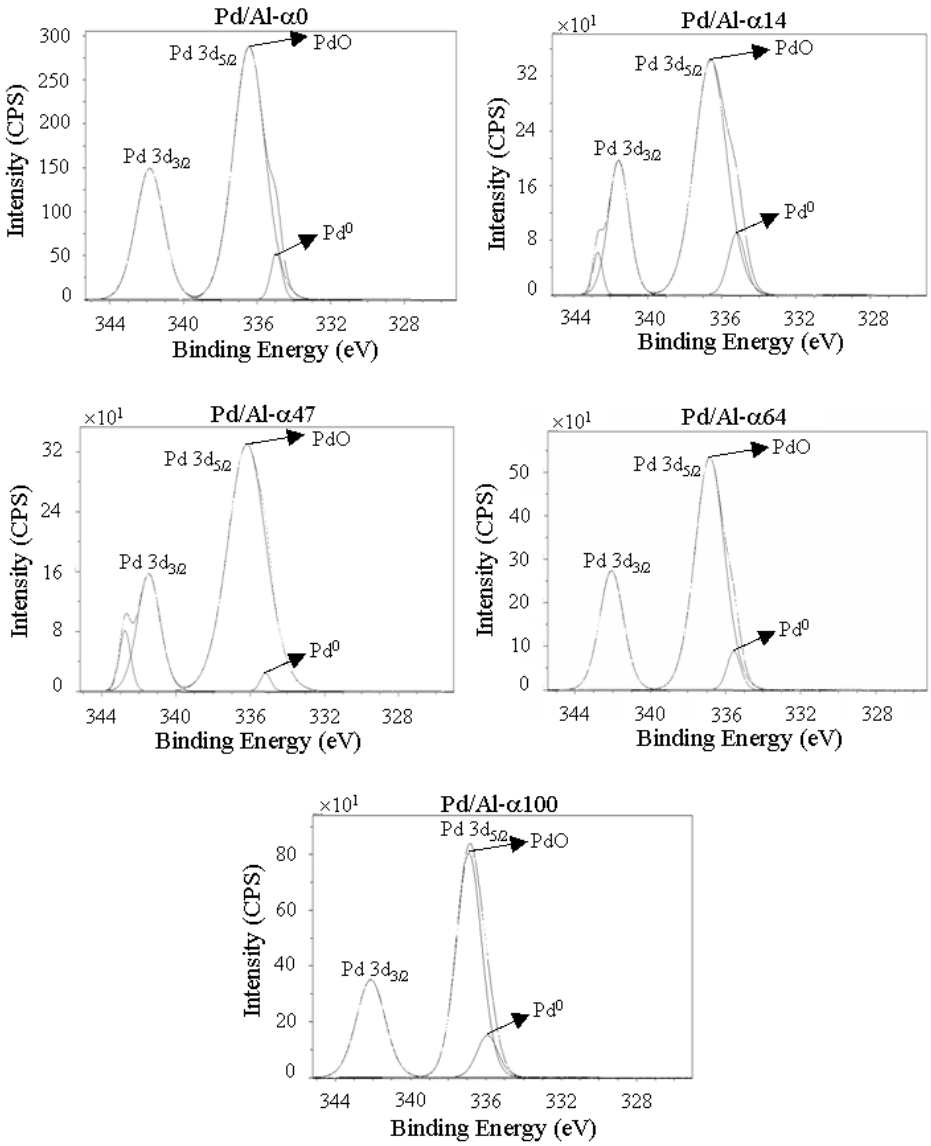

Figure 7.3 The XPS deconvoluted spectra of the Pd/Al_2O_3 catalysts

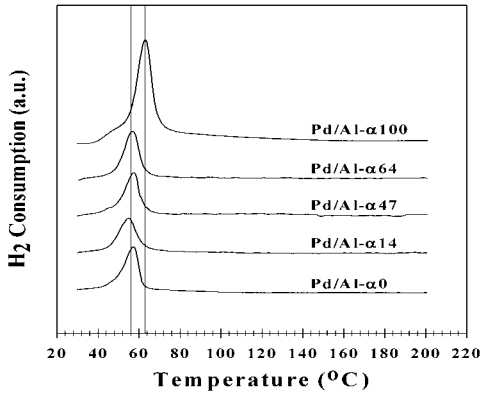

Figure 7.4 TPR profiles of the Pd/Al_2O_3 catalysts

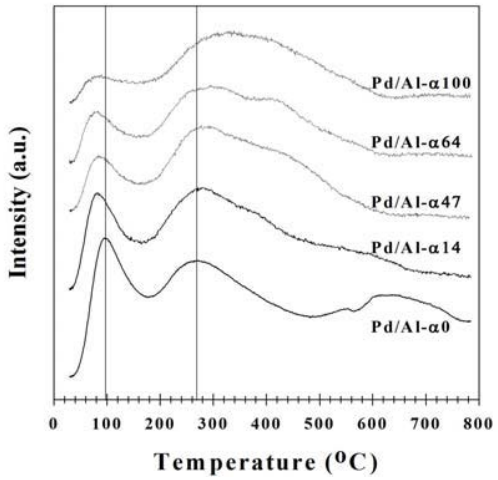

Figure 7.5 Ethylene TPD results of the Pd/Al_2O_3 catalysts

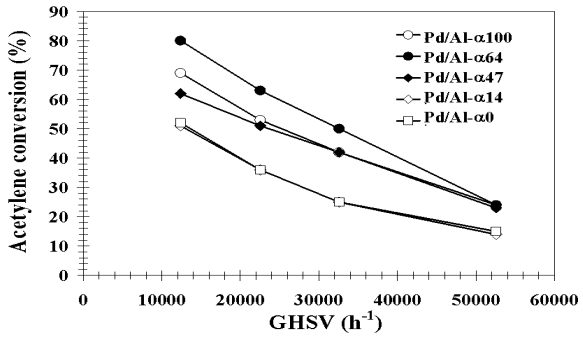

Figure 7.6 Catalyst performances in selective hydrogenation of acetylene in terms of GHSV values and acetylene conversion (%)

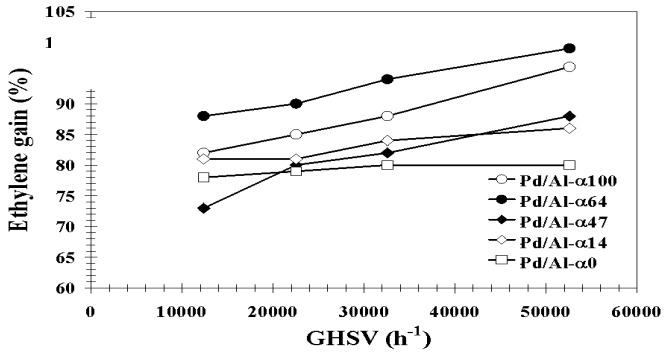

Figure 7.7 Catalyst performances in selective hydrogenation of acetylene in terms of GHSV values and ethylene gain (%)

4.5.8 Effect of Support Crystallite Size on Catalytic Activity and Deactivation of Nanocrystalline $ZnAl_2O_4$ Supported Pd Catalysts in Liquid-Phase Hydrogenation

The catalytic activity and deactivation of nanocrystalline $ZnAl_2O_4$-supported Pd catalysts were investigated for the liquid-phase hydrogenation under mild conditions. Nanocrystalline $ZnAl_2O_4$ spinels with average crystallite size between 8-33 nm were synthesized by the solvothermal method in toluene. Higher turnover frequencies for 1-heptyne hydrogenation and less deactivation due to Pd leaching were obtained for the Pd/$ZnAl_2O_4$-33 nm catalyst. XPS and ESR results suggest that the presence of defects in larger crystallite size $ZnAl_2O_4$ resulted in higher Pd dispersion and stronger interaction between Pd and the support.

Table 8.1 N_2 physisorption results[a] and XRD determined average crystallite sizes of the as-synthesized and the calcined $ZnAl_2O_4$ supports prepared by the solvothermal method

Sample	BET S.A. (m^2/g)	Pore Volume (m^3/g)	Avg. Pore Diameter (nm)	Avg. XRD Crystallite Size (nm)
$ZnAl_2O_4$-as-syn	130	0.18	4.2	8.2
$ZnAl_2O_4$-500	116	0.19	4.6	9.0
$ZnAl_2O_4$-700	63	0.20	8.5	10.9
$ZnAl_2O_4$-900	28	0.19	22.0	17.6
$ZnAl_2O_4$-1150	15	0.08	36.6	33.3

[a] Error of measurements as determined directly were ± 10%.

Table 8.2 Physicochemical properties of the various Pd catalysts

Catalyst	BET S.A.[a] (m^2/g)	Pore Vol.[a] (m^3/g)	Avg. Pore Diameter[a] (nm)	CO chemisorption[b] (10^{18} molecules CO/g cat.)	%dispersion[c]	Pd^0 d_P,[d] (nm)
$Pd/ZnAl_2O_4$-as-syn	106	0.20	4.6	7.4	13.0	7.8
$Pd/ZnAl_2O_4$-500	104	0.21	4.8	7.4	13.1	7.8
$Pd/ZnAl_2O_4$-700	66	0.21	8.9	7.2	12.8	7.4
$Pd/ZnAl_2O_4$-900	28	0.18	21.5	7.3	12.8	8.0
$Pd/ZnAl_2O_4$-1150	16	0.10	29.2	8.7	15.3	6.7

Table 8.3 Catalytic properties for liquid-phase 1-heptyne hydrogenation[a]

Catalysts	Conversion of 1-heptyne (%)	1-Heptene selectivity (%)	Estimated TOF[b] (s^{-1})[c]	%Pd leached[d]
$Pd/ZnAl_2O_4$-as-syn	52	97	0.24	36
$Pd/ZnAl_2O_4$-500	51	100	0.23	38
$Pd/ZnAl_2O_4$-700	45	100	0.22	30
$Pd/ZnAl_2O_4$-900	49	100	0.24	35
$Pd/ZnAl_2O_4$-1150	66	100	0.32	6

[a] Reaction conditions were 105 kPa, 30°C, 5 min, and catalyst/substrate molar ratio = 1,600

[b] TOF = mole product/mole Pd metal surface atoms/s. Based on the amount of potentially active Pd atoms measured by CO chemisorption.

[c] Estimated since at high conversion.

[d] Based on atomic absorption spectroscopy results. Error of measurement as determined directly was ±10%.

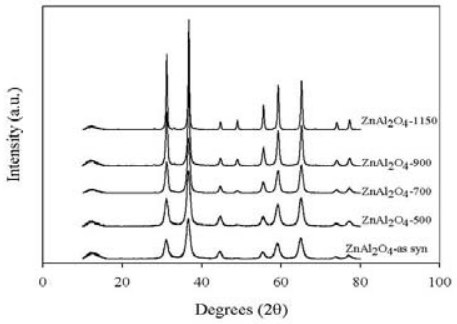

Figure 8.1 XRD patterns of the as-synthesized and the calcined $ZnAl_2O_4$

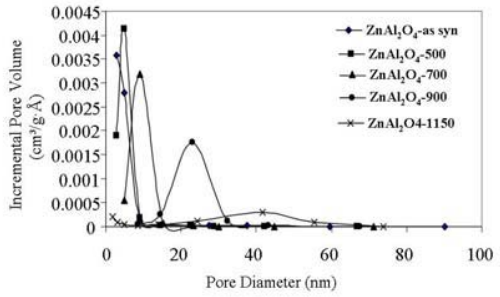

Figure 8.2 Pore size distribution of the as-synthesized and the calcined $ZnAl_2O_4$

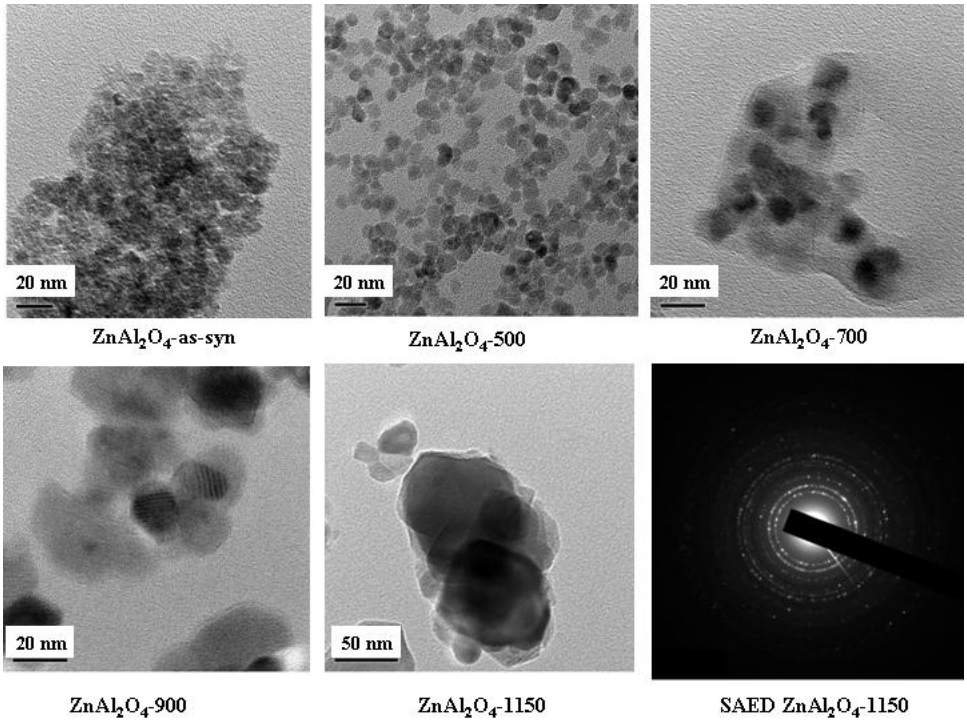

Figure 8.3 TEM micrographs and selected area electron diffraction of various $ZnAl_2O_4$ samples

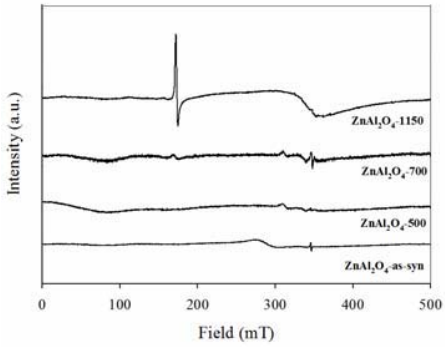

Figure 8.4 ESR results of the solvothermal-derived $ZnAl_2O_4$

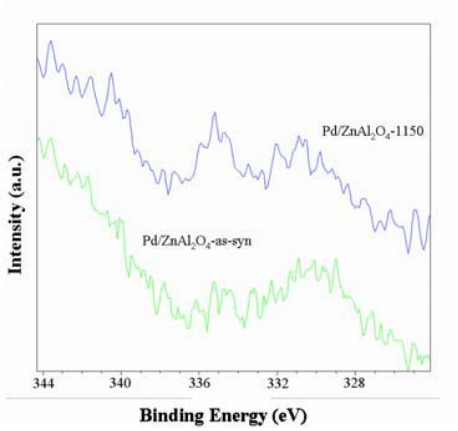

Figure 8.5 XPS spectra of Pd $3d_{5/2}$ for $Pd/ZnAl_2O_4$ catalysts

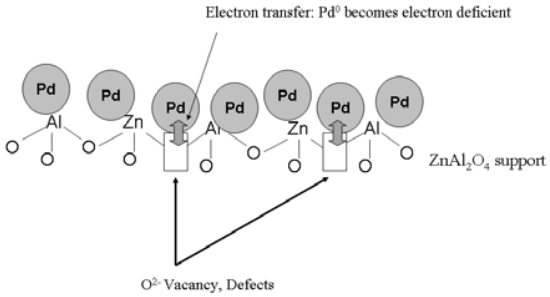

Figure 8.6 A conceptual model for stronger metal-support interaction induced by defect sites of the nanocrystalline material

4.5.9 Effect of Fe-modified α-Al_2O_3 on the properties of Pd/α-Al_2O_3 catalysts in selective acetylene hydrogenation

The use of nanocrystalline Fe-modified α-Al_2O_3 prepared by sol-gel and solvothermal method as supports for Pd catalysts resulted in an improved catalyst performance in selective acetylene hydrogenation. Moreover, the amount of coke deposits was reduced due to lower acidity of the Fe-modified α-Al_2O_3 supports.

Table 9.1 Physicochemical properties of Pd/Al_2O_3 and $Pd/Fe\text{-}Al_2O_3$ catalysts

	BET surface area (m^2/g)	Avg. crystallite size[a] (nm)	CO chemisorption ($\times 10^{17}$ site/g cat.)	% Pd Dispersion	d_p Pd^0 (nm)
$Pd/Al_2O_3\_SG$	1.0	46	10.0	8.4	13
$Pd/Fe\text{-}Al_2O_3\_SG$	1.4	62	4.1	2.7	42
$Pd/Al_2O_3\_SV$	5.1	52	11.0	7.2	16
$Pd/Fe\text{-}Al_2O_3\_SV$	3.9	63	7.8	5.1	22

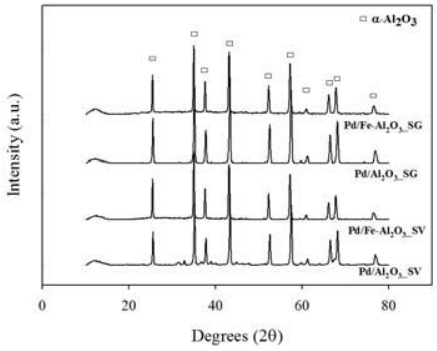

Figure 9.1 XRD patterns of the $Pd/\alpha\text{-}Al_2O_3$ and Pd/Fe-modified $\alpha\text{-}Al_2O_3$ prepared by sol-gel (SG) and solvothermal (SV) methods.

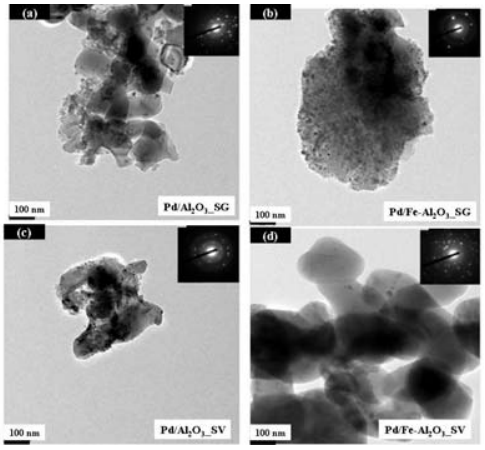

Figure 9.2 TEM micrographs of $Pd/\alpha\text{-}Al_2O_3$ and Pd/Fe-modified $\alpha\text{-}Al_2O_3$ catalysts.

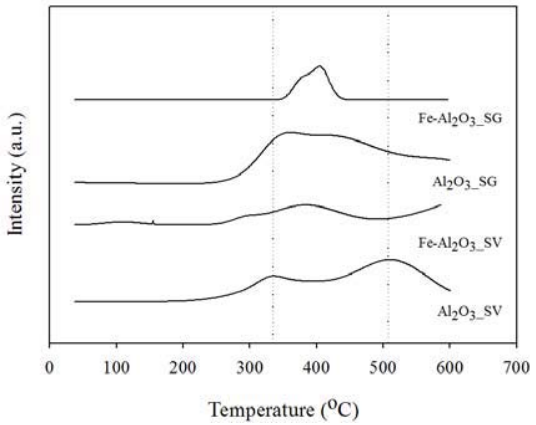

Figure 9.3 NH_3 temperature program desorption profiles for α-Al_2O_3 and Fe-modified α-Al_2O_3 supports.

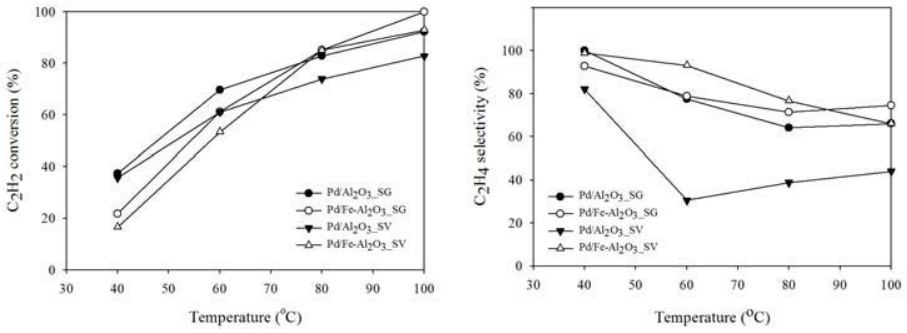

(a) (b)

Figure 9.4 Temperature dependence of the catalytic performance of Pd/α-Al_2O_3 and Pd/Fe-modified α-Al_2O_3 catalysts; (A) % conversion of C_2H_2 (B) % selectivity of C_2H_4.

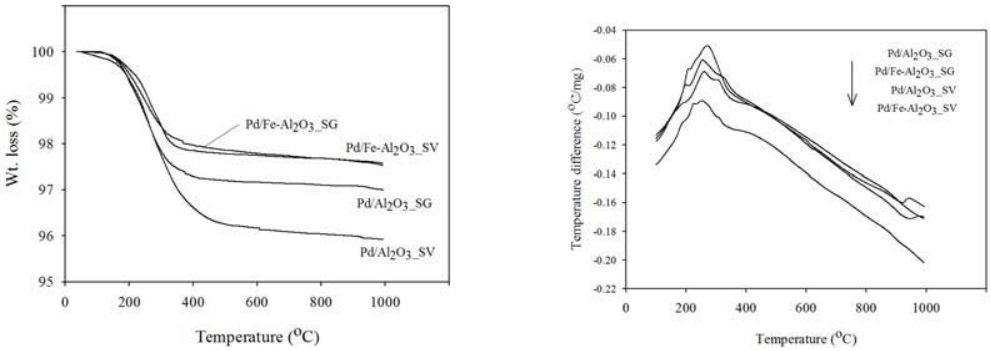

Figure 9.5 Thermal gravimetric and differential temperature analysis (TG/DTA) of Pd/α-Al_2O_3 and Pd/Fe-modified α-Al_2O_3 catalysts after reaction; (A) in terms of temperature (ºC) and weight loss (%), (B) in terms of temperature (ºC) and temperature difference (ºC/mg).

4.5.10 Influence of preparation method on the nanocrystalline porosity of α-Al_2O_3 and the catalytic properties of Pd/α-Al_2O_3 in selective acetylene hydrogenation

Nanocrystalline α-Al_2O_3 powder with average crystallite sizes 34-68 nm have been synthesized by three different methods, namely, solvothermal, sol-gel, and precipitation. Although smallest crystallite size of α-Al_2O_3 was obtained via the sol-gel synthesis, the α-Al_2O_3 sol-gel possessed the least amount of specific surface area and pore volume. A narrow pore size distribution with average pore diameter 15 nm can be obtained via solvothermal method while precipitation method yielded α-Al_2O_3 with larger pore size and wider pore size distribution. When employed as a support for Pd catalyst, the α-Al_2O_3 solvothermal provided the highest Pd dispersion and the best catalyst performance in selective hydrogenation of acetylene. The catalytic properties of Pd/α-Al_2O_3 solvothermal were improved in terms of both acetylene conversion and ethylene selectivity. As shown by temperature program studies, the use of solvothermal-derived α-Al_2O_3 facilitated H_2 reduction at low temperature and desorption of ethylene and CO.

Table 10.1 Physicochemical properties of α-Al_2O_3 various preparation methods and 0.3%Pd/Al_2O_3catalysts.

Catalysts	BET surface area (m^2/g)[a,*]	Pore volume (cm^3/g)[b,*]	Average pore diameter (nm)[b,*]	Crystallite size (nm)[c,*]	Pd active sites ($\times10^{-17}$ sites/g-catalyst)[d]	%Pd dispersion[e]	Average Pd^0 particle size (nm)[f]
Pd/Al_2O_3 Solvothermal	19.8	0.0739	14.9	53	11.5	7.6	14.7
Pd/Al_2O_3 Sol-Gel	1.7	0.0065	46	33.8	3.9	2.6	43.2
Pd/Al_2O_3 Precipitation	41.2	0.2020	26.9	67.6	2.1	1.4	80.2

Table 10.2 Consumption of hydrogen in TPR, amount of ethylene and CO desorption.

Catalysts	Temperature at maximum (°C)			H_2 consumption (μmol)*	Amount of ethylene desorption (μmol)*	Amount of CO desorption (μmol)*
	Peak 1	Peak 2	Peak 3			
Pd/Al_2O_3 Solvothermal	60[a],90[b],90[c]	240[b],230[c]	420[b]	658	131	76
Pd/Al_2O_3 Sol-Gel	65[a],100[b],90[c]	280[b],230[c]	500[b]	488	75	10
Pd/Al_2O_3 Precipitation	70[a],100[b],90[c]	260[b],250[c]	440[b]	610	122	33

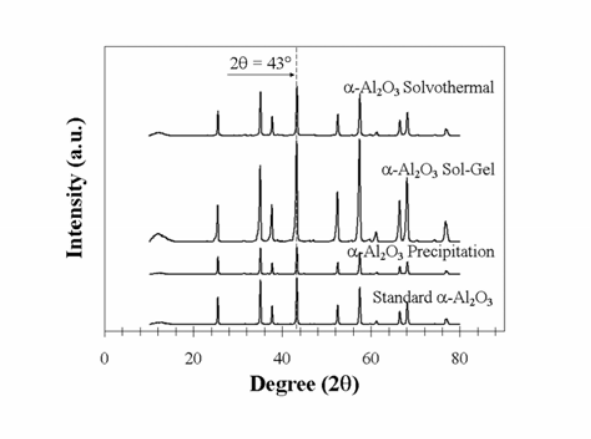

Figure 10.1 XRD patterns of the α-Al_2O_3 supports: solvothermal, sol-gel, and precipitation method.

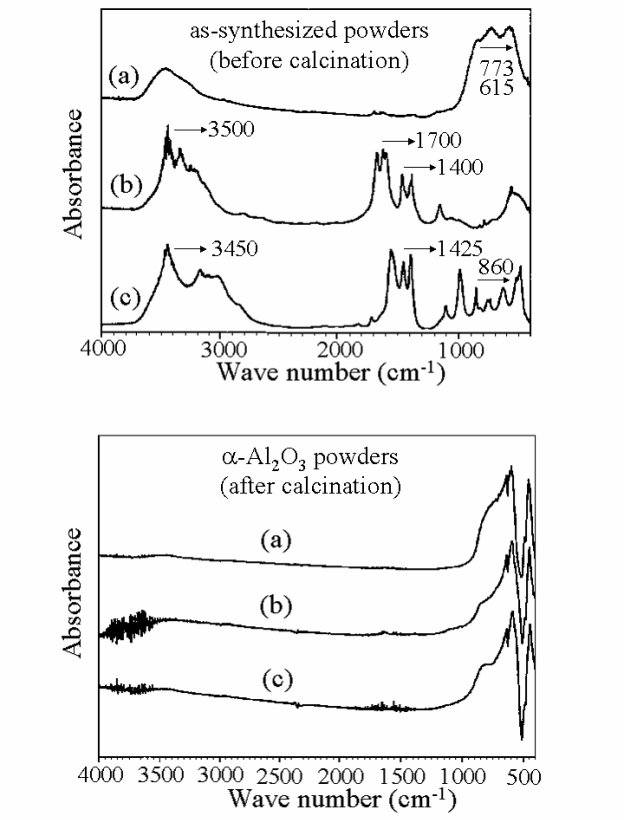

Figure 10.2 IR spectra of α-Al_2O_3 from solvothermal (a), sol-gel (b), and precipitation (c) method.

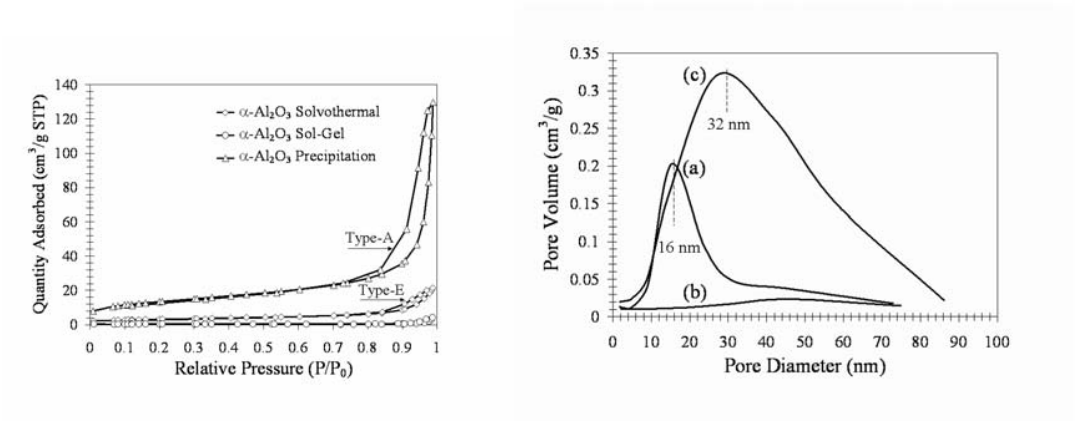

Figure 10.3 Pore size distribution results of the α-Al_2O_3 supports from solvothermal (a), sol-gel (b), and precipitation (c) method. **Figure 10.4** N_2 adsorption isotherms.

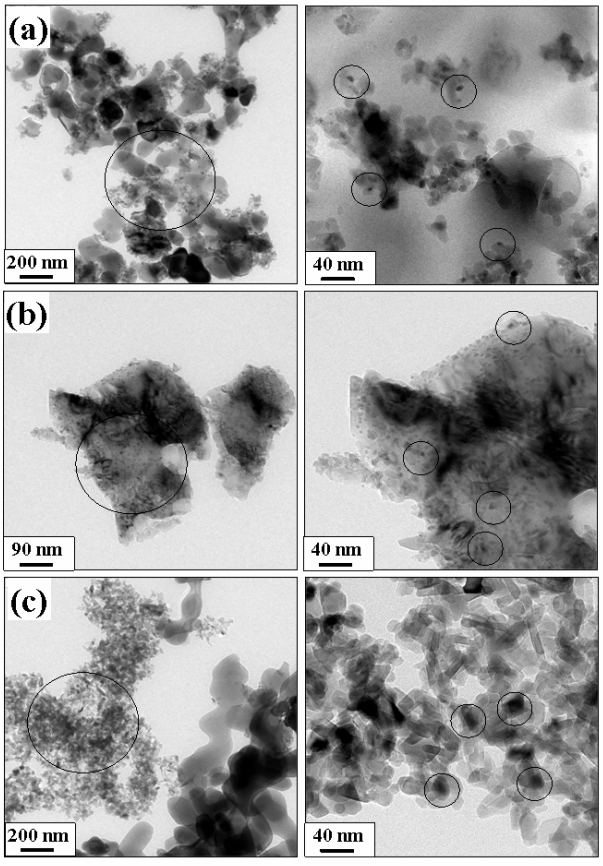

Figure 10.5 TEM image of the Pd supported by α-Al_2O_3 from solvothermal (a), sol-gel (b), and precipitation (c) method, showed Pd characteristics within the circles.

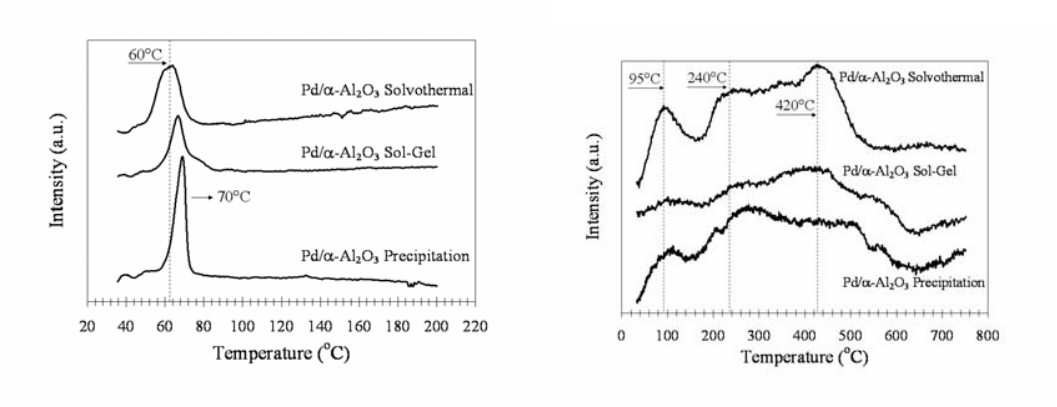

Figure 10.6 H_2-TPR profiles for the various Pd/α-Al_2O_3 catalysts. **Figure 10.7** C_2H_4-TPD profiles for the various Pd/α-Al_2O_3 catalysts.

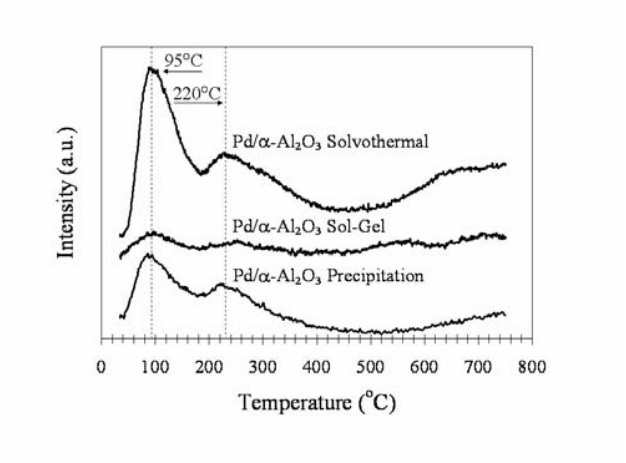

Figure 10.8 CO-TPD profiles for the various Pd/α-Al_2O_3 catalysts.

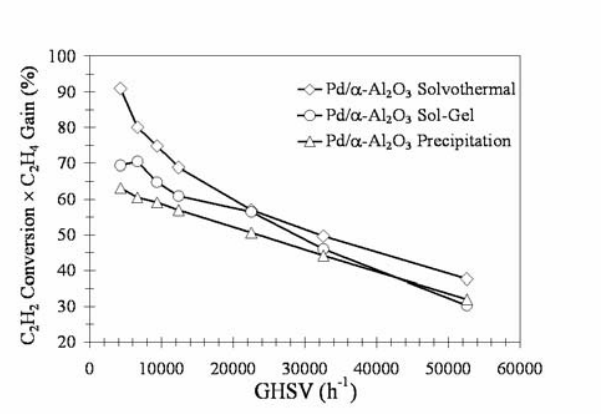

Figure 10.9 Performance of Pd/α-Al_2O_3 catalysts in the selective acetylene hydrogenation.

Output ที่ได้จากโครงการ

งานวิจัยนี้ได้เริ่มดำเนินงานตั้งแต่ 25 มิ.ย. 2550 สิ้นสุดโครงการ 24 มิ.ย. 2553 รวมระยะเวลาดำเนินงาน 3 ปี ผลที่ได้รับจากงานวิจัย ได้แก่

1. สามารถสังเคราะห์ผลึกขนาดนาโนเมตรของโลหะออกไซด์หลายชนิดได้แก่ซิลิกาอะลูมินา ไทเทเนียมไดออกไซด์ซิงค์ออกไซด์ซิงค์อะลูมิเนตและสังเคราะห์ตัวเร่งปฏิกิริยาแพลเลเดียมบนผลึกขนาดนาโนเมตรของโลหะออกไซด์ที่ภาควิชาวิศวกรรมเคมี คณะวิศวกรรมศาสตร์ จุฬาลงกรณ์มหาวิทยาลัย

2. ได้องค์ความรู้ใหม่เกี่ยวกับการสังเคราะห์ตัวเร่งปฏิกิริยาที่มีประสิทธิภาพสูงสำหรับใช้ในปฏิกิริยาไฮโดรจิเนชันของสารไฮโดรคาร์บอนไม่อิ่มตัวต่างๆ

3. ได้ผลงานวิจัยที่ได้รับการตีพิมพ์ในวารสารระดับนานาชาติที่มีค่าImpact Factor สูงทางด้านคาตาไลซิสและวิศวกรรมเคมี อาทิ ***Journal of Catalysis*** (IF 2009 = 5.288), ***Applied Catalysis A. General*** (IF2009 = 3.564), ***Catalysis Today*** (IF2009 = 3.526), ***Journal of Molecular Catalysis A. Chemical*** (IF2009 = 3.135), ***Catalysis Communications*** (IF2009 = 3.00) จำนวน 17 บทความ Impact factor (ปี 2009) **รวม 43.858** โดยเป็น Corresponding author 13 บทความและเป็นผู้ร่วมวิจัย (co-author) 4 บทตวาม (ภาคผนวก ก และ ข)

ภาคผนวก ก

บทความที่เป็นผู้วิจัยหลัก (Corresponding author) Impact factor รวม 34.643

เอกสารแนบ 1-13

No.	ชื่อบทความ	ผู้แต่ง	Corresponding Author	วารสาร	Impact factor (FY2008)
1	Selective Hydrogenation of Acetylene in Excess Ethylene on Micron-Sized and Nanocrystalline TiO_2 Supported Pd Catalysts	Joongjai Panpranot, Kunyaluck Kontapakdee, Piyasan Praserthdam	Joongjai Panpranot	Applied Catalysis A: General 314 (2006) 128-133.	3.564
2	Characteristics and Catalytic Properties of Pd/SiO_2 Synthesized by One-Step Flame Spray Pyrolysis in Liquid-Phase Hydrogenation of 1-Heptyne	Sirima Somboonthanakij, Okorn Mekasuwandumrong, Joongjai Panpranot*, Tarit Nimmanwudtipong, Reto Strobel, Sotiris E. Pratsinis, and Piyasan Praserthdam	Joongjai Panpranot	Catalysis Letters, 119 (2007) 346-352	2.021
3	Performance of Pd Catalysts Supported on Nanocrystalline a-Al_2O_3 and Ni-Modified a-Al_2O_3 in Selective Hydrogenation of Acetylene	Nitikon Wongwaranon, Okorn Mekasuwandumrong, Piyasan Praserthdam, and Joongjai Panpranot	Joongjai Panpranot	Catalysis Today 131 (2008) 553-558	3.526
4	A Comparative Study of Strong Metal-Support Interaction and Catalytic Behaviors of Pd Catalysts Supported on Micron- and Nano-sized TiO_2 in Liquid-Phase Selective Hydrogenation of Phenylacetylene	Patcharaporn Weerachawanasak, Piyasan Praserthdam, Masahiko Arai, and Joongjai Panpranot	Joongjai Panpranot	Journal of Molecular Catalysis A. Chemical, 279 (2007) 133-139	3.135
5	Effect of Ni-Modified a-Al_2O_3 Prepared by Sol-Gel and Solvothermal Methods on the Characteristics and Catalytic Properties of Pd/a-Al_2O_3 Catalysts	Okorn Mekasuwandumrong, Nitikon Wongwaranon, Piyasan Praserthdam, and Joongjai Panpranot	Joongjai Panpranot	Materials Chemistry and Physics, 111 (2008) 431-437	2.015
6	Selective Hydrogenation of Acetylene over Pd Catalysts Supported on Nanocrystalline a-Al_2O_3 and Zn-Modified a-Al_2O_3	Suthana Chinayon, Okorn Mekasuwandumrong, Piyasan Praserthdam, and Joongjai Panpranot	Joongjai Panpranot	Catalysis Communications, 9 (2008) 2297-2302	3.000
7	Improvement of Pd/Al_2O_3 Catalyst Performance in Selective Acetylene Hydrogenation using Mixed-Phases Al_2O_3 Support	Sataporn Komhom, Piyasan Praserthdam, Okorn Mekasuwandumrong, Joongjai Panpranot	Joongjai Panpranot	Catalysis Communications, 10 (2008) 86-91	3.000
8	Effect of Support Crystallite Size on Catalytic Activity and Deactivation of Nanocrystalline $ZnAl_2O_4$ Supported Pd Catalysts in Liquid-Phase Hydrogenation	Terachai Sirikajorn, Okorn Mekasuwandumrong, Piyasan Praserthdam, James G. Goodwin, Jr., and Joongjai Panpranot	Joongjai Panpranot	Catalysis Letters, 126 (2008) 313-318	2.021
9	Effect of strong metal-support interaction on the catalytic performance of Pd/TiO_2 in the liquid-phase semihydrogenation of phenylacetylene	Patcharaporn Weerachawanasak, Okorn Mekasuwandumrong, Piyasan Praserthdam, Masahiko Arai, Shin-Ichiro Fujita, Joongjai Panpranot	Joongjai Panpranot	Journal of Catalysis, 262 (2009) 199-205	5.288
10	Preparation of Nano-Pd/SiO_2 by One-Step Flame Spray Pyrolysis and its Hydrogenation Activities: Comparison to Conventional Impregnation Method	Okorn Mekasuwandumrong, Sirima Somboonthanakij, Piyasan Praserthdam, and Joongjai Panpranot	Joongjai Panpranot	Industrial Engineering and Chemistry Research, 48 (2009) 2819-2825	1.758
11	Synthesis of nanocrystalline Au-ZnO and Pt-ZnO by flame spray pyrolysis and its application for photocatalytic degradation of dyes	Pongsapak Pawinrat, Okorn Mekasuwandumrong, Joongjai Panpranot	Joongjai Panpranot	Catalysis Communications, 10 (2009) 1380-1385	3.000
12	Influence of preparation method on the nanocrystalline porosity of α-Al_2O_3 and the catalytic properties of Pd/α-Al_2O_3 in selective acetylene hydrogenation	Sataporn Komhom, Okorn Mekasuwandumrong, Joongjai Panpranot, Piyasan Praserthdam	Joongjai Panpranot	Industrial Engineering and Chemistry Research, 48 (2009) 6273-6279.	1.758
13	Effect of Fe-Modified a-Al_2O_3 on the Properties of Pd/a-Al_2O_3 Catalysts in Selective Hydrogenation of Acetylene	Tatiya Sangkam, Okorn Mekasuwandumrong, Piyasan Praserthdam, Joongjai Panpranot	Joongjai Panpranot	Reaction Kinetics and Catalysis, 97 (2009) 115-123.	0.557

ภาคผนวก ข

บทความที่เป็นผู้ร่วมวิจัย Impact factor รวม 9.215

เอกสารแนบ 14-17

No.	ชื่อบทความ	ผู้แต่ง	Corresponding Author	วารสาร	Impact factor (FY2008)
14	Synthesis of Nanocrystalline Al_2O_3 by Thermal Decomposition of Aluminum Isopropoxide and its Application as Co Catalyst Support for Carbon Monoxide Hydrogenation	Kamonchanok Pansanga, Okorn Mekasuwandumrong, Joongjai Panpranot, and Piyasan Praserthdam	Piyasan Praserthdam	Korean Journal of Chemical Engineering 24 (2007) 397-402	0.893
15	Copper-Modified Alumina as a Support for Iron Fischer-Tropsch Synthesis Catalysts	Kamonchanok Pansanga, Nattaporn Lohitharn, Andrew C. Y. Chien, Edgar Lotero, Joongjai Panpranot, Piyasan Praserthdam, and James G. Goodwin, Jr.	James G. Goodwin, Jr.	Applied Catalysis A. General, 332 (2007) 130-137.	3.564
16	Effect of Mixed g and χ Crystalline Phases in Nanocrystalline Al_2O_3 on the Dispersion of Cobalt on Al_2O_3	Kamonchanok Pansanga, Joongjai Panpranot, Okorn Mekasuwandumrong, Chairit Satayaprasert, James G. Goodwin, Jr., and Piyasan Praserthdam	Piyasan Praserthdam	Catalysis Communications 9 (2008) 207-212.	3.000
17	Dependence of Quenching Process on the Photocatalytic Activity of Solvothermal-Derived TiO_2 with Various Crystallite Sizes	Piyawat Supphasrirongjaroen, Wilasinee Kongsuebchart, Joongjai Panpranot, Okorn Mekasuwandumrong, Chairit Satayaprasert, and Piyasan Praserthdam	Piyasan Praserthdam	Industrial Engineering and Chemistry Research 47 (2008) 693-697	1.758

Available online at www.sciencedirect.com
ScienceDirect
Applied Catalysis A: General 314 (2006) 128–133
APPLIED CATALYSIS A: GENERAL
www.elsevier.com/locate/apcata

Selective hydrogenation of acetylene in excess ethylene on micron-sized and nanocrystalline TiO_2 supported Pd catalysts

Joongjai Panpranot *, Kunyaluck Kontapakdee, Piyasan Praserthdam

Center of Excellence on Catalysis and Catalytic Reaction Engineering, Department of Chemical Engineering, Faculty of Engineering, Chulalongkorn University, Bangkok 10330, Thailand

Received 11 April 2006; received in revised form 22 July 2006; accepted 7 August 2006
Available online 20 September 2006

Abstract

Physicochemical properties and catalytic performances of Pd catalysts supported on commercial micron-sized and nanocrystalline TiO_2 synthesized by sol–gel and solvothermal method were studied for the selective hydrogenation of acetylene in the presence of excess ethylene. While acetylene conversions were found to be merely dependent on Pd dispersion, ethylene selectivity appeared to be strongly affected by the presence of Ti^{3+} in the TiO_2 samples. The use of pure anatase TiO_2 (either micron- or nano-sized) that contained significant amount of Ti^{3+} as supports for Pd catalysts gave high ethylene selectivities, while the use of pure rutile TiO_2 (without Ti^{3+} present) resulted in ethylene loss. The results suggest that the effect of Ti^{3+} on the TiO_2 supports was more important for high ethylene selectivity than the effect of TiO_2 crystallite size for selective acetylene hydrogenation over Pd/TiO_2 catalysts.

Keywords: Selective acetylene hydrogenation; Pd/TiO_2; Nanocrystalline TiO_2; Sol–gel; Solvothermal; Defect

1. Introduction

Removal of trace amount of acetylene in ethylene feed stream is vital for the commercial production of polyethylene since acetylene acts as a poison to the polymerization catalysts. In order to prevent ethylene loss, when acetylene is catalytically hydrogenated, it is desirable that ethylene remains intact during hydrogenation. Supported Pd-based catalyst is known to be the best catalyst so far for such reaction with good activity and selectivity. The commonly used support for palladium catalyst in selective acetylene hydrogenation is α-alumina, however, oligomer or green oil formation during reaction is inevitable over Pd/Al_2O_3 catalysts resulting in ethylene loss and shorten catalyst lifetime especially at high levels of acetylene conversion [1–6]. Several attempts to improve ethylene selectivity of the palladium catalyst have been made by many researchers, including incorporation of a second metal such as Ag [7–10], Au [11,12], Cu [13], Si [14], K [15], and Co [16], pre-treatment with oxygen-containing compounds such as CO and N_2O [17–20], and modification of the catalyst supports [21,22].

Among the various supports studied, TiO_2 is of particular interest because of its ability to manifest a strong metal–support interaction (SMSI) with group VIII metals and its low acidity compared to alumina. Moon and co-workers [21] reported an improved selectivity for ethylene production in selective acetylene hydrogenation over TiO_2-modified Pd catalysts. The authors suggest that charge transfer from Ti species to Pd weakened the adsorption strength of ethylene on the Pd surface hence higher ethylene selectivity was obtained. Moreover, the amount of green oil formation was reduced on the TiO_2-added Pd catalysts due to suppression of the multiply coordinated Pd sites resulting in an improved catalyst lifetime [23]. Fan and co-workers [24] studied selective hydrogenation of long chain alkadienes, it was shown that the presence of SMSI for Pd/TiO_2 catalysts led to higher selectivity of alkenes.

Recently, our group has reported the synthesis of nanocrystalline TiO_2 by solvothermal method and their applications as Pd catalyst supports in selective acetylene hydrogenation [25]. The solvothermal-derived TiO_2 supported Pd catalysts exhibited relatively high acetylene conversions and ethylene selectivities in the temperature range 40–90 °C in selective acetylene hydrogenation using trace amount of C_2H_2

* Corresponding author. Tel.: +66 2218 6878; fax: +66 2218 6877.
E-mail address: joongjai.p@eng.chula.ac.th (J. Panpranot).

0926-860X/$ – see front matter © 2006 Elsevier B.V. All rights reserved.
doi:10.1016/j.apcata.2006.08.024

in N_2 balance. Nevertheless, their catalytic activities and selectivities have not yet been compared to those of commercial TiO_2 supported ones under real commercial ethylene feed stocks. Thus, it is the aim of this study to investigate and compare the catalytic performances of commercial micron-sized and nanocrystalline TiO_2 supported Pd catalysts in selective acetylene hydrogenation in the presence of excess ethylene. The effects of crystallite size as well as other physicochemical properties such as the presence of Ti^{3+} defective sites of the TiO_2 on the catalytic properties of Pd/TiO_2 catalysts were investigated by means of X-ray diffraction (XRD), N_2 physisorption, X-ray photoelectron spectroscopy (XPS), CO chemisorption, scanning electron microscopy (SEM), and electron spin resonance (ESR).

2. Experimental

2.1. Preparation of TiO_2 and Pd/TiO_2 catalyst samples

The commercial anatase TiO_2 was obtained from Aldrich. By calcination in air at 1010 °C for 4 h using a space velocity of air flow 16,000 h^{-1}, the anatase TiO_2 was gradually transformed into rutile TiO_2. The commercial anatase and rutile TiO_2 were denoted as TiO_2-com-A and TiO_2-com-R, respectively.

Titanium ethoxide (Ti 20%) from Aldrich was used as Ti precursor for preparation of the nanocrystalline TiO_2 by sol–gel method [26]. A specific amount of the precursor was dissolved in ethanol and mixed with a water–ethanol solution at water to alkoxide molar ratio 165. The precursor solution was added drop wise to the aqueous solution and stirred by ultrasonic vibration at room temperature. White precipitates of hydrous oxides formed instantly and the mixture was stirred for at least two more hours. The amorphous precipitates were separated from the mother liquor by centrifugation and were re-dispersed in ethanol for five times to minimize particle agglomeration. The resulting materials were then dried and calcined at 450 °C in flowing oxygen for 2 h at the heating rate of 10 °C/min. The sol–gel derived TiO_2 was denoted hereafter as TiO_2-sol–gel.

The solvothermal-derived TiO_2 was prepared according to the method described in Ref. [27] using 25 g of titanium(IV) *n*-butoxide (TNB) 97% from Aldrich. The starting material was suspended in 100 ml of 1,4-butanediol in a test tube and then set up in an autoclave. In the gap between the test tube and autoclave wall, 30 ml of solvent was added. After the autoclave was completely purged with nitrogen, the autoclave was heated to 320 °C at 2.5 °C/min and held at that temperature for 6 h. Autogenous pressure during the reaction gradually increased as the temperature was raised. After the reaction, the autoclave was cooled to room temperature. The resulting powders were collected after repeated washing with methanol by centrifugation. They were then air-dried at room temperature. The solvothermal derived TiO_2 was denoted hereafter as TiO_2-solvothermal.

One percent Pd/TiO_2 were prepared by the incipient wetness impregnation technique using an aqueous solution of the desired amount of $Pd(NO_3)_2$ (Wako). The catalysts were dried overnight at 110 °C and then calcined in N_2 flow 60 cm^3/min with a heating rate of 10 °C/min until the temperature reached 500 °C and then in air flow 100 cm^3/min at 500 °C for 2 h.

2.2. Catalyst characterization

The BET surface areas of the samples were determined by N_2 physisorption using a Micromeritics ASAP 2000 automated system. Each sample was degassed under vacuum at <10 μm Hg in the Micromeritics ASAP 2000 at 150 °C for 4 h prior to N_2 physisorption. The XRD spectra of the catalyst samples were measured from 20–80° 2θ using a SIEMENS D5000 X-ray diffractometer and Cu Kα radiation with a Ni filter. Electron spin resonance spectra were taken at −150 °C using a JEOL JES-RE2X spectrometer. Relative percentages of palladium dispersion were determined by pulsing carbon monoxide over the reduced catalyst. Approximately 0.2 g of catalyst was placed in a quartz tube in a temperature-controlled oven. The amounts of CO chemisorbed on the catalysts were measured using a Micromeritic Chemisorb 2750 automated system attached with ChemiSoft TPx software at room temperature. Prior to chemisorption, the sample was reduced in a H_2 flow at 500 °C for 2 h then cooled down to ambient temperature in a He flow. The particle morphology was obtained using a JEOL JSM-35CF scanning electron microscope operated at 20 kV. Surface compositions of the catalysts were analyzed using an AMICUS photoelectron spectrometer equipped with a Mg Kα X-ray as a primary excitation and a KRATOS VISION2 software. XPS elemental spectra were acquired with 0.1 eV energy step at a pass energy of 75 kV. The C 1s line was taken as an internal standard at 285.0 eV.

2.3. Reaction study

Selective acetylene hydrogenation was performed in a quartz tube reactor (i.d. 9 mm). Prior to the start of each run, the catalyst was reduced in H_2 at 500 °C for 2 h. Then the reactor was purged with argon and cooled down to the reaction temperature, 40 °C. Feed gas composed of 1.46% C_2H_2, 1.71% H_2, 15.47% C_2H_6 and balanced C_2H_4 (Rayong Olefin Co., Ltd.) and a GHSV of 5400 h^{-1} were used. The composition of product and feed stream were analyzed by a Shimadzu GC 8A equipped with TCD and FID detectors (molecular sieve-5A and carbosieve S2 columns, respectively). Acetylene conversion as used herein is defined as moles of acetylene converted with respect to acetylene in feed. Ethylene selectivity is defined as the percentage of acetylene hydrogenated to ethylene over totally hydrogenated acetylene. The ethylene being hydrogenated to ethane (ethylene loss) is the difference between all the hydrogen consumed and all the acetylene which has been totally hydrogenated.

3. Results and discussion

3.1. Physicochemical properties of the TiO_2 supports

The SEM micrographs of various titania samples are shown in Fig. 1. The commercial anatase TiO_2 had a uniform particle

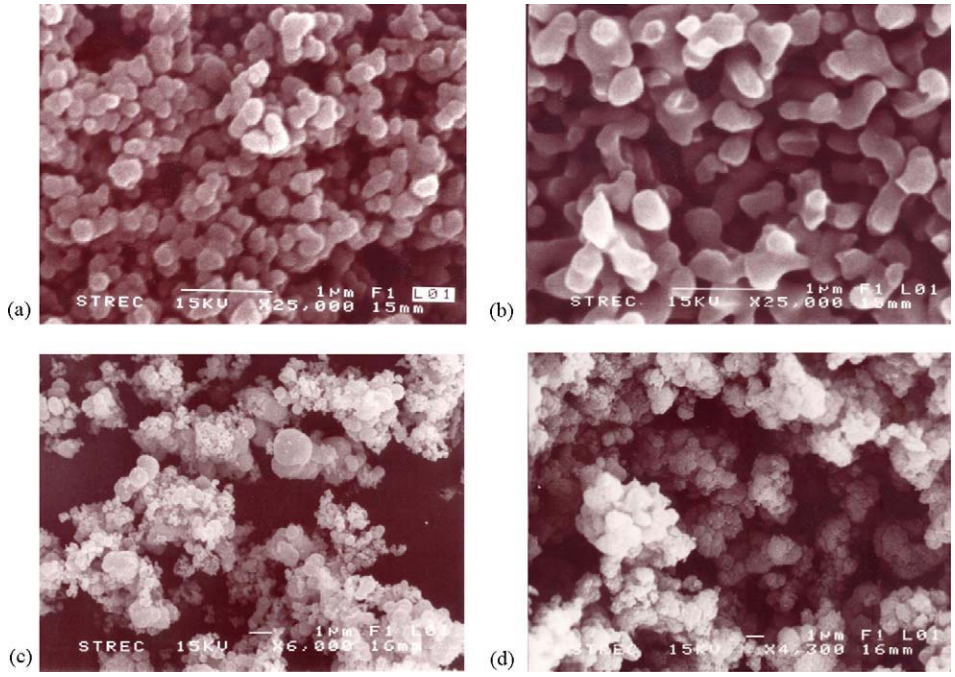

Fig. 1. SEM micrographs of: (a) TiO_2-com-A (b) TiO_2-com-R (c) TiO_2-sol–gel and (d) TiO_2-solvothermal.

size ca. 0.2 μm. After being subjected to thermal treatment (calcination) at 1010 °C for 4 h, pure anatase titania was gradually transformed into rutile titania and the particle size increased to ca. 0.4 μm. The morphology of pure anatase nanocrystalline TiO_2 prepared by sol–gel and solvothermal method was consisted of irregular shape of fine particles. However, some of the particles of those synthesized by the sol–gel method appeared to agglomerate into spherical micron-size particles. The crystallization mechanism of TiO_2 was probably different for these two methods resulting in different properties of the TiO_2 obtained. It was suggested that anatase titania synthesized by solvothermal in 1,4-butanediol was resulted from direct crystallization [27] while sol–gel method yielded a solid precipitate at relatively low temperature used and crystallization occurred during the subsequent calcination step. XRD patterns of the calcined TiO_2 samples are shown in Fig. 2. For the anatase titania (TiO_2-com-A, TiO_2-sol–gel, and TiO_2-solvothermal), XRD peaks at $2\theta = 25$ (major), 37, 48, 55, 56, 62, 71, and 75° 2θ were evident. The TiO_2-com-R exhibited XRD peaks for rutile phase at $2\theta = 28$ (major), 36, 42, and 57°. BET surface areas, average crystallite sizes, and percentages of atomic concentration (Ti/O) of the various TiO_2 samples are given in Table 1. The average crystallite sizes of the TiO_2 prepared by sol–gel and solvothermal calculated from the full width at half maximum of the XRD peak at $2\theta = 25°$ using Scherrer equation are in nanometer range (10 and 17, respectively) while those of the commercial ones could not be determined by this method due to the calculation limit of the Scherrer equation (the crystallite size may be too large). BET surface areas of the commercial anatase TiO_2 decreased essentially from 64.4 to 18.3 m^2/g after calcination in order to transform the crystalline phase to rutile phase TiO_2. It is surprising that the BET surface areas of the nano-sized TiO_2 prepared by sol–gel and solvothermal method were much lower

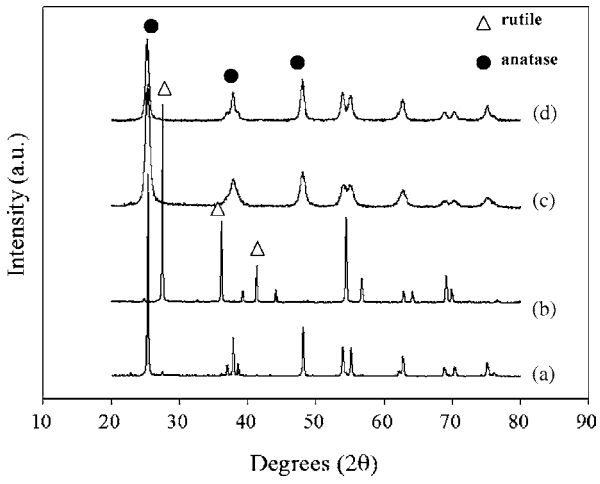

Fig. 2. XRD results of: (a) TiO_2-com-A (b) TiO_2-com-R (c) TiO_2-sol–gel and (d) TiO_2-solvothermal.

Table 1
Properties of the various TiO_2 supports

Sample	BET surface area[a] (m^2/g)	Crystallite size[b] (nm)	Atomic concentration[c] (%), Ti/O
TiO_2-com-A	64.4	n.d.	0.287
TiO_2-com-R	18.3	n.d.	0.250
TiO_2-sol–gel	39.3	10	0.232
TiO_2-solvothermal	26.8	17	0.220

[a] Error of measurement = ±10%.
[b] Determined from XRD line broadening.
[c] Determined from XPS analysis.

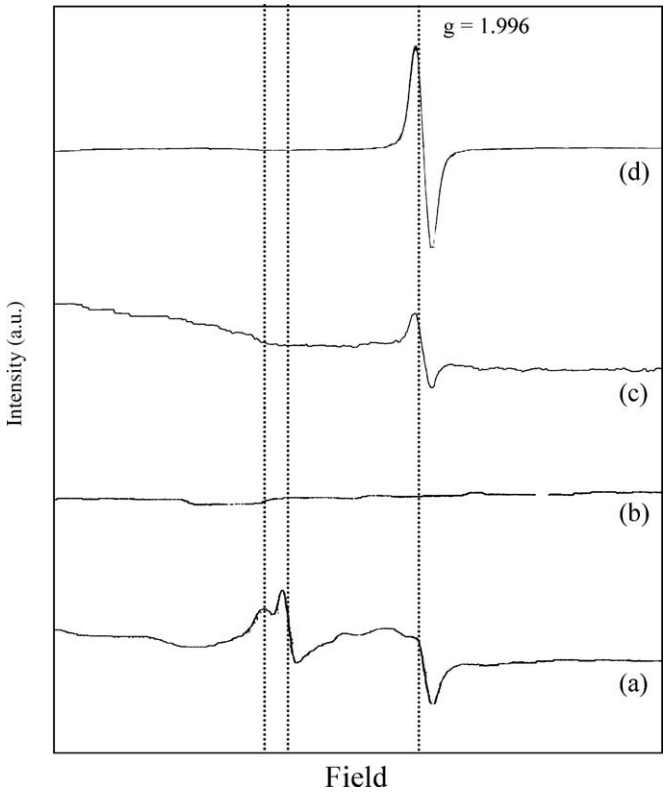

Fig. 3. ESR spectra of: (a) TiO_2-com-A (b) TiO_2-com-R (c) TiO_2-sol–gel and (d) TiO_2-solvothermal.

than that of the commercial anatase TiO_2. Such results suggest that the nano-crystals were closely packed resulting in low pore volume in the samples. Percentages of atomic concentrations of Ti and O on the surface of the TiO_2 were determined by the X-ray photoelectron spectroscopy. The Ti/O ratios were not significantly different among the four TiO_2 samples. There was probably an oxygen-rich layer near the surface of the TiO_2 particles, which is formed by oxygen adsorption and easy oxidation of titanium surface [28]. The ESR spectra of the TiO_2 samples are shown in Fig. 3. The signals of g values less than 2 were assigned to Ti^{3+} ($3d^1$) [29,30]. Nakaoka and Nosaka [31] reported six signals of ESR measurement occurring on the surface of titania: (i) $Ti^{4+}O^{-}Ti^{4+}OH^{-}$, (ii) surface Ti^{3+}, (iii) adsorbed oxygen (O^{2-}), (iv) $Ti^{4+}O^{2-}Ti^{4+}O^{2-}$, (v) inner Ti^{3+}, and

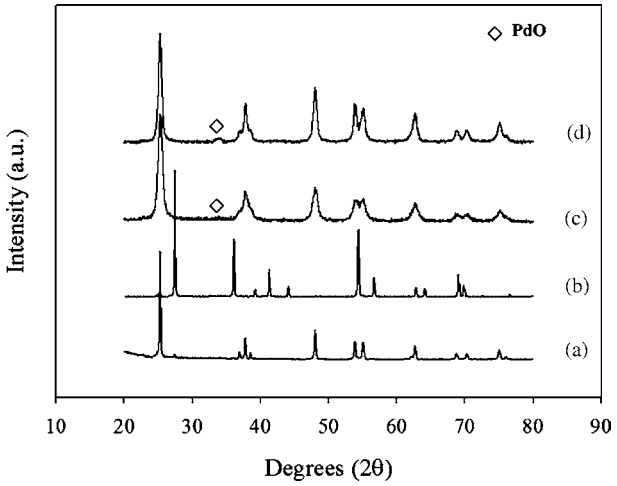

Fig. 4. XRD results of: (a) Pd/TiO_2-com-A (b) Pd/TiO_2-com-R (c) Pd/TiO_2-sol–gel and (d) Pd/TiO_2-solvothermal.

(vi) adsorbed water. In this study, it is seen that the sol–gel and solvothermal-derived TiO_2 exhibited only one signal at g value of 1.996 which can be attributed to Ti^{3+} at the surface. Many Ti^{3+} ESR signals were observed for the commercial anatase TiO_2, it is indicated that more than one type of Ti^{3+} defects were presented in the sample, i.e. surface Ti^{3+} and inner Ti^{3+}. It should be noted that the Ti^{3+} ESR signal was observed only for the anatase TiO_2 (both micron- and nano-sized). The rutile TiO_2 did not exhibit any ESR signal. It is suggested that Ti^{4+} in the rutile TiO_2 is more difficult to be reduced to Ti^{3+}. As rutile titania is more thermodynamically and structurally stable than anatase titania so that the Ti^{3+} ions fixed in the surface lattice of anatase TiO_2 is easier to diffuse to the surface than one in the surface lattice of rutile TiO_2 [24]. The intensity of the Ti^{3+} signal was highest for the solvothermal-derived TiO_2 suggesting that this preparation method produces the highest amount of defects on the TiO_2.

3.2. Characteristics and catalytic properties of Pd/TiO_2 catalysts

The XRD patterns of the various Pd/TiO_2 catalysts are shown in Fig. 4. There were no changes in the crystalline phase of the TiO_2 after impregnation of palladium for all the catalyst samples. The major XRD characteristic peak for PdO at $2\theta = 33.8^\circ$ were

Table 2
Characteristics of the various TiO_2-supported Pd catalysts

Catalyst	BET surface area[a] (m^2/g)	CO pulse chemisorption[b] ($\times 10^{-18}$ molecule CO/g catalyst)	Pd dispersion[c] (%)	d_P[d] Pd^0 (nm)	Atomic concentration[e] (%)	
					Ti/O	Pd/Ti
Pd/TiO_2-com-A	44.5	2.23	3.93	28.5	0.253	0.084
Pd/TiO_2-com-R	17.2	1.55	2.73	41.0	0.240	0.168
TiO_2-sol–gel	33.8	1.19	2.10	53.3	0.282	0.011
Pd/TiO_2-solvothermal	26.0	0.49	0.86	130.2	0.274	0.006

[a] Error of measurement = ±10%.
[b] Error of measurement = ±5%.
[c] Based on the total amount of palladium loaded.
[d] Based on $d = 1.12/D$ (nm), where D = fractional metal dispersion [34].
[e] Determined from XPS analysis.

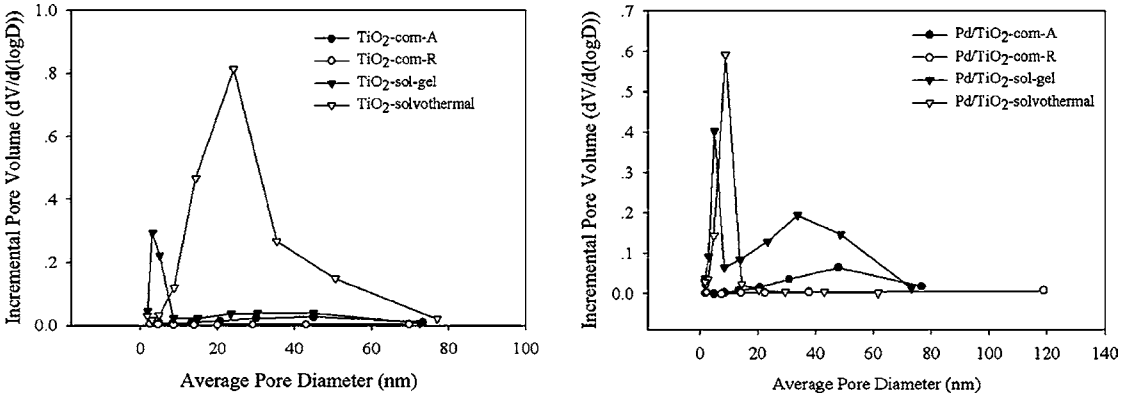

Fig. 5. Pore size distribution results of the various Pd/TiO_2 catalysts.

evident only for the catalyst prepared with the solvothermal-derived TiO_2. The BET surface areas, CO chemisorption results, and atomic concentration of surface element of the Pd/TiO_2 catalyst samples are given in Table 2. The BET surface area of the Pd catalysts were not significantly different form the original TiO_2 supports, however, changes in the pore size distribution of the catalysts due to Pd loading were observed for both sol–gel and solvothermal-derived TiO_2 supported ones suggesting that Pd was deposited in some of the pores of the TiO_2 (Fig. 5). It should also be noted that Pd/TiO_2-com-A was not heat-treated prior to the impregnation step, while the other supports were treated at 1010, 450, and 320 °C. Accordingly, it is also possible that a large decrease in the surface area of the anatase supported catalyst is caused by the calcination of the catalyst at 500 °C after the Pd loading. The percentages of Pd dispersion calculated from the CO chemisorption results were in the order Pd/TiO_2-com-A > Pd/TiO_2-com-R > Pd/TiO_2-sol–gel > Pd/TiO_2-solvothermal. The largest Pd particle size calculated from the CO chemisorption for the Pd/TiO_2-solvothermal catalyst is in a good agreement with the XRD results. It should be noted that as the anatase TiO_2 was transformed to rutile phase TiO_2, the amount of CO chemisorption decreased from 2.23×10^{18} to 1.55×10^{18} molecules CO while the calculated average particle size of Pd^0 metal increased from 28.5 to 41.0 nm. Thus, the presence of rutile phase significantly decreased dispersion of palladium on the titania supports. XPS analysis revealed an increasing Pd/Ti surface concentration from 0.084 to 0.168 when rutile TiO_2 was employed instead of anatase TiO_2. In contrast, the Pd/Ti atomic concentration ratios for those supported on sol–gel and solvothermal derived TiO_2 were much lower than those of the commercial TiO_2 supported ones.

In order to investigate the catalytic performance of the different types of TiO_2 supported Pd catalysts, selective hydrogenation of acetylene in excess ethylene was performed in a fixed bed flow reactor. Fig. 6 shows acetylene conversions and ethylene selectivities obtained from the various Pd/TiO_2 catalysts. Acetylene conversions were in the range of 20–59% and were found to be merely dependent on the Pd dispersion. The selectivities of ethylene were varied from −1.4 to 76.2% with the commercial rutile and the sol–gel derived TiO_2 supported Pd catalysts exhibited the lowest and the highest selectivities, respectively. However, it should be noted that the high ethylene selectivities of the nano-TiO_2 supported Pd catalysts may be because their conversions of acetylene were low. It is thus more appropriate to use the results from Fig. 6 only to compare the selectivities of Pd/TiO_2-com-A and Pd/TiO_2-com-R catalysts. The use of anatase TiO_2 as supports for Pd catalysts resulted in positive values of ethylene selectivity while the use of rutile TiO_2 produced ethylene loss due to over-hydrogenation of ethylene to ethane. Ethylene hydrogenation is usually believed to take place on the support by means of a hydrogen transfer mechanism [32]. Thus, the rutile phase of TiO_2 may be responsible for such reaction. Moreover, the presence of Ti^{3+} ions in anatase TiO_2 supports has a positive effect on high ethylene selectivity, i.e. increasing desorption of ethylene from the catalyst surface. It has been reported that the presence of Ti^{3+} on TiO_2 can lower the temperature to induce a strong metal–support interaction [24]. The SMSI between Pd and TiO_2 support can result in lower adsorption strength of ethylene on the catalyst surface and promotes ethylene desorption [21]. There were no such differences in ethylene selectivities for the micron- and the nano-anatase TiO_2 supported Pd catalysts. This indicates that the crystallite size of TiO_2 support did not have a significant impact on ethylene selectivity; the difference in selectivity of ethylene was due mainly to the presence/absence of Ti^{3+} defective sites on the TiO_2 support. However, in the other studies reported previously by our group [25,33], we have found that there was an optimum amount of Ti^{3+} sites to produce high ethylene selectivity since

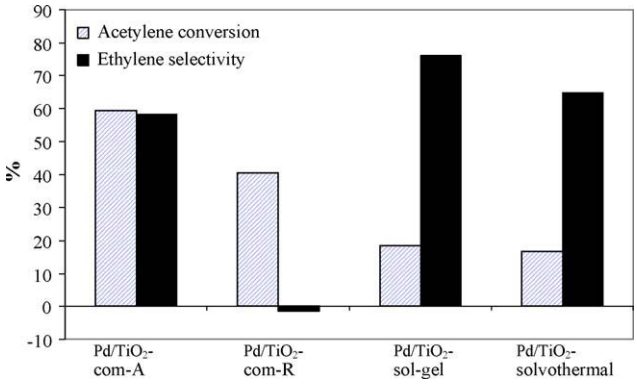

Fig. 6. Catalyst performances in selective acetylene hydrogenation.

only Ti^{3+} species that were in contact with palladium surface promoted SMSI effect and ethylene desorption [24]. Too many Ti^{3+} sites that were not in contact with Pd may result in an over-hydrogenation of ethylene to ethane. This is probably why ethylene selectivity of the Pd/TiO_2-solvothermal is not the highest among four catalysts although the ESR results of Fig. 3 indicated that the intensity of the Ti^{3+} signal was the highest for TiO_2-solvothermal.

4. Conclusions

The use of pure anatase TiO_2 (either micron- or nano-sized) as supports for Pd catalysts produced high ethylene selectivities during selective acetylene hydrogenation in excess ethylene. In contrast, the use of pure rutile TiO_2 supported ones resulted in ethylene loss due to over-hydrogenation of ethylene to ethane. The differences in ethylene selectivity of the various Pd/TiO_2 were due mainly to the presence/absence of the Ti^{3+} defective sites on the TiO_2 support, rather than the difference in the crystallite sizes of the TiO_2 support.

Acknowledgements

Financial supports from the Thailand Research Fund (TRF), Rayong Olefins Co., Ltd., and the Commission on Higher Education are gratefully acknowledged.

References

[1] M.M. Johnson, D.W. Walker, G.P. Nowack, US Patent 4,484,015 (1984).
[2] G.C. Bond, P.B. Wells, J. Catal. 5 (1965) 65.
[3] G.C. Bond, P.B. Wells, Trans. Faraday Soc. 54 (1958) 1537.
[4] M. Larsson, J. Jansson, S. Asplund, J. Catal. 162 (1996) 365.
[5] Y.-J. Huang, C.F. Shun, L.G. Daniel, E.L. Mohundro, J.E. Hartgerink, US Patent 5,332,705 (1994).
[6] K. Flick, C. Herion, H.-M. Allman, US Patent 5,856,262 (1999).
[7] J. Phillips, A. Auroux, G. Bergeret, J. Massardier, A. Renoupez, J. Phys. Chem. 97 (1993) 3565.
[8] D.C. Huang, K.H. Chang, W.F. Pong, P.K. Tseng, K.J. Hung, W.F. Huang, Catal. Lett. 53 (1998) 155.
[9] Q. Zhang, J. Li, X. Liu, Q. Zhu, Appl. Catal. A 197 (2000) 221.
[10] Y. Jin, A.K. Dayte, E. Rightor, R. Gulotty, W. Waterman, M. Smith, M. Holbrook, J. Maj, J. Blackson, J. Catal. 203 (2001) 292.
[11] C. Visser, G.P. Zuidwijk, V. Ponec, J. Catal. 35 (1974) 407.
[12] A. Sarkany, A. Horvath, A. Beck, Appl. Catal. A 229 (2002) 117.
[13] S. LeViness, V. Nair, A. Weiss, J. Mol. Catal. 25 (1984) 131.
[14] E.W. Shin, C.H. Choi, K.S. Chang, Y.H. Na, S.H. Moon, Catal. Today 44 (1998) 137.
[15] Y.H. Park, G.L. Price, Ind. Eng. Chem. Res. 31 (1992) 469.
[16] A. Sarkany, Z. Zsoldos, G. Stefler, W. Hightower, L. Guczi, J. Catal. 157 (1995) 179.
[17] L. Cider, N.-H. Schoon, Ind. Eng. Chem. Res. 30 (1991) 1437.
[18] P. Praserthdam, B. Ngamsom, N. Bogdanchikova, S. Phatanasri, M. Pramotthana, Appl. Catal. A 230 (2002) 41.
[19] B. Ngamsom, N. Bogdanchikova, M.A. Borja, P. Praserthdam, Catal. Commun. 5 (2004) 243.
[20] R.N. Lamb, B. Ngamsom, D.L. Trimm, B. Gong, P.L. Silveston, P. Praserthdam, Appl. Catal. 268 (2004) 43.
[21] J.H. Kang, E.W. Shin, W.J. Kim, J.D. Park, S.H. Moon, J. Catal. 208 (2002) 310.
[22] A. Monzón, E. Romeo, C. Royo, R. Trujillano, F.M. Labajos, V. Rives, Appl. Catal. A 185 (1999) 53.
[23] W.J. Kim, J.H. Kang, I.Y. Ahn, S.H. Moon, J. Catal. 226 (2004) 226.
[24] Y. Li, B. Xu, Y. Fan, N. Feng, A. Qiu, J. Miao, J. He, H. Yang, Y. Chen, J. Mol. Catal. A 216 (2004) 107.
[25] J. Panpranot, L. Nakkararuang, B. Ngamsom, P. Praserthdam, Catal. Lett. 103 (2005) 53.
[26] K. Suriye, P. Praserthdam, B. Jongsomjit, Ind. Eng. Chem. Res. 44 (2005) 6599.
[27] W. Payakgul, O. Mekasuwandumrong, V. Pavarajarn, P. Praserthdam, Ceram. Int. 31 (2005) 391.
[28] F. Zhang, Z. Zheng, D. Liu, Y. Mao, Y. Chen, Z. Zhou, S. Yang, X. Liu, Nucl. Instrum. Meth. B 132 (1997) 620.
[29] J.C. Conesa, P. Malet, G.M. Unuera, J. Sanz, J. Soria, J. Phys. Chem. 88 (1984) 2986.
[30] T.M. Salama, H. Hattori, H. Kita, K. Ebitani, T. Tanaka, J. Chem. Soc. Faraday Trans. 89 (1993) 2067.
[31] Y. Nakaoka, Y. Nosaka, J. Photochem. Photobiol. A 110 (1997) 299.
[32] S. Aplund, J. Catal. 158 (1996) 267.
[33] J. Panpranot, K. Kontapakdee, P. Praserthdam, J. Phys. Chem. B 110 (2006) 8019.
[34] N. Mahata, V. Vishwanathan, J. Catal. 196 (2000) 262.

Catal Lett (2007) 119:346–352
DOI 10.1007/s10562-007-9242-2

Characteristics and Catalytic Properties of Pd/SiO_2 Synthesized by One-step Flame Spray Pyrolysis in Liquid-phase Hydrogenation of 1-Heptyne

Sirima Somboonthanakij · Okorn Mekasuwandumrong · Joongjai Panpranot · Tarit Nimmanwudtipong · Reto Strobel · Sotiris E. Pratsinis · Piyasan Praserthdam

Received: 10 June 2007 / Accepted: 2 August 2007 / Published online: 7 September 2007

Abstract In this study, Pd/SiO_2 catalysts with 0.5–10 wt.% Pd loadings were prepared by one-step flame spray pyrolysis (FSP) and characterized by N_2 physisorption, X-ray diffraction (XRD), transmission electron microscopy (TEM), CO chemisorption, and X-ray photoelectron spectroscopy (XPS). The average cluster/particles size of Pd as revealed by TEM were *ca.* 0.5–3 nm. The turnover frequencies (TOFs) of the flame-made catalysts decreased from 66.2 to 4.3 per s as Pd loading increased from 0.5 to 10 wt.%, suggesting that the catalytic activity was dependent on Pd particle/cluster size. However, there were no appreciable influences on 1-heptene selectivity. The flame-made Pd/SiO_2 showed better properties than the conventional prepared catalysts. Their advantages are not only the presence of large pores that facilitates diffusion of the reactants and products, but also the high-catalytic activity of as-synthesized catalysts so that further pretreatment is not necessary.

S. Somboonthanakij · J. Panpranot (✉) · T. Nimmanwudtipong · P. Praserthdam
Center of Excellence on Catalysis and Catalytic Reaction Engineering, Department of Chemical Engineering, Faculty of Engineering, Chulalongkorn University, Bangkok 10330, Thailand
e-mail: joongjai.p@eng.chula.ac.th

O. Mekasuwandumrong
Department of Chemical Engineering, Faculty of Engineering and Industrial Technology, Silpakorn University, Nakorn Pathom 73000, Thailand

R. Strobel · S. E. Pratsinis
Particle Technology Laboratory, Department of Mechanical and Process Engineering, ETH Zentrum, Swiss Federal Institute of Technology, CH-8092 Zurich, Switzerland

Keywords Flame spray pyrolysis · Pd/SiO_2 · Liquid phase hydrogenation · 1-Heptyne hydrogenation · Pd nanoparticle

1 Introduction

The selective hydrogenation of alkynes to alkenes is an important reaction in the synthesis of biologically active compounds such as insect sex pheromones (pest control) and vitamins [1]. Palladium (Pd) is the most selective of the noble metal catalysts for alkyne semihydrogenation with respect to over all alkene formation [2]. The classic Lindlar catalyst, consisting of metallic Pd on calcium carbonate support modified with lead(II) acetate, is the well known commercially available catalyst for such reaction. As reported by several authors, high activity and selectivity may be obtained over other catalyst systems in which modifiers are not necessary such as supported Pd complexes [3–5], bimetallic $Pd–Cu/SiO_2$ [6], Pd/montmorillonite [7], Pd/pumice [8], Pd/MCM-41 [9], Pd/activated carbon, and Pd/Al_2O_3 [10]. The advantages of the reaction in heterogeneous conditions are easy separation from the reaction media and possibility of continuous operation [11]. These catalyst systems, however, may require several steps during preparation such as calcination and high-temperature reduction pretreatment in order to obtain high-catalytically active components.

Flame synthesis, especially flame spray pyrolysis (FSP), is a relatively new process for one-step synthesis of supported metal catalysts. It is generally known as a method for making nanoparticles such as fume silica, titania, and carbon black in large quantity at low cost [12]. Supported metal catalysts synthesized via one-step FSP have been employed in various catalytic reactions

and they often showed improved catalytic performances [13–18]. Their differences in catalytic behaviors were suggested to be due to the structural differences of the flame-made and the conventionally prepared catalysts.

In this work, Pd/SiO_2 catalysts with 0.5–10 wt.% Pd loadings were prepared in one-step by FSP. The catalysts were characterized by N_2 physisorption, X-ray diffraction (XRD), CO pulse chemisorption, transmission electron spectroscopy (TEM), and X-ray photoelectron spectroscopy (XPS). The catalytic behaviors of the flame-made Pd/SiO_2 were evaluated in the liquid-phase selective hydrogenation of 1-heptyne under mild conditions.

2 Experimental

2.1 Catalyst Preparation

Synthesis of Pd/SiO_2 was carried out using a flame spray reactor similar to that of Ref. [19]. Palladium actetylacetonate and tetraethylorthosilicate (TEOS) from Aldrich, Tanfkirchen, Germany, were used as palladium and silicon precursors, respectively. Precursors were prepared by dissolving in xylene (MERCK, Hohenbrumn, Germany; 99.8 vol.%)/acetonitrile (Fluka, Steinheim, Germany; 99.5 vol.%) mixtures (70/30 vol.%) with total metal concentration maintained at 0.5 M. The palladium concentration was ranged between 0.5 and 10 wt.%. Using a syringe pump, 5 ml/min of precursor solution was dispersed into fine droplets by a gas-assist nozzle fed by 5 l/min of oxygen (Thai Industrial Gas Limited, Bangkok, Thailand; purity >99%). The pressure drop at the capillary tip was maintained at 1.5 bar by adjusting the orifice gap area at the nozzle. The spray was ignited by supporting flamelets fed with oxygen (3 l/min) and methane (1.5 l/min) which are positioned in a ring around the nozzle outlet. A sintered metal plate ring (8 mm wide, starting at a radius of 8 mm) provided additional 10 l/min of oxygen as sheath for the supporting flame. The product particles were collected on a glass fiber filter (Whatman GF/C, Kent, UK, 15 cm in diameter) with the aid of a vacuum pump.

For comparison purposes, 1 wt.% Pd on a commercial SiO_2 (Strem Chemicals, Newburyport, MA, USA, *specific surface area* 243.8 m^2/g V_{Pore} 1.06 m^3/g d_{Pore} 17.4 nm) was prepared by incipient wetness impregnation using $Pd(NH_3)_4Cl_2$ (Aldrich) as palladium precursor. The catalyst was dried in oven at 100 °C and calcined in air at 450 °C for 3 h. Prior to reaction, the catalyst was reduced ex situ in H_2 flow at room temperature for 2 h. Properties of the reference catalyst can be found in Ref. [20].

2.2 Catalyst Characterization

X-ray diffraction patterns were recorded with a Siemens D5000 using nickel filtered CuK_α radiation. The crystallite size (d_{XRD}) was determined using the Scherrer equation and α-alumina as the external standard. The Brunauer Emmett Teller (BET) surface area, average pore size diameters, and pore size distribution are determined by physisorption of nitrogen (N_2) using a Micromeritics ASAP 2020 automated system. The average palladium cluster/particle size and distribution of palladium on silica was observed using a JEOL-JEM 200CX transmission electron microscope operated at 100 kV. The active sites and relative percentages dispersion of palladium catalyst were determined by CO-pulse chemisorption technique using a Micromeritics ChemiSorb 2750 system attached with ChemiSoft TPx software at room temperature. XPS analysis was performed using an AMICUS photoelectron spectrometer equipped with a Mg K_α X-ray as a primary excitation and a KRATOS VISION2 software. XPS elemental spectra were acquired with 0.1 eV energy step at a pass energy of 75 kV. The C 1 s line was taken as an internal standard at 285.0 eV.

2.3 Catalytic Evaluation

The selective hydrogenation of 1-heptyne (Aldrich) was carried out in magnetically stirred 50-ml stainless steel autoclave reactor (JASCO, Tokyo, Japan). Approximately 20 mg of Pd/SiO_2 catalyst was dispersed in a 10 ml of 2% (v/v) solution of 1-heptyne (Fluka) in toluene. The reaction was carried out under ultra high-purity hydrogen atmosphere at 1 bar and 30 °C for 5 min. The liquid reactants and products were analyzed by gas chromatography equipped with an FID detector (Shimadzu GC-14A, Kyoto, Japan) and a GS-alumina (length = 30 m, I.D. = 0.53 mm) packed column.

3 Results and Discussion

3.1 Catalyst Properties

Figure 1 shows the XRD patterns of the flame-made SiO_2 and Pd/SiO_2 catalysts with Pd loadings 0.5–10 wt.%. All the catalyst samples exhibited only the characteristic peaks of amorphous silica except that of 10 wt.% Pd/SiO_2 where additional peaks corresponding to Pd^0 metal were apparent (major peak at 40.1° 2θ). It is suggested that very fine palladium metal clusters/particles were finely dispersed in the silica matrix for the catalysts with low-Pd loadings. Unlike typical supported metal catalysts prepared by wet

impregnation that calcination and reduction steps are required in order to obtain catalytically active metal surface, the flame-made supported metal catalysts can be used as synthesized and calcination/reduction step is not necessary since the metal is available in its reduced form as synthesized [14–16]. Figure 2a shows typical TEM micrographs of the flame-made Pd/SiO_2 catalysts with different Pd contents. The Pd clusters were found to be in spherical shape with average diameters *ca.* 0.5–3 nm with narrow size distribution confined to the surface of SiO_2 particles. The TEM images were quite similar to those of Pd/Al_2O_3 catalysts prepared via flame process reported by Strobel et al. [16]. However, it is surprising that for Pt/SiO_2 prepared by FSP under similar conditions using platinum acetylacetonate as Pt precursor, some very large Pt particles (>100 nm) were obtained due to incomplete evaporation [15]. This was not the case for the flame-derived Pd/SiO_2 in which only small Pd particles were observed. The average clusters sizes of palladium increased from 0.5 to 3 nm as Pd loading increased from 0.5 to 2 wt.% and remained at *ca.* 3 nm even after increasing of Pd loading to 10 wt.%.

Table 1 summarizes some physicochemical properties of the SiO_2, the flame-made Pd/SiO_2 catalysts, and the 1%Pd on commercial SiO_2. The BET surface area of the flame-made SiO_2 was 196 m^2/g whereas those of the flame-made Pd/SiO_2 catalysts were in the range of 246–306 m^2/g. The BET surface areas of the flame-made catalysts increased as Pd contents increased from 0.5 to 5 wt.% and were slightly decreased when Pd loading was increased from 5 to 10 wt.% (from 306 to 299 m^2/g). An increase in BET surface areas of the flame-made catalysts compared to the SiO_2 support was due probably to inhibition of the growth of the SiO_2 particles by Pd dopant. Such result is similar to the works reported by Hannemann et al. [21] for $Au–Ag/SiO_2$ nanoparticles prepared by FSP

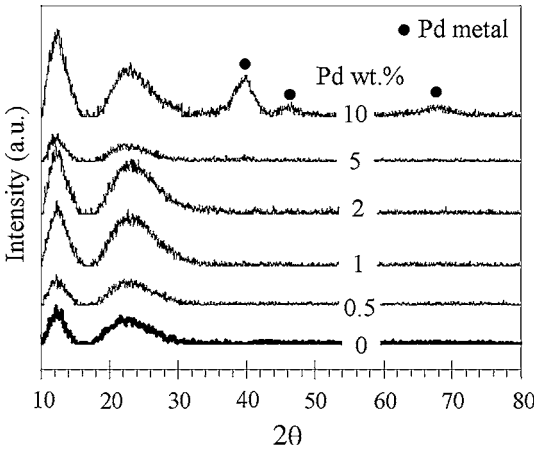

Fig. 1 XRD patterns of the flame-made Pd/SiO_2 catalysts (as synthesized)

that adding metal particles resulted in an increase in BET surface area of the SiO_2 support. Pore volumes of the flame-made catalysts also increased with increasing Pd loading and were determined to be 0.43–0.69 cm^3/g. The pore size distribution patterns of the flame-made samples as calculated by BJH desorption equation suggest the presence of mostly meso- and macro-pores (Fig. 3). The average pore diameters were unaltered for the flame-made Pd/SiO_2 catalysts with Pd loading between 0.5 and 5 wt.% while that of the 10%Pd/SiO_2 increased slightly. The presence of large pores in the flame-made catalysts can help facilitating diffusion of both reactants and products. It has been reported that diffusion limitation of reactants occurred when much smaller pore sizes of the supports were used (average pore size <10 nm) for Pd catalysts in liquid phase hydrogenation [22, 23]. These pores were larger than that of the commercial SiO_2 used in this study.

Typically, BET surface areas of supported metal catalysts are less than that of the original support due to pore blockages of metal particles during impregnation and/or calcination step. Structural difference of the flame-made catalysts suggests different mechanism for the formation of metal/metal oxide particles. Formation of Pd/SiO_2 nanoparticles by FSP was considered as follows: the sprayed droplets of precursor solution were evaporated and combusted as soon as they met the flame at very high temperature and released the metal atoms, then nucleation and growth of particles by coagulation and condensation occurred along the axial direction of the flame. Comparing to silica, the vapor pressure of Pd/PdO was higher in the hot flame environment, and consequently SiO_2 particle formation started earlier. Further downstream of the flame at lower temperatures, Pd/PdO started to form small particles which were deposited directly on the SiO_2. Similar particle formation mechanism has been suggested for Pd/Al_2O_3 and Pt/TiO_2 [16–24].

On the other hand, the 1%Pd/SiO_2-com exhibited XRD characteristic peaks of PdO at 2θ degree = 33.8, and less so at 42.0, 54.8, 60.7, and 71.4 (results not shown). The average PdO crystallite sizes calculated from the full width at half maximum of the XRD peak at $2\theta = 33.8°$ using Scherrer equation was 11.4 nm. The relative amounts of active surface Pd metal on the as-synthesized FSP-catalyst samples were calculated from CO chemisorption experiments at room temperature and are given in Table 1. It has been confirmed by CO chemisorption experiments that these FSP-derived Pd/SiO_2 catalysts with or without H_2 reduction adsorbed similar amounts of CO. Thus, it is likely that palladium were deposited on the as-synthesized Pd/SiO_2 catalysts as Pd^0 metal. The Pd active sites were then calculated based on the assumption that one carbon monoxide molecule adsorbs on one palladium site [25, 26]. The Pd active sites were found to increase from

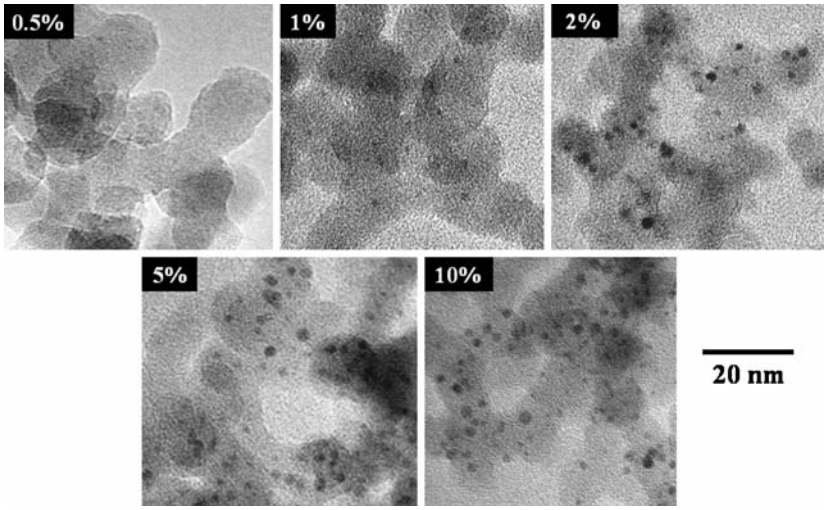

Fig. 2 TEM micrographs of (**a**) the as-synthesized and (**b**) the spent flame-made Pd/SiO_2 catalysts (after reaction)

0.97×10^{18} to 25.84×10^{18} sites/g catalyst as the Pd contents increased from 0.5 to 10 wt.% and corresponding to increasing of %Pd metal dispersion from 3.4 to 4.6%. The average Pd^0 metal particle sizes calculated from CO chemisorption were found to be in the range of 24–39 nm which were much larger than those based on XRD and TEM analyses. In general, low-metal dispersion and overestimation of metal particle sizes in supported metal catalysts based on CO chemisorption have possibly been due to (a) partial blockage of CO adsorption as a result of pore blockage by agglomeration of metal particles [27] and (b) localized destruction of the pore structure forming cracks and holes where larger metal particles could form and chemisorption would also be restricted [28], or (c) chemisorption suppression due to strong support-metal interactions [29]. In this case, low-CO chemisorption uptake of the catalysts with relatively low-metal loadings may be due to the formation of Si–O groups covering the small Pd metal clusters/particles resulting in an inhibition of CO chemisorption. Otherwise, an alloy of Pd and Si may be formed resulted in a strong interaction between Pd and SiO_2. Chemisorption suppression may relate to a decrease in the kinetics of chemisorption as a result of it becoming highly activated, therefore, resulting in poor uptake at a given temperature.

X-ray photoelectron spectroscopy is a powerful tool for determination of the surface compositions of the catalysts and the interaction between Pd and silica supports. The

Table 1 Physicochemical properties of flame-made SiO_2 and Pd/SiO_2 catalysts

Catalyst	BET surface areas[a] (m^2/g)	Pore volume[a] (cm^3/g)	CO chemisorption results[b]			XPS results Pd $3d_{5/2}$		Atomic ratio[e] (Pd/Si)
			CO uptake ($\times 10^{-18}$ molecule CO/g cat.)	%Pd dispersion[c]	$d_P Pd^{0,d}$ (nm)	B.E. (eV)	FWHM	
SiO_2	196	0.48	n/a[f]	n/a	n/a	n/a	n/a	n/a
0.5%Pd/SiO_2	246	0.43	1.0	3.42	33	n/a	n/a	0.0011
0.5%Pd/SiO_2_R[g]	–	–	1.1	3.53	32	–	–	–
1%Pd/SiO_2	251	0.46	1.9	3.40	33	n/a	n/a	0.0014
2%Pd/SiO_2	260	0.49	3.3	2.88	39	n/a	n/a	0.0018
5%Pd/SiO_2	306	0.59	13.4	4.71	24	337.4	2.389	0.0139
10%Pd/SiO_2	299	0.69	25.8	4.55	25	337.4	3.189	0.0404
1%Pd/SiO_2-com	234	1.02	3.3	5.81	19	–	–	0.0033

[a] Error of measurement was ± 10%

[b] Error of measurement was ± 5% as determined directly

[c] Based on the total palladium loaded and an assumption of CO/Pd = 1

[d] Based on d = (1.12/D) nm [25], where D = fractional metal dispersion

[e] Based on XPS results

[f] n/a = not available

[g] R = after reduced for 2 h in H_2 at room temperature

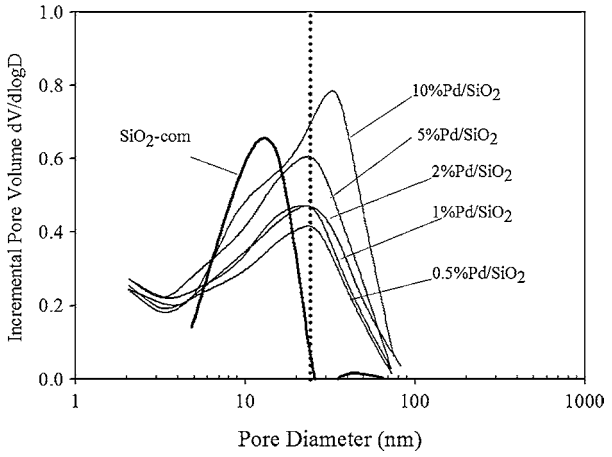

Fig. 3 Pore size distribution of the flame-made Pd/SiO_2 catalysts with 0.5–10 wt.% Pd loading

elemental scans for Pd $3d_{5/2}$ of the various flame-made Pd/SiO_2 catalysts are shown in Fig. 4. No distinctive peaks for Pd $3d_{5/2}$ were observed for the flame-made Pd/SiO_2 with Pd loading between 0.5 and 2 wt.% suggesting that very low amount of Pd present on the catalyst surface. The binding energies of Pd $3d_{5/2}$ for the 5 and 10 wt.% Pd/SiO_2 were 337.4 eV which was 0.2 eV higher than Pd $3d_{5/2}$ on the classic Lindlar catalysts according to the literature [2]. It was also 2.3 eV higher than that corresponding to Pd^0 (335.1 eV) [30], which indicating that Pd in the flame-made Pd/SiO_2 catalyst is electron-deficient. The FWHM values, higher than 2.0 eV, are also indicative that more than one Pd species may be present in the flame-made Pd/SiO_2 as have been suggested for Pd/Al_2O_3 and Pd/C catalysts prepared by conventional impregnation technique [31]. The percentages of atomic concentration for Si 2p, O 1 s, and Pd 3d are also given in Table 1. For the catalysts with Pd loading 0.5–2 wt.%, much lower Pd/Si ratios were observed compared to those with higher Pd loadings (5–10 wt.%). Such results are in good agreement with the CO chemisorption results that for the catalysts with relative low-metal loadings, the metal surface may be covered by Si–O groups due to simultaneous crystallization of Pd and SiO_2 in gas-phase during FSP. It is also possible that some of the Pd metal surfaces were partially oxidized, while the kernel of the Pd particles is metallic. This would also explain the broad and not very intense XPS lines.

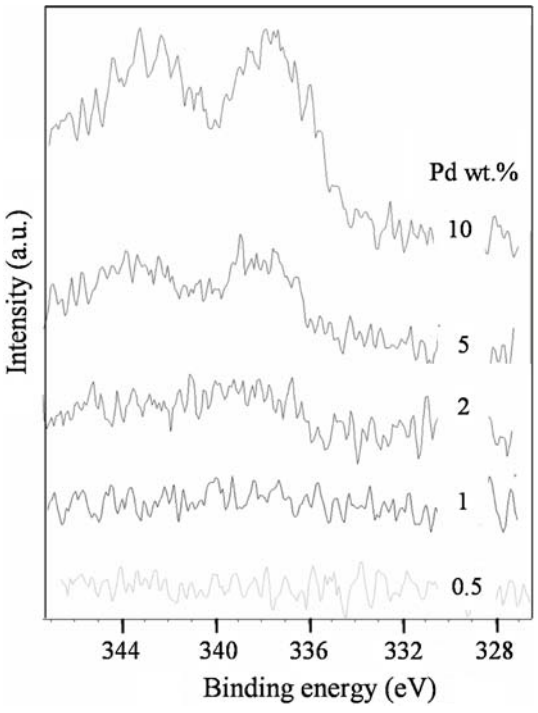

Fig. 4 XPS results for Pd $3d_{5/2}$ of the flame-made Pd/SiO_2 catalysts

3.2 Selective Hydrogenation of 1-Heptyne

The catalytic behavior of the flame-made Pd/SiO_2 catalysts was investigated in the liquid-phase selective hydrogenation of 1-heptyne in a batch system. High-stirring rate (1,000 rpm) was used in order to ensure that the reaction rate does not depend on the external mass transfer of hydrogen. However, it should be noted that external mass transfer control may still exist if the relative velocity between fluid and particles is close to zero. As mentioned earlier, the average pore sizes of all the flame-made Pd/SiO_2 catalysts were much larger than those reported in the literature in which diffusion limitation of reactants occurred (usually average pore size of the supports <10 nm), therefore, the effect of pore size on the reaction rate could be negligible in this study. The catalytic performance in terms of 1-heptyne conversions and selectivities to 1-heptene and the turnover frequencies (TOFs) calculated based on CO chemisorption results of the flame-made Pd/SiO_2 catalysts are given in Table 2. The conversion of 1-heptyne increased from 42 to 75% as Pd loading increased from 0.5 to 5 wt.% and remained relatively constant when Pd loading was increased to 10 wt.%. The selectivities for 1-heptene were in the range of 92–95% for all the Pd/SiO_2 catalysts. Based on the conditions and the column used in our GC analysis, the other product found in the reaction besides 1-heptene is *n*-heptane. No other by-products were observed. For similar Pd loading, the catalytic activity of the flame-made catalyst was considerably higher than that of Pd/SiO_2 catalyst prepared by incipient wetness impregnation on a commercial SiO_2 support. The results of this study follow the trend in the literature that alkyne hydrogenation activity of Pd catalyst depends largely on Pd dispersion and there is no appreciable influence on

Table 2 Catalytic properties for liquid-phase 1-heptyne selective hydrogenation

Catalyst	Conversion (%)	1-Heptene selective (%)	TOF[a] (s^{-1})
0.5%Pd/SiO_2	42	93	66.2
1%Pd/SiO_2	43	92	34.1
	100[b]	62[b]	–
2%Pd/SiO_2	54	94	25.3
5%Pd/SiO_2	75	95	8.6
10%Pd/SiO_2	73	94	4.3
1%Pd/SiO_2-com	20	100	7.7
	100[b]	13[b]	–

Reaction conditions were 105 kPa, 30 °C, 5 min, and catalyst/substrate molar ratio = 1/1,600

[a] TOF = mole product/mole Pd metal/s. Based on the amount of active Pd atoms measured by CO chemisorption

[b] Reaction conditions were 105 kPa, 30 °C, 40 min, and catalyst/substrate molar ratio = 1/500

alkene selectivity [32, 33]. In general, 1-heptene selectivity decreases with increasing 1-heptyne conversion. Under similar reaction conditions, the flame-derived catalysts exhibited higher 1-heptyne conversion than the impregnated ones and slightly lower 1-heptene selectivity. However, at 100% conversion of 1-heptyne, the selectivities for 1-heptene for the flame-made and the impregnated catalysts were 62 and 13%, respectively. The specific activities of the flame-made catalysts are also expressed in terms of TOF which is defined as mole of product/mole of metal/time. As the palladium loading increased from 0.5 to 10 wt.%, the TOFs of the flame-made catalysts decreased from 66.2 to 4.3 per s. Much higher TOFs values for the catalysts with relatively low-metal loadings (≤2 wt.%) are another evidence that CO chemisorption suppression occurred on these catalysts. It was probably due to the formation of very fine palladium metal clusters/particles or an alloy of Pd and Si which resulted in a strong interaction between Pd and SiO_2. Moreover, formation of Si–O groups at the metal surface due to homogeneous crystallization of Pd^0 and SiO_2 in gas phase during flame spray synthesis or partially oxidized Pd at the surface could also result in the inhibition of CO chemisorption. For the 10 wt.% Pd/SiO_2, there was probably no CO chemisorption suppression since most of the Pd was in metallic state as indicated by XRD so the TOFs still decreased from 2 to 10 wt.% Pd loadings in spite of similar particle size of these catalysts. The remarkable high-catalytic hydrogenation activities (TOFs) of Pd nanoparticles, however, have also been reported for other Pd/SiO_2 systems [34–36]. The durability of the catalysts under repeated catalytic cycles was tested on both the flame-made 1%Pd/SiO_2 and 1%Pd/SiO_2-com catalysts. After different numbers of reaction cycles (0, 1, 2, or 3), the used catalyst was filtered out and dried at room temperature before being re-used in the reaction. It was found that the catalytic activity decreased by *ca.* 50 and 30% after the third cycle of run, respectively. Such results suggest that catalyst deactivation is still a problem in the liquid-phase reaction.

4 Conclusions

Flame spray pyrolysis is an effective method for one-step synthesis of Pd nanoparticles with average size of 0.5–3 nm on SiO_2 supports. The as-synthesized FSP-derived catalysts showed higher catalytic activities for selective hydrogenation of 1-heptyne under mild conditions than the conventional prepared Pd/SiO_2 catalyst. The TOFs of the flame-made Pd/SiO_2 decreased with increasing Pd particle/cluster size suggesting that alkyne hydrogenation activity depends on Pd dispersion. However, there is no appreciable influence on alkene selectivity.

Acknowledgments The authors would like to thank the financial supports from the Graduate School of Chulalongkorn University (the 90th Anniversary of Chulalongkorn University-the Golden Jubilee Fund), the Thailand Research Fund (TRF), the National Science and Technology Development Agency (NSTDA), and the Research and Development Institute of Silpakorn University.

References

1. Bailey S, King F (2000) In: Sheldon RA, van Bekkum H (eds) Fine chemicals through heterogeneous catalysis, Chap. 8. Wiley-VCH, Germany
2. Marin-Astorga N, Alvez-Manoli G, Reyes P (2005) J Mol Catal A 226:81
3. L'Argentiere PC, Cagnola EA, Quiroga ME, Liprandi DA (2002) Appl Catal A 226:253
4. Cagnola E, Liprandi D, Quiroga M, L'Argentiere P (2003) React Kinet Catal Lett 80:277
5. L'Argentiere PC, Quiroga ME, Liprandi DA, Cagnola EA, Roman-Martinez MC, Diaz-Aunon JA, Salinas-Martinez de Lecea C (2003) Catal Lett 87:97
6. Nijhuis TA, van Koten G, Moulijn JA (2003) Appl Catal A 238:259
7. Mastalir A, Kiraly Z, Szollosi G, Bartok M (2000) J Catal 194:146
8. Gruttadauria M, Liotta LF, Noto R, Deganello G (2001) Tetrahedron Lett 42:2015
9. Marin-Astorga N, Pecchi G, Fierro JLG, Reyes P (2003) Catal Lett 91:115
10. Lederhos CR, L'Argentiere PC, Figoli NS (2005) Ind Eng Chem Res 44:1752
11. Lennon D, Marshall R, Webb R, Jackson SD (2000) Stud Surf Sci Catal 130:245
12. Stark WJ, Pratsinis SE (2002) Powder Technol 126:103
13. Piacentini M, Strobel R, Maciejewski M, Pratsinis SE, Baiker A (2006) J Catal 243:43
14. Strobel R, Krumeich F, Pratsinis SE, Baiker A (2006) J Catal 243:229

15. Height MJ, Pratsinis SE, Mekasuwandunrong O, Praserthdam P (2006) Appl Catal B 63:305
16. Strobel R, Stark WJ, Madler L, Pratsinis SE, Baiker A (2003) J Catal 213:296
17. Strobel R, Krumeich F, Stark WJ, Pratsinis SE, Baiker A (2004) J Catal 222:307
18. Hannemann S, Grunwaldt J-D, Lienemann P, Gunther D, Krumeich F, Pratsinis SE, Baiker A (2007) Appl Catal A 316:226
19. Mädler L, Stark WJ, Pratsinis SE (2002) J Mater Res 17:1356
20. Panpranot J, Phandinthong K, Sirikajorn T, Arai M, Praserthdam P (2007) J Mol Catal A 261:29
21. Hannemann S, Grunwaldt J, Krumeich F, Kappen P, Baiker A (2006) Appl Surf Sci 52:7862
22. Sato S, Takahashi R, Sodesawa T, Koubata M (2005) Appl Catal A 284:247
23. Mastalir A, Rac B, Kiraly Z, Molnar A (2007) J Mol Catal A 264:170
24. Teoh WY, Mädler L, Beydoun D, Pratsinis SE, Amal R (2005) Chem Eng Sci 60:5852
25. Mahata N, Vishwanathan V (2000) J Catal 196:262
26. Ali SH, Goodwin JG Jr (1998) J Catal 176:3
27. Verdonck JJ, Jacobs PA, Genet M, Poncelet G (1980) J Chem Soc Faraday Trans 76:403
28. Gustafson BL, Lunsford JH (1982) J Catal 74:393
29. Tauster S J, Fung SC, Garten RL (1978) J Am Chem Soc 100:170
30. Wagner CD, Riggs WM, Davis LE, Moulder JF (1978) In: Muilenberg GE (ed) Handbook of X-ray photoelectron spectroscopy. Perkin-Elmer Corporation, Eden Prairie, MN
31. Lederhos RC, L'Argentiere PC, Fıgoli NS (2005) Ind Eng Chem Res 44:1752
32. Papp A, Molnar A, Mastalir A (2005) Appl Catal A 289:256
33. Mastalir A, Kiraly Z (2003) J Catal 220:372
34. Dominguez-Quintero O, Martinez S, Henriquez Y, D'Ornelas L, Krentzien H, Osuna J (2003) J Mol Catal A 197:185
35. Mu X, Bartmann U, Guraya M, Busser GW, Weckenmann U, Fischer R, Muhler M (2003) Appl Catal 248:85
36. Kim N, Kwon MS, Park CM, Park J (2004) Tetrahedron Lett 45:7057

Available online at www.sciencedirect.com
ScienceDirect
Catalysis Today 131 (2008) 553–558
CATALYSIS TODAY
www.elsevier.com/locate/cattod

Performance of Pd catalysts supported on nanocrystalline α-Al_2O_3 and Ni-modified α-Al_2O_3 in selective hydrogenation of acetylene

Nitikon Wongwaranon [a], Okorn Mekasuwandumrong [b], Piyasan Praserthdam [a], Joongjai Panpranot [a,*]

[a] Center of Excellence on Catalysis and Catalytic Reaction Engineering, Department of Chemical Engineering, Faculty of Engineering, Chulalongkorn University, Bangkok 10330, Thailand
[b] Department of Chemical Engineering, Faculty of Engineering and Industrial Technology, Silpakorn University, Nakhonpathom, Thailand

Available online 26 November 2007

Abstract

Nanocrystalline α-Al_2O_3 and Ni-modified α-Al_2O_3 have been prepared by sol–gel and solvothermal methods and employed as supports for Pd catalysts. Regardless of the preparation method used, $NiAl_2O_4$ spinel was formed on the Ni-modified α-Al_2O_3 after calcination at 1150 °C. However, an addition of NiO peaks was also observed by X-ray diffraction for the solvothermal-made Ni-modified α-Al_2O_3 powder. Catalytic performances of the Pd catalysts supported on these nanocrystalline α-Al_2O_3 and Ni-modified α-Al_2O_3 in selective hydrogenation of acetylene were found to be superior to those of the commercial α-Al_2O_3 supported one. Ethylene selectivities were improved in the order: Pd/Ni-modified α-Al_2O_3–sol–gel > Pd/Ni-modified α-Al_2O_3-solvothermal ≈ Pd/α-Al_2O_3–sol–gel > Pd/α-Al_2O_3-solvothermal ≫ Pd/α-Al_2O_3-commerical. As revealed by NH_3 temperature program desorption studies, incorporation of Ni atoms in α-Al_2O_3 resulted in a significant decrease of acid sites on the alumina supports. Moreover, XPS revealed a shift of Pd 3d binding energy for Pd catalyst supported on Ni-modified α-Al_2O_3–sol–gel where only $NiAl_2O_4$ was formed, suggesting that the electronic properties of Pd may be modified.

Keywords: Nanocrystalline α-Al_2O_3; Ni-modified α-Al_2O_3; Solvothermal; Sol–gel; Selective acetylene hydrogenation; Nickel aluminate

1. Introduction

The selective hydrogenation of acetylene in ethylene rich stream is a crucial process in polyethylene production since acetylene poisons the polymerization catalysts [1,2]. Pd-based catalyst supported on alumina with low Pd loading (0.1–0.3 wt.%) is typically employed for this reaction due to its good activity and selectivity and the easily desorption of ethylene on the catalyst surface. With respect to selectivity changes, catalysts of low Pd dispersion have been suggested to give better selectivity towards ethylene at high acetylene conversions [3–5]. The alumina used as Pd catalyst support in this reaction contains mostly the alpha phase alumina since it possesses relatively low specific surface area and low acidity compared to other 'transition' alumina. Recent reports have shown development of new efficient catalysts for the selective hydrogenation of acetylene including the glow discharge plasma-prepared Pd/α-Al_2O_3 [6], Pd on nano-sized TiO_2 [7,8], and zeolite-supported Pd-Ag catalysts [9].

In recent years, nanocrystalline materials have gained considerable interest in the field of catalysis because they show significant differences in terms of catalytic activity and selectivity compared with those synthesized in micron scale. For examples, Co catalysts supported on nanocrystalline Al_2O_3 [10] and ZrO_2 [11] have been found to exhibit higher hydrogenation activities and selectivities toward long chain hydrocarbons than those of the commercial micron-sized Al_2O_3 and ZrO_2 supported ones. Physical and chemical properties of TiO_2 are modified when they are synthesized in the nanometer range resulting in an improvement of its photocatalytic activity [12].

Several techniques have been reported for preparation of nanocrystalline 'transition' alumina such as sol–gel method [13], hydrothermal synthesis [14], microwave synthesis [15], emulsion evaporation [16,17], precipitation from solution [18],

* Corresponding author. Tel.: +66 2 2186869; fax: +66 2 2186877.
E-mail address: joongjai.p@eng.chula.ac.th (J. Panpranot).

0920-5861/$ – see front matter © 2007 Elsevier B.V. All rights reserved.
doi:10.1016/j.cattod.2007.10.036

and solvothermal synthesis [19,20]. The sol–gel method is widely used due to its simplicity, however, the precipitated powders obtained are amorphous in nature and further heat treatment is required for crystallization. Solvothermal method is an alternative route for one-step synthesis of nanocrystalline material. Desired shape and size of particles can be produced by controlling process conditions such as solute concentration, reaction temperature, reaction time, and the type of solvent [21].

In the present study, nanocrystalline α-Al_2O_3 and Ni-modified α-Al_2O_3 have been synthesized via sol–gel and solvothermal methods and employed as supports for Pd catalysts for selective hydrogenation of acetylene. Modification of nanocrystalline α-Al_2O_3 with nickel is also interesting because it can form nickel aluminate spinel ($NiAl_2O_4$) which is a highly stable material that can have beneficial effect on the catalyst performance. Moreover, formation of $NiAl_2O_4$ in some Ni-based hydrogenation catalysts has shown high resistance to coke formation [22–24].

2. Experimental

2.1. Preparation of Nanocrystalline α-Al_2O_3 and Ni-modified α-Al_2O_3

Nanocrystalline α-Al_2O_3 and Ni-modified α-Al_2O_3 were prepared by sol–gel and solvothermal methods. For the sol–gel method, 24 g of aluminium nitrate nonahydrate (Aldrich) was dissolved in 50 cc of ethanol. The experiment was conducted in the reflux-condenser reactor at the temperature about 70–80 °C for 18 h. Then, urea solution, which consist of 60 g of urea and 50 ml of distilled water, was added to adjust pH of sol. The mixture was rested at the same temperature for 24 h to be gelled at neutral condition. The obtained product was calcined with 2 steps heating rate to avoid overflowing of gel during calcinations, i.e. 3 °C/min from room temperature to 500 °C and continue heating at 5 °C/min to 1150 °C. Then, temperature was hold for 3 h. For the preparation of Ni-modified α-Al_2O_3, a desired amount of nickel nitrate-6-hydrate (Aldrich) was added to the precursor mixture and then followed the same procedures as that of α-Al_2O_3.

For the solvothermal method, α-Al_2O_3 and Ni-modified α-Al_2O_3 were prepared using a mixture of aluminum isopropoxide 15.0 g and appropriate amount of nickel(II) acetylacetonate. The starting materials were suspended in 100 mL of toluene in beaker, and then set up in autoclave. In the gap between the beaker and autoclave wall, 40 mL of toluene was added. After the autoclave was completely, the suspension was heated to 300 °C at the rate of 2.5 °C/min and held at that temperature for 2 h. However, the same synthesis method is performed at various holding temperature. Autogenous pressure during the reaction gradually increased as temperature was raised. Then the autoclave was cooled to room temperature. After the autoclave was cooled, the resulting products were washed repeatedly with methanol by centrifugation and dried in air. The calcination of the obtained product carried out in a furnace. The product was heated at a rate of 10 °C/min to a desired temperature 1150 °C and held at that temperature for 1 h. For comparison purposes, a commercial α-Al_2O_3 (JRC-ALO2) was also employed as Pd catalyst support.

2.2. Preparation of α-Al_2O_3 supported Pd catalysts

The Pd/α-Al_2O_3 catalysts were prepared by incipient wetness impregnation of Al_2O_3 support with a desired amount of an aqueous solution of palladium(II) nitrate hydrate (Aldrich). The catalysts were dried overnight at 110 °C and then calcined in N_2 flow 60 cm^3/min with a heating rate of 10 °C/min until the temperature reached 500 °C and then in air flow 100 cm^3/min at 500 °C for 2 h. The final Pd loading of the catalysts was determined by atomic absorption spectroscopy (Varian Spectra A800) to be ca. 0.3 wt.%.

2.3. Catalyst Characterization

Surface area measurements were carried out by nitrogen adsorption in a Micromeritic Chemisorb 2750 system. Each sample was degassed at 200 °C for 2 h. The analysis gas consisting of 30% N_2 in helium was adsorbed on the samples at low temperature by dipping cell into liquid nitrogen dewar. X-ray diffraction patterns of the catalyst samples were obtained with a SIEMENS D5000 X-ray diffractometer using Cu Kα radiation with a Ni filter. The pattern were recorded between 20° and 80° (2θ) using a scanning velocity of 0.02°/s. Metal active sites were measured using CO chemisorption technique at room temperature in a Micromeritic Chemisorb 2750 automated system attached with ChemiSoft TPx software. Before chemisorption measurement, the sample was reduced in a H_2 flow at 150 °C for 2 h then cooled down to ambient temperature in a He flow. Ammonia temperature program desorption (NH_3-TPD) was also performed in a Micromeritic Chemisorb 2750 automated system attached with ChemiSoft TPx software. Approximately 100 mg of catalyst was placed in a quartz tube in a temperature-controlled oven. The samples adsorbed ammonia at 40 °C, then heated up to 650 °C at a heating rate of 10 °C/min. The distribution of palladium on catalyst supports were observed using AJEM-200CX transmission electron microscope operated at 160 kV. Surface compositions of the catalysts were analyzed using an AMICUS photoelectron spectrometer equipped with Mg Kα X-ray as primary excitation and KRATOS VISION2 software. XPS elemental spectra were acquired with 0.1 eV energy step at a pass energy of 75 kV. The C 1s line was taken as an internal standard at 285.0 eV.

2.4. Reaction study

Catalytic performance of the catalysts was studied in selective hydrogenation of acetylene. The experiment was performed in a quartz tube reactor (i.d. 10.1 mm). Before starting of the reaction, the catalyst was reduced in H_2 at 150 °C for 2 h. Then the reactor was purged with argon and cooled down to the reaction temperature, 40 °C. Feed gas composed of 1.5% C_2H_2, 1.7% H_2, and balanced C_2H_4 (TIG Co., Ltd.), a GHSV of 39435, 24433, 16901 and 9288 h^{-1} were used. The

composition of product and feed stream were analyzed by a Shimadzu GC 8A equipped with TCD and FID detectors (molecular sieve-5A and carbosieve S2 columns, respectively). Acetylene conversion as used herein is defined as moles of acetylene converted with respect to acetylene in feed. Ethylene selectivity is defined as the percentage of acetylene hydrogenated to ethylene over totally hydrogenated acetylene. The ethylene being hydrogenated to ethane (ethylene loss) is the difference between all the hydrogen consumed and all the acetylene which has been totally hydrogenated.

3. Results and discussion

3.1. Catalyst characterization

The XRD patterns of the sol–gel- and the solvothermal-made Pd/α-Al_2O_3 and the Pd/Ni-modified α-Al_2O_3 catalysts with Ni/Al atomic ratio 0.5 after calcinations at 1150 °C are shown in Fig. 1. The patterns in the lower half of the figure correspond to the sol–gel-made powder while the patterns in the upper part of the figure are for those prepared by solvothermal synthesis. Both the sol–gel- and solvothermal-made Pd/α-Al_2O_3 catalysts exhibited all the characteristic peaks of α-Al_2O_3 structure. While the diffraction lines for Pd/Ni-modified α-Al_2O_3 catalyst could be assigned to a spinel-type $NiAl_2O_4$ structure; space group Fd3m [25]. Additional peaks corresponding to NiO were also presented at 43.3 and 62.9° 2θ for the product obtained from solvothermal synthesis. The XRD characteristic peaks associated with Pd^0 or PdO phase were not observed in all the samples. This was probably due to the very low amount of Pd present and/or a very good dispersion of Pd phase on all the alumina supports.

TEM micrographs were taken in order to physically measure the size of the palladium oxide particles and/or palladium clusters. It can be seen that the sol–gel made catalyst (Fig. 2a and b) was consisted of agglomerated particles with primarily irregular shape structure. For those prepared by solvothermal method, agglomeration of finger-like particles were observed for the Pd/α-Al_2O_3 whereas spherical-shape particles were found for the Pd/Ni-modified α-Al_2O_3 catalysts (Fig. 2c and d, respectively). The finger-like α-Al_2O_3 particles are normally obtained by calcination of the solvothermal-made α-Al_2O_3 powders at high temperature [26,27]. Based on TEM analysis, palladium particles/clusters with average particle size ca. 5–10 nm were found to be deposited on the alumina supports.

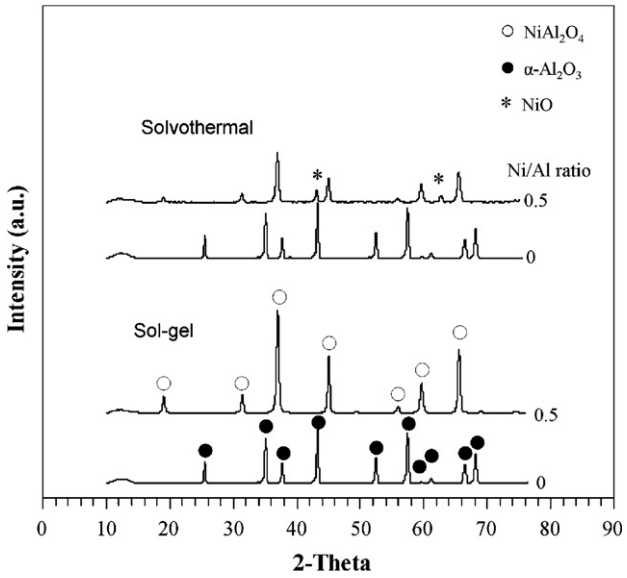

Fig. 1. XRD patterns of the various Pd catalysts supported on nanocrystalline α-Al_2O_3 and Ni-modified α-Al_2O_3 prepared by sol–gel and solvothermal methods.

The physical and chemical properties of Pd/α-Al_2O_3 and Pd/Ni-modified α-Al_2O_3 catalysts are summarized in Table 1. The average crystallite size of each crystal phase was calculated from the Scherrer equation. The average crystallite sizes of the α-Al_2O_3 prepared by sol–gel and solvothermal method were 34 and 58 nm, respectively. While, the crystallite sizes of $NiAl_2O_4$ formed in the Ni-modified α-Al_2O_3 prepared by sol–gel and solvothermal method were 23 and 27 nm, respectively. In all cases, the average crystallite sizes of $NiAl_2O_4$ were smaller than those of α-Al_2O_3. Such results suggest that crystal growth rate for $NiAl_2O_4$ was slower than that of α-Al_2O_3. The surface areas of all the catalysts were not significantly different and still quite low, due probably to high agglomeration of these nanocrystalline particles during calcinations at high temperature. The amounts of CO chemisorption on the catalysts, the Pd dispersions, and the average Pd metal particle sizes determined from CO chemisorption are also given in Table 1. The pulse CO chemisorption technique was based on the assumption that one carbon monoxide molecule adsorbs on one palladium site [28–32]. The amounts of CO chemisorption decreased from 7.5 to 5.4×10^{17} and 8.1 to 7.4×10^{17} sites/g cat. corresponding to the decreasing in Pd metal dispersion from 4.4 to 3.2 and 4.8 to 4.3% by modification with Ni atoms by sol–gel and solvothermal method, respectively. The percentages of Pd dispersion calculated from the CO chemisorption results were in the order Pd/α-Al_2O_3-solvothermal > Pd/α-Al_2O_3–sol–gel ≈ Pd/Ni-modified α-Al_2O_3-solvothermal > Pd/Ni-modified α-Al_2O_3–sol–gel. The average Pd^0 particle sizes for all the catalysts were calculated to be 24–35 nm.

Fig. 3 shows the NH_3 temperature program desorption profiles for the sol–gel and solvothermal-made α-Al_2O_3 and the Ni-modified α-Al_2O_3 supports. Comparing the desorption peak area of the reference γ-alumina, the desorption peak areas of the nanocrystalline α-Al_2O_3 powders obtained from both sol–gel and solvothermal syntheses were relatively low due probably to the dramatically decrease of the surface area after calcination at high temperature. However, two desorption peaks corresponding to different acid sites were still observed at ca. 320 and 400–500 °C for both α-Al_2O_3 samples. For the Ni-modified α-Al_2O_3–sol–gel, no distinctive peaks were observed and the profiles became almost flat. Such results indicate that acidity of the α-Al_2O_3 samples was drastically decreased by incorporation of Ni atoms. The results are in good agreement with those reported by other researchers. For examples, Otero Areán et al. [33] measured acidity of Ni-doped alumina by IR spectroscopy of CO adsorbed at liquid nitrogen temperature. A

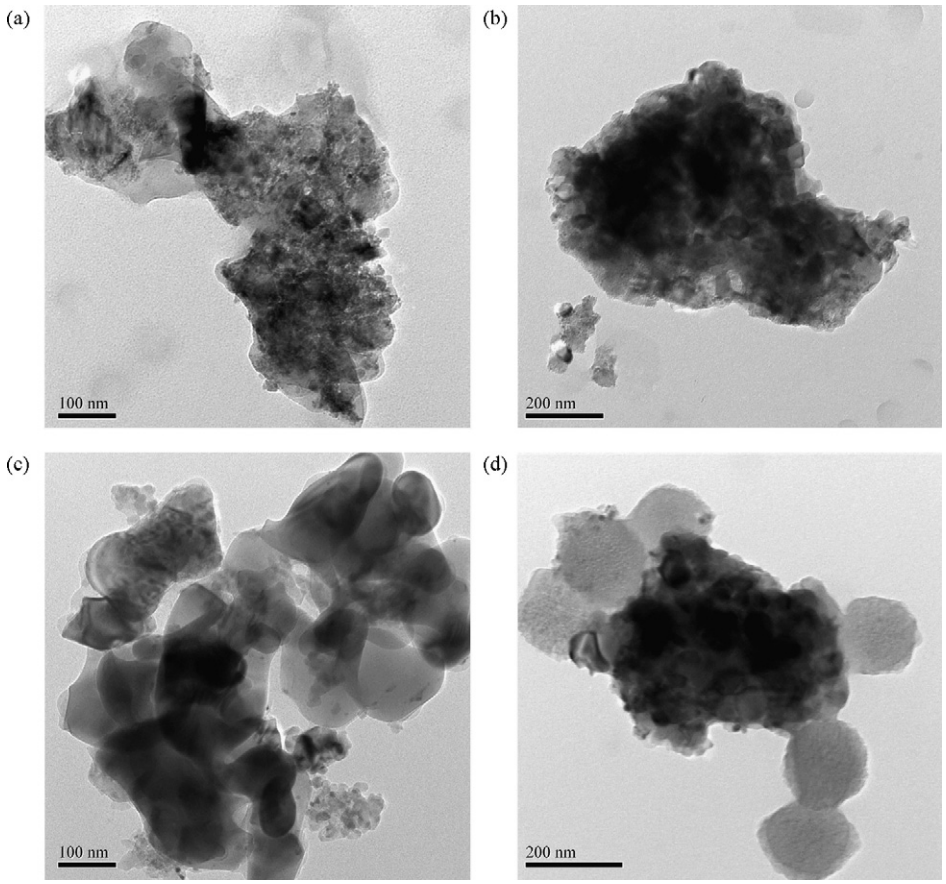

Fig. 2. TEM micrographs of (a) Pd/α-Al_2O_3–sol–gel, (b) Pd/Ni-modified α-Al_2O_3–sol–gel, (c) Pd/α-Al_2O_3-solvothermal, and (d) Pd/Ni-modified α-Al_2O_3-solvothermal.

decrease in both Lewis and Brønsted acidity was observed as the Ni contents increased in the Ni-alumina solid solution. The very low Brønsted acidity also appears to be typical for many oxide spinels as well as other aluminate spinels such as $MgAl_2O_4$ and $ZnAl_2O_4$ [34,35]. A small broad peak was observed for the Ni-modified α-Al_2O_3-solvothermal due probably to the formation of NiO species in which some acidity may be remained.

Because of its surface sensitivity, XPS is used to monitor the interaction between surface Pd and the alumina supports. The elemental scans for Pd 3d of the Pd/α-Al_2O_3 and the Pd/Ni-modified α-Al_2O_3 catalysts are shown in Fig. 4. It was found that the binding energy of Pd 3d for the Pd catalyst supported Ni-modified α-Al_2O_3 prepared by sol–gel shifted to lower binding energy while for those of all the other catalysts, the binding energies for Pd 3d were at the same binding energies. It

Table 1
Characteristics of the various Pd/α-Al_2O_3 and Pd/Ni-modified α-Al_2O_3 catalysts

Sample	d_{XRD}[a] (nm)	BET surface area (m^2/g)	CO chemisorption ($\times 10^{17}$ sites/g cat.)	% Dispersion	d_P[b] Pd^0 (nm)
Sol–gel					
Pd/α-Al_2O_3	34[c]	1.5	7.51	4.42	25
Pd/Ni-α-Al_2O_3	27[d]	1.9	5.37	3.16	35
Solvothermal					
Pd/α-Al_2O_3	54[c]	4.7	8.10	4.76	24
Pd/Ni-α-Al_2O_3	23[d], 26[e]	1.4	7.35	4.32	26
Commercial					
Pd/α-Al_2O_3	391.6[c]	0.5	5.91	3.48	32

[a] Average crystallite size calculated by Scherrer equation.
[b] Average Pd metal particle size calculated from CO chemisorption results. $d_P = 1.12/D$ where D = Pd dispersion [25].
[c] α-Al_2O_3.
[d] $NiAl_2O_4$.
[e] NiO.

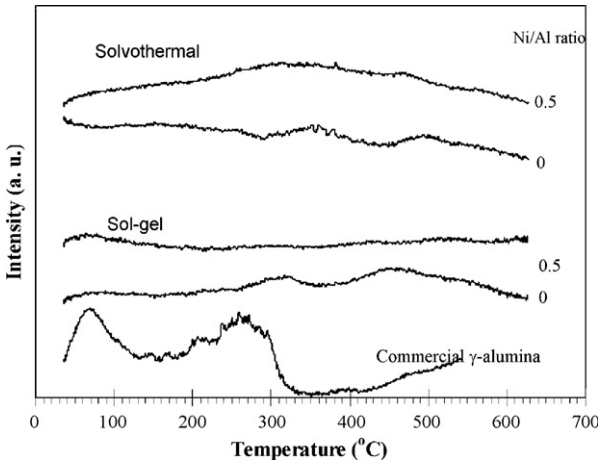

Fig. 3. NH_3 temperature program desorption profiles for the sol–gel and solvothermal-made α-Al_2O_3 and the Ni-modified α-Al_2O_3 supports.

is likely that Pd catalyst supported on $NiAl_2O_4$ spinel may result in a lower interaction between Pd and the alumina support.

3.2. Catalyst performance in selective acetylene hydrogenation

The catalyst performance in selective hydrogenation of acetylene to ethylene was studied for all the catalyst samples using a fixed bed flow reactor. Changes in ethylene selectivity with acetylene conversion for Pd/α-Al_2O_3 and Pd/Ni-modified α-Al_2O_3 catalysts are shown in Fig. 5. In general, ethylene selectivity decreases with increasing acetylene conversion due to the fact that the ethylene is produced as an intermediate in acetylene hydrogenation reaction. Compared to Pd catalyst supported on the commercial α-Al_2O_3, the ones supported on

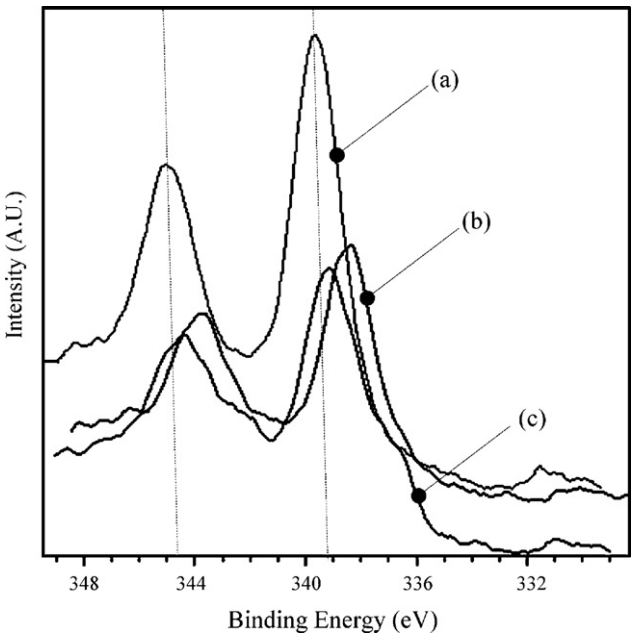

Fig. 4. XPS results of Pd 3d for (a) Pd/α-Al_2O_3–sol–gel, (b) Pd/Ni-modified α-Al_2O_3–sol–gel and (c) Pd/Ni-modified α-Al_2O_3-solvothermal.

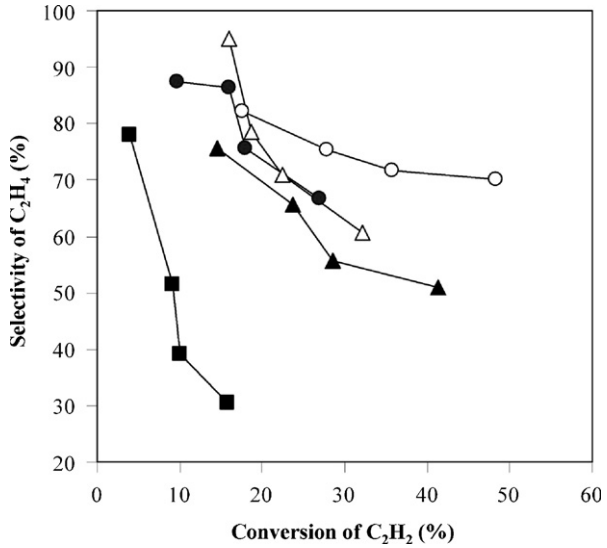

Fig. 5. Performance of sol–gel (circle; ○) and solvothermal (triangle; △) made Pd/α-Al_2O_3 (filled symbols), Pd/commercial α-Al_2O_3 (filled square; ■) and Pd/Ni-modified α-Al_2O_3 (open symbols) catalysts in selective acetylene hydrogenation.

nanocrystalline α-Al_2O_3 and Ni-modified α-Al_2O_3 showed superior catalytic performances in selective acetylene hydrogenation with Pd/Ni-modified α-Al_2O_3 exhibited higher selectivity than Pd/α-Al_2O_3. When comparing the samples prepared by different techniques, the sol–gel-made samples showed higher ethylene selectivity than those of the solvothermal-derived ones. The ethylene selectivity was improved in the order: Pd/Ni-modified α-Al_2O_3-sol–gel > Pd/Ni-modified α-Al_2O_3-solvothermal ≈ Pd/α-Al_2O_3–sol–gel > Pd/α-Al_2O_3-solvothermal ≫ Pd/α-Al_2O_3-commercial.

During long-time investigation by many research groups, the catalytic activity and ethylene selectivity in the selective acetylene hydrogenation in excess ethylene over Pd-based catalysts are found to be dependent on many factors such as metal dispersion (Pd metal particle size) [7], thermodynamic adsorption differences between acetylene and ethylene [36], and carbonaceous product formation [37,38], etc. Based on the reaction mechanisms for acetylene hydrogenation on Pd/Al_2O_3 catalysts in the literatures [39], there are three active sites on the Pd metal surface and one active site on the alumina support. The three sites on the palladium surface are responsible for selective hydrogenation of acetylene to ethylene, direct ethane formation from acetylene and oligomer formation whereas ethylene hydrogenation is believed to take place on the support by means of a hydrogen transfer mechanism. It was claimed that the carbonaceous deposits present act as bridges for hydrogen spillover [40]. It is well known that acidity on alumina surface promotes formation of carbonaceous deposits on catalyst surface. When Ni was incorporated in alumina lattice (i.e., in terms of $NiAl_2O_4$ formation), the acidity of alumina decreased drastically and thus reduced the formation of carbonaceous deposits and hydrogen spillover. In summary, Pd catalyst supported on Ni-modified α-Al_2O_3 can be used as an effective catalyst for producing high ethylene selectivities at relatively high acetylene conversions especially when $NiAl_2O_4$ are

formed. Promotion with other second metals such as Ag is then not necessary in order to improve the catalytic performance of these Pd-based catalysts.

4. Conclusions

The catalytic performance of Pd catalysts supported on nanocrystalline α-Al_2O_3 and Ni-modified α-Al_2O_3 prepared by sol–gel and solvothermal methods was studied in the selective hydrogenation of acetylene in excess ethylene. While the use of sol–gel method resulted in only $NiAl_2O_4$ formation, those prepared by solvothermal gave both $NiAl_2O_4$ and NiO species. Acidity of the nanocrystalline α-Al_2O_3 was significantly decreased by incorporation of Ni atoms in α-Al_2O_3. Ethylene selectivities were improved in the order: Pd/Ni-modified α-Al_2O_3–sol–gel > Pd/Ni-modified α-Al_2O_3-solvothermal $\approx$ Pd/α-Al_2O_3–sol–gel > Pd/α-Al_2O_3-solvothermal $\gg$ Pd/α-Al_2O_3-commercial. The improvement in catalyst performance is probably due to both a decrease in surface acidity of α-Al_2O_3 and modification of Pd surface activity due to $NiAl_2O_4$ formation.

Acknowledgements

Financial supports from the Thailand Research Fund (TRF), the Research and Development Institute of Silpakorn University, and the Graduate School of Chulalongkorn University are gratefully acknowledged.

References

[1] Y.-J.Huang, C.F. Shun, L.G. Daniel, E.L. Mohundro, J.E. Hartgerink, US Patent 5,332,705 (1994).
[2] Q. Zhang, J. Li, X. Liu, Q. Zhu, Appl. Catal. A 197 (2000) 221.
[3] S. Hub, L. Hilaire, R. Touroude, Appl. Catal. 36 (1988) 307.
[4] J.P. Boitiaux, J. Cosyns, S. Vasudevan, Appl. Catal. 6 (1983) 41.
[5] Á. Sárkány, A.H. Weiss, L. Guczi, J. Catal. 98 (1986) 550.
[6] M.H. Chen, W. Chu, X.Y. Dai, X.W. Zhang, Catal. Today 89 (2004) 201.
[7] J. Panpranot, K. Kontapakdee, P. Praserthdam, Appl. Catal. A 314 (2006) 128.
[8] J. Hong, W. Chu, M. Chen, X. Wang, T. Zhang, Catal. Commun. 8 (2007) 593.
[9] W. Huang, J.R. McCormick, R.F. Lobo, J.G. Chen, J. Catal. 246 (2007) 40.
[10] K. Pansanga, O. Mekasuwandumrong, J. Panpranot, P. Praserthdam, Korean J. Chem. Eng. 24 (2007) 397.
[11] J. Panpranot, N. Taochaiyaphoom, P. Praserthdam, Mater. Chem. Phys. 94 (2005) 207.
[12] U. Diebold, Surf. Sci. Rep. 48 (2003) 53.
[13] C.J. Brinker, G.W. Scherrer, Sol–Gel Science: The Physics and Chemistry of Sol–Gel Processing, Academic Press, San Diego, 1990.
[14] W.H. Dawson, Am. Ceram. Soc. Bull. 67 (1988) 1673.
[15] S.G. Deng, Y.S. Lin, J. Mater. Sci. Lett. 16 (1997) 1291.
[16] Y. Sarikaya, I. Sevinc, M. Akinc, Powder Technol. 116 (2001) 109.
[17] I. Sevinc, Y. Sarikaya, M. Akinc, Ceram. Int. 1 (1991) 17.
[18] W.B. Scott, E. Matijevic, J. Colloid Interface Sci. 66 (1978) 447.
[19] M. Inoue, H. Kominami, T. Inui, J. Am. Ceram. Soc. 73 (1990) 1100.
[20] M. Inoue, H. Kominami, T. Inui, J. Am. Ceram. Soc. 75 (1996) 2597.
[21] Y. Deng, X. Zhou, G. Wei, J. Liu, C.W. Nan, S. Zhao, J. Phys. Chem. Solids 63 (2002) 2119.
[22] A. Al-Ubaid, E.E. Wolf, Appl. Catal. 40 (1998) 73.
[23] A. Bhattacharyya, V.W. Chang, Stud. Surf. Sci. Catal. 88 (1994) 207.
[24] J.A. Peña, J. Herguido, C. Guimon, A. Monzón, J. Santamaría, J. Catal. 159 (1996) 313.
[25] A.R. West, Solid State Chemistry and its Application, John Wiley & Sons, New York, 1997.
[26] O. Mekasuwandumrong, V. Pavarajarn, M. Inoue, P. Praserthdam, Mater. Chem. Phys. 100 (2006) 445.
[27] O. Mekasuwandumrong, P.L. Silveston, P. Praserthdam, M. Inoue, V. Pavarajarn, W. Tanakulrungsank, Inorg. Chem. Commun. 6 (2003) 930.
[28] N. Mahata, V. Vishwanathan, J. Catal. 196 (2000) 262.
[29] S.H. Ali, J.G. Goodwin Jr., J. Catal. 176 (1998) 3.
[30] E.A. Sales, G. Bugli, A. Ensuque, M.J. Mendes, F. Bozon-Verduraz, Phys. Chem. Chem. Phys. 1 (1999) 491.
[31] A. Sarkany, Z. Zsoldos, B. Furlong, J.W. Hightower, L. Guczi, J. Catal. 141 (1993) 566.
[32] N.K. Nag, Catal. Lett. 24 (1994) 37.
[33] C. Otero Arean, M. Penarroya Mentruit, A.J. Lopez Lopez, J.B. Parra, Colloids Surf. A 180 (2001) 253.
[34] C. Otero Arean, C. Mas Carbonell, Vib. Spectrofc. 8 (1995) 411.
[35] C. Otero Arean, B. Sintes Sintes, G. Turnes Palomino, C. Mas Carbonell, E. Escalona Platero, J.B. Parra Soto, Microporous Mater. 8 (1997) 187.
[36] G.C. Bond, Catalysis by Metals, Academic Press, London, 1962.
[37] A. Borodzinski, A. Cybulski, Langmuir 13 (1997) 883.
[38] A. Borodzinski, A. Cybulski, Appl. Catal. A 198 (2000) 51.
[39] R.N. Lamb, B. Ngamsom, D.L. Trimm, B. Gong, P.L. Silveston, P. Praserthdam, Appl. Catal. A 268 (2004) 43.
[40] S. Asplund, J. Catal. 158 (1996) 267.

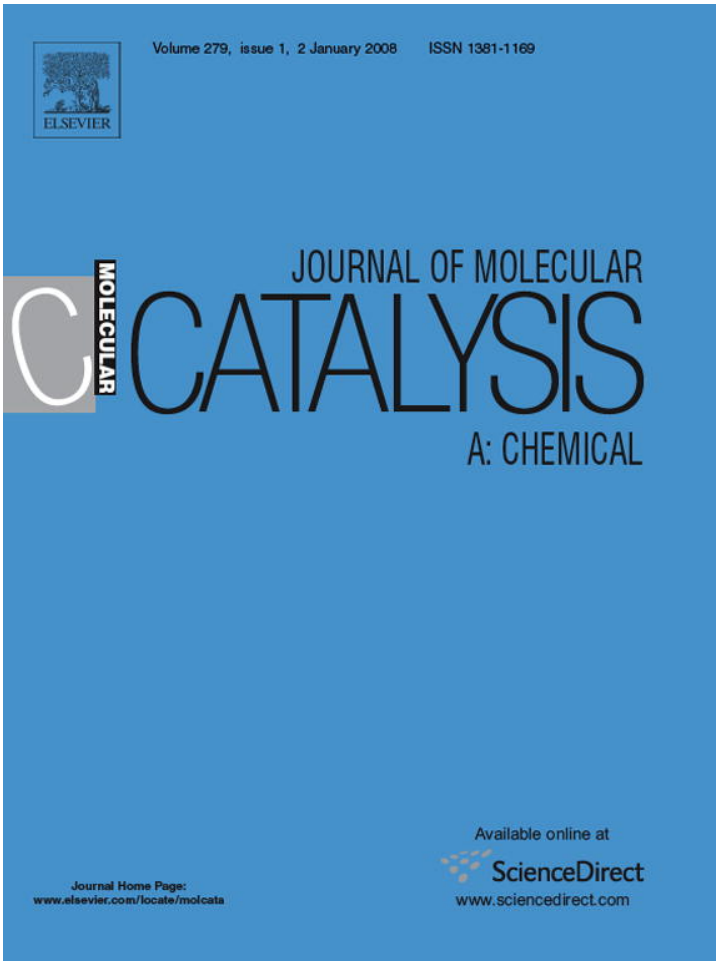

Available online at www.sciencedirect.com
ScienceDirect
Journal of Molecular Catalysis A: Chemical 279 (2008) 133–139
JOURNAL OF MOLECULAR CATALYSIS A: CHEMICAL
www.elsevier.com/locate/molcata

A comparative study of strong metal–support interaction and catalytic behavior of Pd catalysts supported on micron- and nano-sized TiO_2 in liquid-phase selective hydrogenation of phenylacetylene

Patcharaporn Weerachawanasak [a], Piyasan Praserthdam [a], Masahiko Arai [b], Joongjai Panpranot [a,*]

[a] *Center of Excellence on Catalysis and Catalytic Reaction Engineering, Department of Chemical Engineering, Faculty of Engineering Chulalongkorn University, Bangkok, Thailand*
[b] *Division of Chemical Process Engineering, Graduate School of Engineering, Hokkaido University, Sapporo, Japan*

Received 21 September 2007; accepted 3 October 2007
Available online 9 October 2007

Abstract

The strong metal–support interaction and catalytic behaviors of Pd catalysts supported on micron(0.1 μm)- and nano-sized (14 nm) TiO_2 were investigated in the liquid-phase selective hydrogenation of phenylacetylene to styrene. It was found that when supported on the nano-sized TiO_2, the Pd/TiO_2 catalyst that reduced by H_2 at 500 °C exhibited strong metal–support interaction (SMSI) and much improved catalytic performance in liquid-phase selective hydrogenation of phenylacetylene. However, as revealed by CO pulse chemisorption, X-ray photoelectron spectroscopy (XPS), transmission electron microscopy (TEM), and CO-temperature program desorption, the SMSI effect was not detected for the micron-sized TiO_2 supported ones. It is suggested during high-temperature reduction, the inner Ti^{3+} in large crystallite size TiO_2 was more difficult to diffuse to the Pd^0 surface than the surface Ti^{3+} in the smaller crystallite size ones. Sintering of Pd^0 metal was observed instead.

Keywords: Pd/TiO_2; Liquid-phase hydrogenation; Phenylacetylene hydrogenation; Strong metal–support interaction

1. Introduction

The selective hydrogenation of alkynes to alkenes has fundamental importance in the fine chemicals production and industrial polymerization processes [1–4]. A large number of these reactions are carried out in liquid phase using batch type slurry reactors. The major advantages of supported noble metal catalysts in liquid-phase hydrogenation are their relatively high activity, mild process conditions, easy separation, and better handling properties. Pd is one of the most frequently used metals in such processes because of its unique ability to selectively hydrogenation.

Various supports have been employed for recent development of supported Pd catalysts for liquid-phase selective alkyne hydrogenation such as silica [5–8], MCM-41 [9–11], carbon [12], and titania [13–16]. Among these, titania is of particular interest because it exhibits the strong metal–support interaction (SMSI) phenomenon after reduction at high temperatures due to the decoration of the metal surface by partially reducible metal oxides [17,18] or by an electron transfer between the support and the metals [19,20]. In selective hydrogenation of acetylene to ethylene on Pd/TiO_2 catalysts, the charge transfer from Ti species to Pd weakened the adsorption strength of ethylene on the Pd surface hence higher ethylene selectivity was obtained [21]. Fan and coworkers [13] found that Pd/TiO_2 catalysts with SMSI exhibited higher selectivity for alkenes in liquid-phase hydrogenation of long chain alkadienes. Recently, Xu et al. [16] reported that Pd/TiO_2 catalyst prepared by sol–gel produced high conversion and high yield towards butyric acid in liquid-phase hydrogenation of maleic anhydride. The excellent catalyst performances were attributed to the strong interaction between metal and support and the formation of interfacial $Pd–TiO_x$ site, which was induced by high-temperature reduction step.

Recently, there has been a growing interest in the application of nano-sized TiO_2 in the field of catalysis. With the

* Corresponding author. Tel.: +66 2218 6869; fax: +66 2218 6877.
E-mail address: joongjai.p@eng.chula.ac.th (J. Panpranot).

1381-1169/$ – see front matter © 2007 Elsevier B.V. All rights reserved.
doi:10.1016/j.molcata.2007.10.006

decrease in particle size to nanometer scale, photocatalytic activity of TiO_2 is enhanced because the optical band gap is widened due to surface defect [22,23] and an increase in surface area [24,25]. Various techniques have been reported for the preparation of nano-sized TiO_2 such as solvothermal method [26–28], precipitation method [29], sol–gel method [30–32], and thermal decomposition of alkoxide [33]. The sol–gel method is an easy method but the precipitated powders obtained are amorphous in nature and further heat treatment is required for crystallization. Solvothermal method is an alternative route for direct (one-step) synthesis of pure anatase TiO_2. Particle morphology, crystalline phase, and surface chemistry of the solvothermal-derived TiO_2 can be controlled by regulating precursor composition, reaction temperature, pressure, solvent property, and aging time.

In previous studies, the effect of TiO_2 polymorphs (anatase and rutile) on the strong metal–support interaction and catalytic properties of Pd/TiO_2 have been studied and compared [13,34]. It was shown that pre-reduction by H_2 at lower temperature results in SMSI for anatase titania supported palladium catalyst, but not for rutile titania supported one. A recent study from our group has shown that the use of pure anatase TiO_2 that contained significant amount of Ti^{3+} defects as supports for Pd catalysts gave high ethylene selectivities in gas-phase selective acetylene hydrogenation, while the use of pure rutile TiO_2 resulted in ethylene loss [35]. Nevertheless, the effects of Ti^{3+} and/or the TiO_2 crystallite size on the strong metal–support interaction of Pd/TiO_2 and their catalytic behavior in liquid-phase selective hydrogenation have never been reported.

Thus, it is the aim of this study to investigate the SMSI phenomena and catalytic behavior of Pd catalysts supported on micron- and nano-size TiO_2 in liquid-phase selective hydrogenation of phenylacetylene under mild reaction conditions. The nano-TiO_2 was synthesized by the solvothermal method in 1,4-butanediol using titanium *n*-butoxide as a titanium precursor. The catalysts were characterized by N_2 physisorption, X-ray diffraction (XRD), CO-temperature programmed desorption (CO-TPD), scanning electron microscopy (SEM), transmission electron microscopy (TEM), CO pulse chemisorption, electron spin resonance (ESR) and X-ray photoelectron spectroscopy (XPS).

2. Experimental

2.1. Preparation of TiO_2 and Pd/TiO_2 catalysts

The solvothermal-derived nano-TiO_2 was prepared according to the method described in Ref. [36] using 25 g of titanium(IV) *n*-butoxide (TNB) 97% from Aldrich. The starting material was suspended in 100 ml of 1,4-butanediol in a test tube and then set up in an autoclave. In the gap between the test tube and autoclave wall, 30 ml of solvent was added. After the autoclave was completely purged with nitrogen, the autoclave was heated to desired temperature (320 °C) at the rate of 2.5 K min^{-1} and held at that temperature for 6 h. Autogeneous pressure during the reaction gradually increased as the temperature was raised. After the reaction, the autoclave was cooled to room temperature. The resulting powders were collected after repeated washing with methanol by centrifugation. They were then air-dried at room temperature. For comparison purposes, the micron-sized anatase TiO_2 was obtained commercially from Aldrich. The micron- and nano-sized TiO_2 were denoted herein as TiO_2-micron and TiO_2-nano, respectively.

The 1%Pd/TiO_2 catalysts were prepared by the incipient wetness impregnation technique using an aqueous solution of the desired amount of $Pd(NO_3)_2{\cdot}6H_2O$ (Aldrich). The catalysts were dried overnight at 110 °C and then calcined in air at 450 °C for 3 h.

2.2. Catalyst characterization

The specific surface areas, pore volumes, and average pore diameters were determined by N_2 physisorption using a Micromeritics ASAP 2000 automated system and the Brunauer–Emmet–Teller (BET) method. Each sample was degassed under vacuum at $<1 \times 10^{-5}$ bar in the Micromeritics system at 150 °C for 4 h prior to N_2 physisorption. The XRD patterns of the catalysts were measured from 10° to 80° 2θ using a SIEMENS D5000 X-ray diffractometer and Cu Kα radiation with a Ni filter. The particle morphology was obtained using a JEOL JSM-35CF scanning electron microscope (SEM) operated at 20 kV. Catalyst crystallite sizes were obtained using the JEOL JEM 2010 transmission electron microscope that employed a LaB_6 electron gun in the voltage range of 80–200 kV with an optical point-to-point resolution of 0.23 nm. The amounts of CO chemisorbed on the catalysts were measured using a Micromeritic Chemisorb 2750 automated system with ChemiSoft TPx software. Prior to chemisorption, the sample was reduced in a H_2 flow at a desired temperature for 2 h and then cooled down to ambient temperature in a He flow. XPS analysis was performed using an AMICUS photoelectron spectrometer with Mg Kα X-ray as primary excitation and equipped with KRATOS VISION2 software. XPS elemental spectra were acquired with 0.1 eV energy step at pass energy of 75 kV. The C 1s line was taken as an internal standard at 285.0 eV. Electron spin resonance spectroscopy (ESR) was conducted using a JEOL JESRE2X electron spin resonance spectrometer. The intensity of ESR was calculated using a computer software program ES-PRIT ESR DATA SYSTEM version 1.6.

2.3. Reaction study

Approximately 0.2 g of 1%Pd/TiO_2 catalyst was placed into the 50 ml autoclave. The reactant consisting of 1 ml of phenyl acetylene and 9 ml of ethanol was mixed in a volumetric flask before being introduced into the autoclave reactor. Afterward the reactor is purged with hydrogen gas. The liquid-phase hydrogenation was carried out with H_2 pressure between 1 and 3 bar at 30 °C for 10–40 min. After the reaction, the vent valve was slowly opened to prevent the loss of product. The product mixture was analyzed by gas chromatography with flame ionization detector (FID).

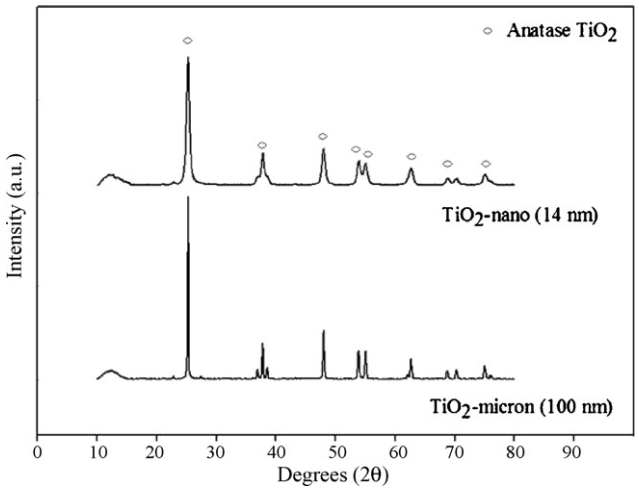

Fig. 1. XRD patterns of nano- and micron-sized TiO_2.

3. Results and discussion

Fig. 1 shows the XRD patterns of the micron- and nano-sized TiO_2. Both samples exhibited the characteristic peaks of the anatase titania at $2\theta = 25°$ (major), 37°, 48°, 55°, 56°, 62°, 71°, and 75°. The average crystallite sizes of the TiO_2-micron and TiO_2-nano calculated from the full width at half maximum of the XRD peak at $2\theta = 25°$ using the Scherrer equation were 100 nm (~0.1 μm) and 14 nm, respectively. The average crystallite size of TiO_2-micron in this study was found to be much larger than many commercially available TiO_2 widely used in the industry such as P-25 (Degussa), PC-500 and AT-1 (Millennium Chemicals), and Hombikat UV-100 (Sachtleben Chemie) in which the TiO_2 crystallite sizes are in the range of 10–30 nm [37]. The XRD characteristic peaks corresponding to PdO and/or Pd^0 metal were not observed after impregnation of Pd, calcination, and reduction steps due probably to the low amount of Pd present or a higher degree of Pd dispersion (results not shown).

Table 1 summarizes physicochemical properties of the TiO_2 and 1%Pd/TiO_2 catalysts. Reduction with H_2 either at 40 or 500 °C did not result in significant changes of the TiO_2 crystallite sizes. The BET surface area of the 1%Pd/TiO_2-micron was not altered from the original TiO_2-micron support suggesting that most of the palladium were deposited on the external surface of the support. In contrast, the BET surface areas of the TiO_2-nano decreased after Pd loading followed by the high-temperature reduction at 500 °C, indicating that Pd was deposited in some of the pores of the TiO_2 support. A slight increase in the TiO_2 crystallite sizes of the TiO_2-nano from 14 to 17 nm was probably caused by high temperature calcination and reduction of the catalysts at 500 °C. The percentage of Pd dispersion estimated from CO chemisorption and Pd^0 metal particle sizes calculated were also given in Table 1. It was found that %Pd dispersion decreased when the catalysts were reduced at 500 °C for both TiO_2-micron and TiO_2-nano-supported Pd catalysts. However, %Pd dispersion for 1%Pd/TiO_2-micron decreased by 80.5% while that of 1%Pd/TiO_2-nano decreased by only 53.5%. The corresponding Pd^0 particle sizes calculated based on CO chemisorption were varied from 6.7 to 48.7 nm.

Fig. 2 shows the SEM micrographs of TiO_2 and 1%Pd/TiO_2 catalysts (calcined). The TiO_2-micron had a uniform particle size of 0.1–0.2 μm while the TiO_2-nano consisted of irregular shape of very fine agglomerated particles. Morphologies of the reduced 1%Pd/TiO_2 catalysts were not significantly different from the corresponding TiO_2 supports suggesting high-thermal stability of the TiO_2. TEM analysis has been carried out in order to physically measure the Pd^0 particle sizes on the various TiO_2 supports and the results are shown in Fig. 3. The particle sizes of various TiO_2 supports were consistent to those obtained from XRD results. It is clearly seen that on the TiO_2-micron, Pd^0 metal particle sizes increased when the catalyst was reduced at 500 °C whereas those on the TiO_2-nano were essentially the same to those reduced at 40 °C. Such results indicate that sintering of Pd^0 metal occurred on the 1%Pd/TiO_2-micron catalyst during high-temperature reduction, in agreement with the lower amount of CO chemisorption observed (Table 1). For the 1%Pd/TiO_2-nano reduced at 500 °C, the results of TEM and low CO chemisorption (giving an over estimation of the Pd^0 metal particle sizes) indicate that the catalyst exhibited strong metal–support interaction under high-temperature reduction since no change in the Pd^0 particle size was observed. The SMSI effect on these catalysts was confirmed by measuring the amounts of CO chemisorption of the re-calcined (at 450 °C) and re-reduced (at 40 °C) catalysts after they were subjected to reduction at 500 °C. The results are illustrated in Fig. 4. The amount of CO chemisorption of the re-calcined and re-reduced 1%Pd/TiO_2-micron was less than that reduced at 40 °C suggesting that sintering of Pd^0 occurred during high-

Table 1
Physicochemical properties of various TiO_2 and 1%Pd/TiO_2 catalysts

Sample[a]	Crystallite size of TiO_2 by XRD (nm)	BET (m^2/g)	Pore volume (cm^3/g)	Pore diameter (nm)	%Pd dispersion[b]	d_pPd^0 (nm)[c]
TiO_2-micron	100	10	0.02	7.6	–	–
TiO_2-nano	14	79	0.40	14.9	–	–
1%Pd/TiO_2-micron-R40	96	9	0.03	1.3	16.4	6.9
1%Pd/TiO_2-micron-R500	94	11	0.03	1.2	3.2	48.7
1%Pd/TiO_2-nano-R40	16	73	0.31	0.6	16.8	6.7
1%Pd/TiO_2-nano-R500	17	68	0.28	0.8	7.8	40.6

[a] R40 and R400 indicate the samples reduced at 40 and 500 °C, respectively.
[b] Determined from CO chemisorption.
[c] Based on d (nm) = (1.12/D) [46], where D is the fractional metal dispersion.

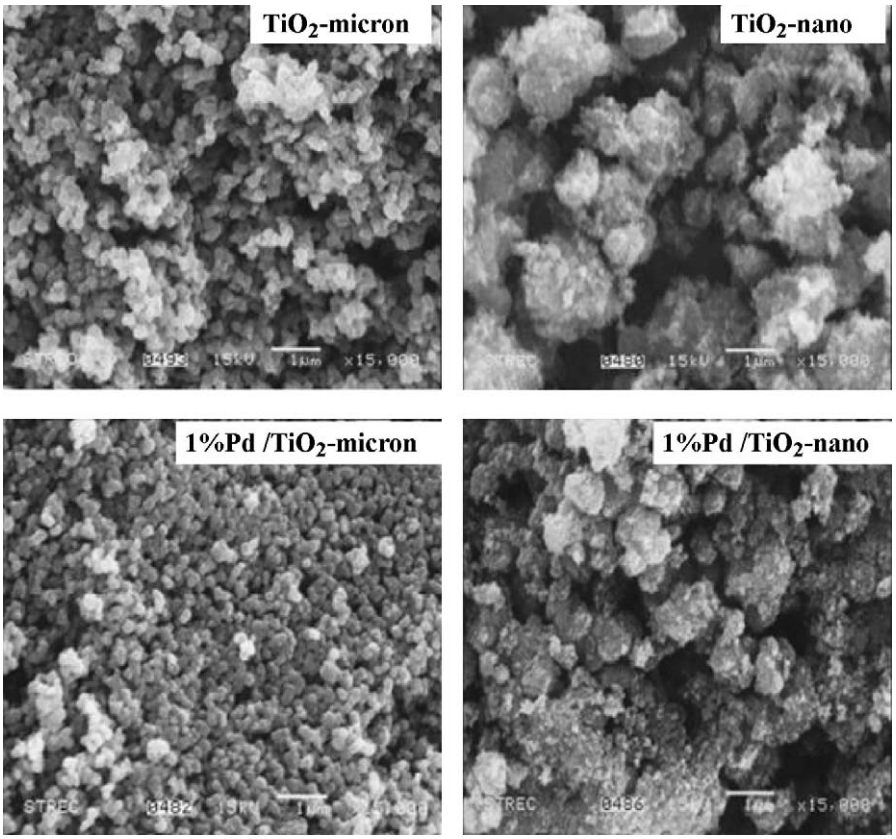

Fig. 2. SEM micrographs of TiO_2 and 1%Pd/TiO_2 (calcined).

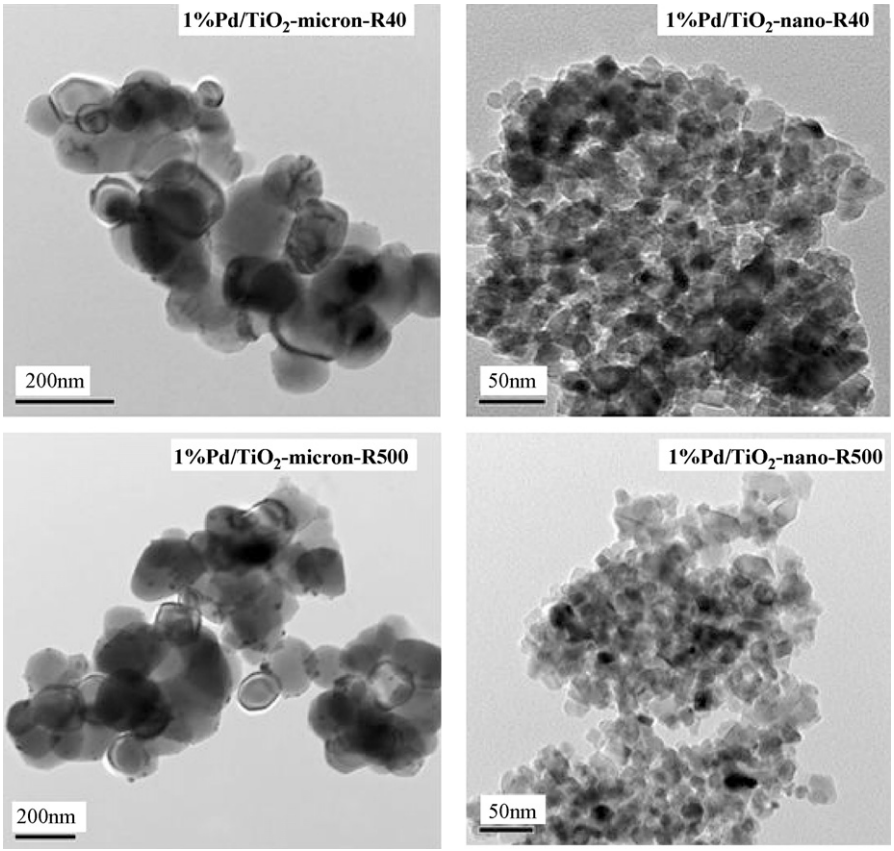

Fig. 3. TEM micrographs of the various Pd/TiO_2 catalysts.

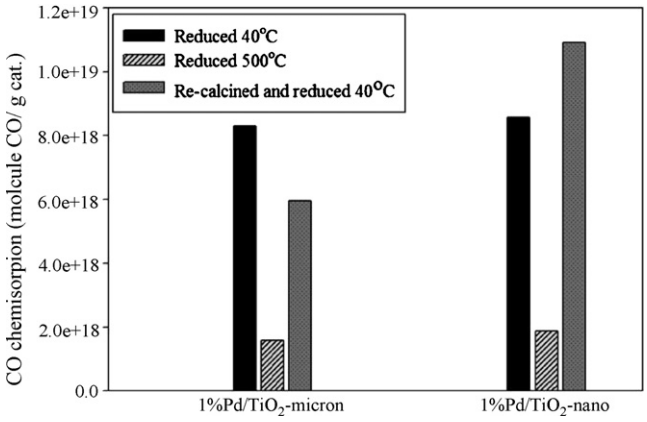

Fig. 4. CO chemisorption results.

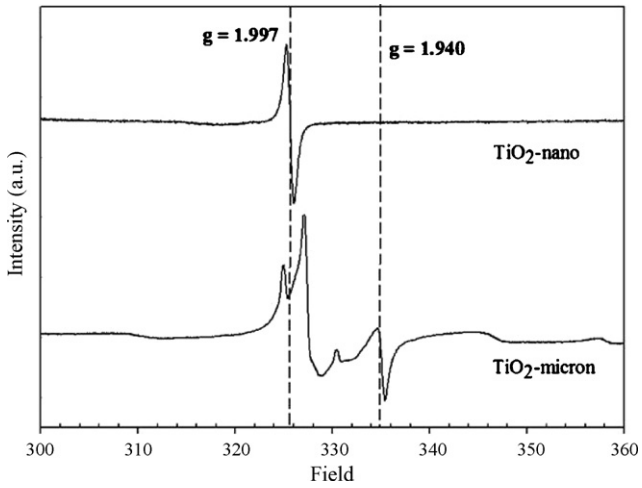

Fig. 5. ESR spectra of nano- and micron-sized TiO_2.

temperature reduction while the amount of CO chemisorption of the re-calcined and re-reduced 1%Pd/TiO_2-nano can be totally recovered. It is generally known that strong metal–support interaction in TiO_2 supported Pd catalysts occurred after a high-temperature reduction ≥500 °C. It is thus surprising that such interaction was not detected on our 1%Pd/TiO_2-micron. However, it should be noticed that the TiO_2 crystallite sizes used for preparation of Pd/TiO_2 catalysts in most studies in the literature were in nanometer range (usually less than 50 nm) [13–15,38]. Panagiotopoulou et al. [39] also reported that formation of sub-stoichiometric TiO_x species started at lower temperature and was more facile over Pt/TiO_2 for small TiO_2 particle sizes (10–35 nm). On the other hand, a recent study by Musolino et al. [14] on the selective liquid-phase hydrogenation of *cis*-2-butene-1,4-diol to 2-hydroxy tetrahydrofuran on various supported Pd catalysts revealed the absence of SMSI effect for the Pd/TiO_2 catalyst reduced at high temperature. The interpretation of the observed behavior has not been given by those authors. However, the TiO_2 support used in their study was also anatase-phase TiO_2 from Aldrich with the specific surface area of ∼9 m^2/g similar to the micron-sized TiO_2 reported in this study.

The surface compositions of the catalysts as well as the interaction between Pd and the TiO_2 supports were confirmed by XPS analysis. The binding energies, FWHM, and atomic concentrations of Ti 2p, O 1s, and Pd 3d on various Pd/TiO_2 catalysts are given in Table 2. The Ti/O atomic ratios were found to be much higher for the TiO_2-nano than the TiO_2-micron suggesting that the solvothermal-derived TiO_2-nano possessed more oxygen vacancies (or so-called Ti^{3+} defective sites) on the TiO_2 surface than the TiO_2-micron. However, there was also probably an oxygen-rich layer near the surface of the TiO_2 particles, which was formed by oxygen adsorption and easy oxidation of titanium surface [40]. When reduced at 500 °C, the Pd/Ti surface concentration decreased by 15 and 55% for 1%Pd/TiO_2-micron and 1%Pd/TiO_2-nano, respectively. A slight decrease of Pd/Ti surface concentration for 1%Pd/TiO_2-micron may be due to larger Pd^0 particle size formed by sintering as shown by TEM and CO chemisorption, while a large decrease of Pd/Ti on the 1%Pd/TiO_2-nano would be due to decoration of Pd^0 metal surface by the reducible TiO_2 support. The binding energies of Pd $3d_{5/2}$ (335.0–335.2 eV) and the FWHM less than 2 eV revealed that palladium was in the form of Pd^0 metal for both cases [41].

The presence of Ti^{3+} in both TiO_2-micron and TiO_2-nano supports was revealed by electron spin resonance technique (Fig. 5). The Ti^{3+} species are produced by trapping of electrons at defective sites of TiO_2 and the amount of accumulated electrons may therefore reflect the number of defective sites [42]. The signal of *g* value less than two was assigned to Ti^{3+} ($3d^1$) [43]. Nakaoka et al. [44] reported six signals of ESR measurement occurring on the surface of titania: (i) $Ti^{4+}O^-Ti^{4+}OH^-$, (ii) surface Ti^{3+}, (iii) adsorbed oxygen (O^{2-}), (iv) $Ti^{4+}O^{2-}Ti^{4+}O^{2-}$, (v) inner Ti^{3+}, and (vi) adsorbed water. In this study, it is clearly seen that the solvothermal-derived TiO_2 exhibited only one strong ESR signal at a *g* value of 1.997, which can be attributed

Table 2
XPS results

Catalysts	Ti 2p		O 1s		Pd 3d		Atomic concentration	
	B.E. (eV)	FWHM	B.E. (eV)	FWHM	B.E. (eV)	FWHM	Ti/O	Pd/Ti
TiO_2-micron	458.6	1.259	532.3	2.362	–	–	0.028	–
TiO_2-nano	458.7	1.308	530.0	1.675	–	–	0.204	–
1%Pd/TiO_2-micron R40	458.7	1.516	530.2	2.324	335.0	1.704	0.123	0.073
1%Pd/TiO_2-micron R500	458.7	1.846	530.2	1.846	335.2	1.849	0.178	0.062
1%Pd/TiO_2-nano-R40	458.7	1.292	530.0	1.596	335.0	1.570	0.210	0.009
1%Pd/TiO_2-nano-R500	458.6	1.319	529.9	1.681	*n/d*	*n/d*	0.190	0.004

to Ti^{3+} at the surface. Many Ti^{3+} ESR signals were observed for the TiO_2-micron indicating that more than one type of Ti^{3+} defects were presented in the sample, i.e., surface Ti^{3+} and inner Ti^{3+}. Moreover, less amount of surface Ti^{3+} was present on the micron-sized TiO_2. Literature data indicate that the presence of Ti^{3+} promotes strong metal–support interaction in Pd/TiO_2 catalysts since Ti^{3+} can easily diffuse from the lattice of TiO_2 to surface of Pd particles [13]. The results in this study, however, have shown that probably only the surface Ti^{3+} has high mobility and the other Ti^{3+} species may not be able to diffuse easily to Pd^0 surface so that Pd catalyst supported on the TiO_2-micron with significant amount of Ti^{3+} did not exhibited the strong metal–support interaction.

Temperature programmed desorption of CO has been carried out in order to elucidate the influence of TiO_2 crystallite size, Pd dispersion, and reduction temperature on the strength and mechanism of CO adsorption on TiO_2 supported Pd catalysts. The results are shown in Fig. 6. For $1\%Pd/TiO_2$-micron reduced at 40 °C, two main desorption peaks were observed at ca. 340 and 640 °C which may be attributed to CO adsorbed on different adsorption sites probably Pd^0 with different particle sizes and/or adsorption on Ti^{3+} sites [45]. Both peaks were slightly shifted to higher temperature for the catalyst reduced at 500 °C. However, the amounts of CO desorption were not significant different for $1\%Pd/TiO_2$-micron reduced at 40 or 500 °C indicating that CO adsorption strength was not much different for the catalysts reduced at low and high temperatures. In contrast, $1\%Pd/TiO_2$-nano reduced at 40 °C exhibited several desorption peaks at 100–800 °C indicating various adsorption sites on the catalyst surface. However, the peaks become almost flat when the catalyst was reduced at 500 °C indicating negligible CO adsorption under such conditions. In other words, CO was weakly adsorbed under high-temperature reduction conditions due to the strong metal–support interaction effect.

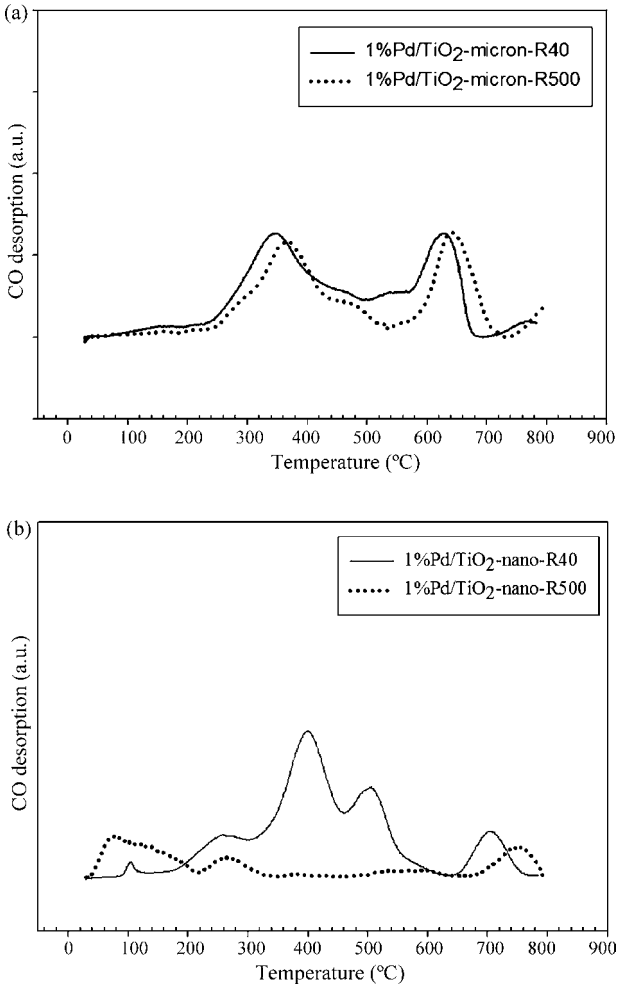

Fig. 6. CO-temperature programmed desorption profiles of (a) micron- and (b) nano-sized TiO_2 supported Pd catalysts.

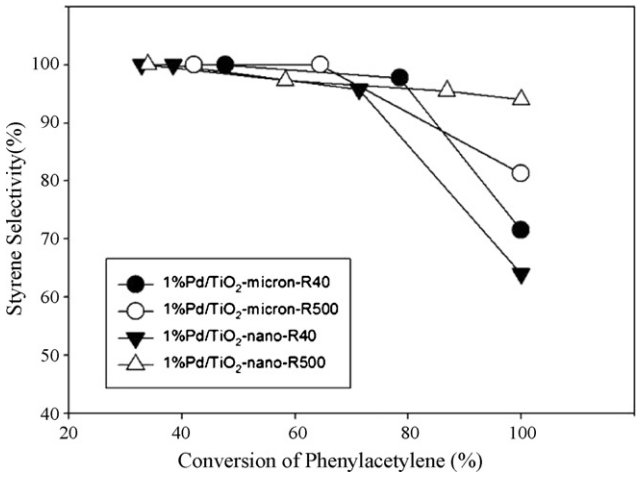

Fig. 7. Catalyst performances in liquid-phase selective hydrogenation of phenylacetylene.

Fig. 7 shows the performance of the $1\%Pd/TiO_2$-micron and $1\%Pd/TiO_2$-nano catalysts in liquid-phase selective hydrogenation of phenylacetylene under mild conditions. Both catalysts exhibited high styrene selectivities (≥95%) for phenylacetylene conversions less than 80%. Based on the conditions and the column used in our GC analysis, the other product found in the reaction besides styrene was ethylbenzene. No other by-products were observed. The selectivity for styrene significantly dropped to 65–80% when conversion of phenylacetylene reached 100% for all the catalysts except $1\%Pd/TiO_2$-nano reduced at 500 °C that retained its high styrene selectivity >90%. Such results suggest that the strong metal–support interaction on $1\%Pd/TiO_2$-nano catalyst produced great beneficial effect on the catalyst performance. The presence of SMSI effect may result in an inhibition of the adsorption of the product styrene on the $1\%Pd/TiO_2$-nano; hence high styrene selectivity was obtained.

The turnover frequencies (TOF) values were calculated from the data at a small conversion level of, for example, 30% for the catalysts except for the SMSI catalyst. It was found that the TOFs increased from 5.5 s^{-1} for $1\%Pd/TiO_2$-micron-R40) to 25.1 s^{-1} for $1\%Pd/TiO_2$-micron-R500) corresponding to the increase of Pd^0 particle size from 7 to 49 nm, respectively. The amount of exposed Pd species were estimated from CO chemisorption data with the assumption that one carbon monoxide molecule adsorbs on one palladium site [46–51]. The specific activity results were found to be in agreement with the well-established trend in the

literature that the liquid-phase hydrogenation activity decreases as Pd^0 particle size decreases [52–58].

4. Conclusions

As revealed by various analytical techniques such as CO pulse chemisorption, X-ray photoelectron spectroscopy (XPS), transmission electron microscopy (TEM), and CO-temperature program desorption, reduction by H_2 at 500 °C resulted in strong metal–support interaction for the nano-sized TiO_2 supported Pd catalyst, but not for the micron-sized TiO_2 supported one. The SMSI effect, however, appeared to be necessary for high catalytic performance of the Pd/TiO_2 catalysts in the liquid-phase selective hydrogenation of phenylacetylene to styrene.

Acknowledgements

Financial supports from the Thailand Research Fund (TRF), the Graduate School of Chulalongkorn University (the 90th Anniversary of Chulalongkorn University-the Golden Jubilee Fund), and the Commission on Higher Education, Thailand are gratefully acknowledged.

References

[1] L. Guczi, A. Horvath, A. Beck, A. Sarkany, Stud. Surf. Sci. Catal. 145 (2003) 351.
[2] O. Dominguez-Quintero, S. Martinez, Y. Henriquez, L. D'Ornelas, H. Krentzien, J. Osuna, J. Mol. Catal. A 197 (2003) 185.
[3] K.J. Stanger, Y. Tang, J. Anderegg, R.J. Angelici, J. Mol. Catal. A 202 (2003) 147.
[4] T.A. Nijhuis, G. van Koten, J.A. Moulijn, Appl. Catal. A 238 (2003) 259.
[5] J.W. Park, Y.M. Chung, Y.W. Suh, H.K. Rhee, Catal. Today 93 (2004) 445.
[6] N. Marin-Astorga, G. Pecchi, J.L.G. Fierro, P. Reyes, Catal. Lett. 91 (2003) 115.
[7] N. Marin-Astorga, G. Pecchi, T.J. Pinnavaia, G. Alvez-Manoli, P. Reyes, J. Mol. Catal. A 247 (2006) 145.
[8] J. Panpranot, K. Phandinthong, T. Sirikajorn, M. Arai, P. Praserthdam, J. Mol. Catal. A 261 (2007) 29.
[9] A. Papp, A. Molnar, A. Mastalir, Appl. Catal. A 289 (2005) 256.
[10] A. Mastalir, B. Rac, Z. Kiraly, A. Molnar, J. Mol. Catal. A 264 (2007) 170.
[11] S. Sato, R. Takahashi, T. Sodesawa, M. Koubata, Appl. Catal. A 284 (2005) 247.
[12] D. Teschner, E. Vass, M. Hävecker, S. Zafeiratos, P. Schnörch, H. Sauer, A. Knop-Gericke, R. Schlögh, M. Chamam, A. Wootsch, A.S. Canning, J.J. Gamman, S.D. Jackson, J. MacGregor, L.F. Gladden, J. Catal. 242 (2006) 26.
[13] Y. Li, B. Xu, Y. Fan, N. Feng, A. Qiu, J. Miao, J. He, H. Yang, Y. Chen, J. Mol. Catal. A 216 (2004) 107.
[14] M.G. Musolino, P. De Maio, A. Donato, R. Pietropaolo, J. Mol. Catal. A 208 (2004) 219.
[15] M.G. Musolino, G. Apa, A. Donato, R. Pietropaolo, F. Frusten, Appl. Catal A 25 (3) (2007) 112.
[16] J. Xu, K. Sun, L. Zhang, Y. Ren, X. Xu, Catal. Commun. 6 (2005) 462.
[17] J. Santos, J. Phillips, J.A. Dumesic, J. Catal. 81 (1983) 147.
[18] G.B. Raupp, J.A. Dumesic, J. Catal. 95 (1985) 587.
[19] J.M. Herrmann, M. Gravelle-Rumeau-Maillot, P.C. Gravelle, J. Catal. 104 (1987) 136.
[20] P. Chou, M.A. Vannice, J. Catal. 104 (1987) 1.
[21] J.H. Kang, E.W. Shin, W.J. Kim, J.D. Park, S.H. Moon, J. Catal. 208 (2002) 310.
[22] C. Shifu, C. Gengyu, Surf. Coat. Technol. 200 (2006) 3637.
[23] K. Suriye, P. Praserthdam, B. Jongsomjit, Ind. Eng. Chem. Res. 44 (2005) 6599.
[24] R.K. Madhusudan, C.V. Gopal, S.V. Manorama, J. Solid State Chem. 158 (2001) 180.
[25] T. Toyoda, H. Kawano, Q. Shen, A. Kotera, M. Ohmori, Jpn. J. Appl. Phys. 39 (2000) 3160.
[26] C.-S. Kim, B.K. Moon, J.-H. Park, S.T. Chung, S.-M. Son, J. Cryst. Growth 254 (2003) 405.
[27] C. Wang, Z.-X. Deng, G. Zhang, S. Fan, Y. Li, Powder Technol. 125 (2002) 39.
[28] M. Kang, B.-J. Kim, S.M. Cho, C.-H. Chung, B.-W. Kim, G.Y. Han, K.J. Yoon, J. Mol. Catal. A 180 (2002) 125.
[29] H.-D. Nam, B.-H. Lee, S.-J. Kim, C.-H. Jung, J.-H. Lee, S. Park, Jpn. J. Appl. Phys. 37 (1998) 4603.
[30] C. Su, B.-Y. Hong, C.-M. Tseng, Catal. Today 96 (2004) 119.
[31] Y. Bessekhouad, D. Robert, J.V. Weber, J. Photochem. Photobiol. A: Chem. 157 (2003) 47.
[32] M.J. Alam, D.C. Cameron, J. Sol–Gel Sci. Technol. 25 (2002) 137.
[33] H. Kominami, J.-I. Kalo, Y. Takada, Y. Doushi, B. Ohtani, S.-I. Nishimoto, M. Inoue, Y. Kera, Catal. Lett. 46 (1997) 235.
[34] J. Panpranot, K. Kontapakdee, P. Praserthdam, J. Phys. Chem. B 110 (2006) 8019.
[35] J. Panpranot, K. Kontapakdee, P. Praserthdam, Appl. Catal. A 314 (2006) 128.
[36] W. Payakgul, O. Mekasuwandumrong, V. Pavarajarn, P. Praserthdam, Ceram. Int. 31 (2005) 391.
[37] P. Panaglotopoulou, D.I. Kondarides, J. Catal. 225 (2004) 327.
[38] R.F. Hicks, A.T. Bell, J. Catal. 90 (1984) 205.
[39] P. Panagiotopoulou, A. Christodoulakis, D.I. Kondarides, S. Boghosian, J. Catal. 40 (2) (2006) 114.
[40] F. Zhang, Z. Zheng, D. Liu, Y. Mao, Y. Chen, Z. Zhou, S. Yang, X.X. Liu, Phys. Res. B 132 (1997) 620.
[41] C.D. Wagner, W.M. Riggs, L.E. Davis, J.F. Moulder, in: G.E. Muilenberg (Ed.), Handbook of X-ray Photoelectron Spectroscopy, Perkin-Elmer Corporation, Eden Prairie, MN, 1978.
[42] S. Ikeda, N. Sugiyama, S. Murakami, H. Kominami, Y. Kera, H. Noguchi, K. Uosaki, T. Torimoto, B. Ohtani, Phys. Chem. Chem. Phys. 5 (2003) 778.
[43] T.M. Salama, H. Hattori, H. Kita, K. Ebitani, T. Tanaka, J. Chem. Soc., Faraday Trans. 89 (1993) 2067.
[44] Y. Nakaoka, Y. Nosaka, J. Photochem. Photobiol. A 110 (1997) 299.
[45] E.V. Benvenutti, L. Franke, C.C. Moro, Langmuir 15 (1999) 3140.
[46] N. Mahata, V. Vishwanathan, J. Catal. 196 (2000) 262.
[47] S.H. Ali, J.G. Goodwin Jr., J. Catal. 176 (1998) 3.
[48] E.A. Sales, G. Bugli, A. Ensuque, M.J. Mendes, F. Bozon-Verduraz, Phys. Chem. Chem. Phys. 1 (1999) 491.
[49] A. Sarkany, Z. Zsoldos, B. Furlong, J.W. Hightower, L. Guczi, J. Catal. 41 (1993) 566.
[50] M.A. Vannice, S.Y. Wang, S.H. Moon, J. Catal. 71 (1981) 152.
[51] N.K. Nag, Catal. Lett. 24 (1994) 37.
[52] N. Marin-Astroga, G. Alvez-Manoli, P. Reyes, J. Mol. Catal. A 226 (2005) 81.
[53] A. Molnar, A. Sarkany, M. Varga, J. Mol. Catal. A 173 (2001) 185.
[54] D. Duca, L.F. Liotta, G. Deganello, J. Catal. 154 (1995) 69.
[55] G. Carturan, G. Facchin, G. Cocco, S. Enzo, G. Navazio, J. Catal. 76 (1982) 405.
[56] A. Sarkany, A.H. Weiss, L. Guczi, J. Catal. 98 (1986) 550.
[57] P. Albers, K. Seibold, G. Prescher, H. Muller, Appl. Catal. A 146 (1999) 135.
[58] G. del Angel, J.L. Benitez, J. Mol. Catal. A 94 (1994) 409.

Materials Chemistry and Physics 111 (2008) 431–437

Contents lists available at ScienceDirect

Materials Chemistry and Physics

journal homepage: www.elsevier.com/locate/matchemphys

Effect of Ni-modified α-Al_2O_3 prepared by sol–gel and solvothermal methods on the characteristics and catalytic properties of Pd/α-Al_2O_3 catalysts

Okorn Mekasuwandumrong[a], Nitikon Wongwaranon[b], Joongjai Panpranot[b,*], Piyasan Praserthdam[b]

[a] Department of Chemical Engineering, Faculty of Engineering and Industrial Technology, Silpakorn University, Nakhonpathom 73000, Thailand
[b] Center of Excellence on Catalysis and Catalytic Reaction Engineering, Department of Chemical Engineering, Faculty of Engineering, Chulalongkorn University, Phayathai Road, Pathumwan, Bangkok 10330, Thailand

ARTICLE INFO

Article history:
Received 21 August 2007
Received in revised form 17 April 2008
Accepted 21 April 2008

Keywords:
Nanocrystalline α-Al_2O_3
Ni-modified α-Al_2O_3
Solvothermal
Sol–gel
Selective acetylene hydrogenation
$NiAl_2O_4$

ABSTRACT

In the present study, Ni-modified α-Al_2O_3 with Ni/Al ratios of 0.3 and 0.5 were prepared by sol–gel and solvothermal method and then were impregnated with 0.3 wt.% Pd. Due to different crystallization mechanism of the two preparation methods used, addition of nickel during preparation of α-Al_2O_3 resulted in various species such as $NiAl_2O_4$, mixed phases between $NiAl_2O_4$ and α-Al_2O_3, and mixed phases between $NiAl_2O_4$ and NiO. As revealed by NH_3-temperature programmed desorption, formation of $NiAl_2O_4$ drastically reduced acidity of alumina, hence lower amounts of coke deposited during acetylene hydrogenation was found for the Ni-modified α-Al_2O_3 supported catalysts. For any given method, ethylene selectivity was improved in the order of Pd/Ni–Al_2O_3-0.5 > Pd/Ni–Al_2O_3-0.3 > Pd/Ni–Al_2O_3-0 ≫ Pd/α–Al_2O_3-commercial. When comparing the samples prepared by different techniques, the sol–gel-made samples showed better performances than the solvothermal-derived ones.

1. Introduction

Alumina powders are very interesting crystalline materials with broad applicability as adsorbents, coatings, soft abrasives, ceramic tools, fillers, wear-resistant ceramics, catalysts, and catalyst supports [1,2]. Because of their fine particle size, high surface area, high melting point (above 2000 °C), high purity, good adsorbent, and high catalytic activity, they have been employed in a wide range of large-scale technological processes [3,4].

Various transition alumina (α, γ, χ, δ, η, and θ) has been prepared by different methods such as, sol–gel synthesis [5], hydrothermal synthesis [6], microwave synthesis [7], emulsion evaporation [8,9], precipitation from solution [10], and solvothermal synthesis [11–13]. The sol–gel method is an easy method but the precipitated powders obtained are amorphous in nature and further heat treatment is required for crystallization. Solvothermal method is an alternative route for direct (one-step) synthesis of Al_2O_3 nanoparticles. Particle morphology, crystalline phase, and surface chemistry of the products can be controlled by regulating precursor composition, reaction temperature, pressure, solvent property, and aging time [14,15]. The α-Al_2O_3 is usually used as a thermal stabilizing material while the γ-Al_2O_3 shows a high surface area and is often used to make a dispersed metal catalyst.

Pd/α-Al_2O_3 is typically employed in gas-phase selective acetylene hydrogenation in commercial ethylene production plant. Removal trace amount of acetylene in ethylene feedstock is very important because acetylene acts as a poison to ethylene polymerization catalysts [16,17]. The Pd/α-Al_2O_3 catalyst is typically macroporous and has a relatively small surface area of approximately 0.1–2 $m^2\ g^{-1}$. In general, α-Al_2O_3 provides low dispersion of active metal than γ-Al_2O_3 but it is desirable in selective acetylene hydrogenation reaction because α-Al_2O_3 is less acidic than γ-Al_2O_3 so that less oligomer or green oil was formed during acetylene hydrogenation reaction. Moreover, Pd/α-Al_2O_3 has lower ability for direct ethane formation than Pd/γ-Al_2O_3 catalyst. Recently, Pd/α-Al_2O_3 prepared by glow discharge plasma has been studied in acetylene hydrogenation [18]. The improved catalyst performance has been suggested to be due to surface modification and changes of the interaction between metal and support as a result of plasma processing.

In this study, the properties of α-Al_2O_3 support have been modified by Ni addition during sol–gel and solvothermal syntheses. The characteristics of Pd/Ni-modified α-Al_2O_3 were investigated by means of N_2 physisorption, X-ray diffraction (XRD), transmission electron microscopy (TEM), CO pulse chemisorption, thermal gravimetric and differential temperature analysis (TG–DTA), and

* Corresponding author. Tel.: +66 2 2186869; fax: +66 2 2186877.
E-mail address: joongjai.p@eng.chula.ac.th (J. Panpranot).

0254-0584/$ – see front matter © 2008 Elsevier B.V. All rights reserved.
doi:10.1016/j.matchemphys.2008.04.042

NH_3 temperature program desorption. Their catalytic properties were tested in the gas-phase selective hydrogenation of acetylene.

2. Experimental

2.1. Preparation of Ni-modified α-Al_2O_3

Ni-modified α-Al_2O_3 samples were prepared by sol–gel and solvothermal methods. For the sol–gel method, mixture of 24 g aluminium nitrate nonahydrate (Aldrich) and a desired amount of nickel nitrate-6-hydrate (Aldrich) were dissolved in 50 cc of ethanol. The experiment was conducted in the reflux-condenser reactor at the temperature about 70–80 °C for 18 h. Then, urea solution, which consist of 60 g of urea and 50 mL of distilled water, was added to adjust pH of sol. The mixture was rested at the same temperature for 24 h to be gelled at neutral condition. The obtained product was calcined with two steps heating rate to avoid overflowing of gel during calcinations, i.e. 3 °C min^{-1} from room temperature to 500 °C and continue heating at 5 °C min^{-1} to 1150 °C. Then, temperature was hold for 3 h.

For the solvothermal method, Ni-modified Al_2O_3 were prepared using a mixture of aluminum isopropoxide 15.0 g and appropriate amount of nickel(II) acetylacetonate. The starting materials were suspended in 100 mL of toluene in beaker, and then set up in autoclave. In the gap between the beaker and autoclave wall, 40 mL of toluene was added. After the autoclave was completely, the suspension was heated to 300 °C at the rate of 2.5 °C min^{-1} and held at that temperature for 2 h. However, the same synthesis method is performed at various holding temperature. Autogenous pressure during the reaction gradually increased as temperature was raised. Then the autoclave was cooled to room temperature. After the autoclave was cooled, the resulting products were washed repeatedly with methanol by centrifugation and dried in air. The calcination of the obtained product carried out in a furnace. The product was heated at a rate of 10 °C min^{-1} to a desired temperature and held at that temperature for 1 h.

2.2. Preparation of Pd supported on Ni-modified α-Al_2O_3

The Pd/Ni-modified Al_2O_3 catalysts were prepared by incipient wetness impregnation of support with a desired amount of an aqueous solution of palladium(II) nitrate hydrate (Aldrich) to obtain the final Pd loading of ca. 0.3 wt%. The catalysts were dried overnight at 110 °C and then calcined in N_2 flow 60 cm^3 min^{-1} with a heating rate of 10 °C min^{-1} until the temperature reached 500 °C and then in air flow 100 cm^3 min^{-1} at 500 °C for 2 h.

2.3. Catalyst characterization

Surface area measurements were carried out by nitrogen adsorption in a Micromeritic Chemisorb 2750 system. Each sample was degassed at 200 °C for 2 h. The analysis gas consisting of 30% N_2 in helium was adsorbed on the samples at low temperature by dipping cell into liquid nitrogen dewar. X-ray diffraction patterns of the catalyst samples were obtained with a SIEMENS D5000 X-ray diffractometer using Cu Kα radiation with a Ni filter. The pattern were recorded between 20° and 80° (2θ) using a scanning velocity of 0.02° s^{-1}. Metal active sites were measured using CO chemisorption technique at room temperature in a Micromeritic Chemisorb 2750 automated system attached with ChemiSoft TPx software. Before chemisorption measurement, the sample was reduced in a H_2 flow at 150 °C for 2 h then cooled down to ambient temperature in a He flow. Ammonia temperature program desorption (NH_3-TPD) was also performed in a Micromeritic Chemisorb 2750 automated system attached with ChemiSoft TPx software. Approximately 0.1 g of catalyst was placed in a quartz tube in a temperature-controlled oven. The samples adsorbed ammonia at 40 °C, then heated up to 650 °C at a heating rate of 10 °C min^{-1}. The amount of acid-sites on the catalyst surface was calculated from the desorption amount of NH_3. It was determined by measuring the areas of the desorption profiles obtained from a Micromeritics ChemiSorb 2750 pulse chemisorption system analyzer. For the broad desorption peak, it was separated into many sub-peaks by using the Fityk program for peak fitting. All areas of sub-peaks were summed to calculate the total amount of acid-sites [19]. The distribution of palladium on catalyst supports were observed using AJEM-200CX transmission electron microscope operated at 160 kV.

2.4. Reaction study

Catalytic performance of the catalysts was studied in selective hydrogenation of acetylene. The experiment was performed in a quartz tube reactor (i.d. 10.1 mm). Before starting of the reaction, the catalyst was reduced in H_2 at 150 °C for 2 h. Then the reactor was purged with argon and cooled down to the reaction temperature, 40 °C. Feed gas composed of 1.5% C_2H_2, 1.7% H_2, and balanced C_2H_4 (TIG Co., Ltd.), a GHSV of 39,435, 24,433, 16,901 and 9288 h^{-1} were used. The composition of product and feed stream were analyzed by a Shimadzu GC 8A equipped with TCD and FID detectors (molecular sieve-5A and carbosieve S2 columns, respectively). Acetylene conversion as used herein is defined as moles of acetylene converted with respect to acetylene in feed. Ethylene selectivity is defined as the percentage of acetylene hydrogenated to ethylene over totally hydrogenated acetylene. The ethylene being hydrogenated to ethane (ethylene loss) is the difference between all the hydrogen consumed and all the acetylene which has been totally hydrogenated.

3. Results and discussion

3.1. Characteristics of the Ni-modified α-Al_2O_3

3.1.1. The solvothermal-made

The XRD patterns of solvothermal-made Al_2O_3 and Ni-modified Al_2O_3 with various Ni/Al ratios (0, 0.3, and 0.5) are shown in Fig. 1. The patterns in the lower half of the figure correspond to the as-synthesized powder while the patterns in the upper part of the figure are for those which have been calcined at 1150 °C for 1 h in a post-synthesis treatment step. The as-synthesized and calcined alumina powders exhibited typical XRD characteristic peaks of χ-alumina and α-alumina, respectively. χ-Alumina powders are normally obtained by the thermal decomposition reaction of AIP in inert organic solvent which transformed directly to α-alumina at high calcination temperature [20,21]. For the as-synthesized Ni-doped samples, XRD characteristic peaks of both χ-Al_2O_3 and Ni^0 metal were observed. After calcination, XRD characteristic peaks of $NiAl_2O_4$ spinel; space group Fd3m [22] (as indicated by circles in the upper frame) were apparent. For the sample with Ni/Al = 0.3, only the $NiAl_2O_4$ spinel was found while for Ni/Al = 0.5, both $NiAl_2O_4$ and NiO characteristic peaks were observed.

Thermal gravimetric and differential temperature analysis of as-synthesized solvothermal-made powders are shown in Fig. 2. The overall weight loss increased from 14 to 20% as the Ni/Al ratios increased from 0 to 0.5. Two weight-decrease steps were clearly detected. The first step observed below 250 °C was due to desorption of the physisorbed water. The second weight decrease at around 250–400 °C could be attributed to the combustion of organic moieties forming on catalyst surface. The exothermic DTA peaks were clearly observed at around 318 °C which should be assigned to the exothermic heat from the combustion process. Intensities of DTA peaks and overall weight loss increased as the

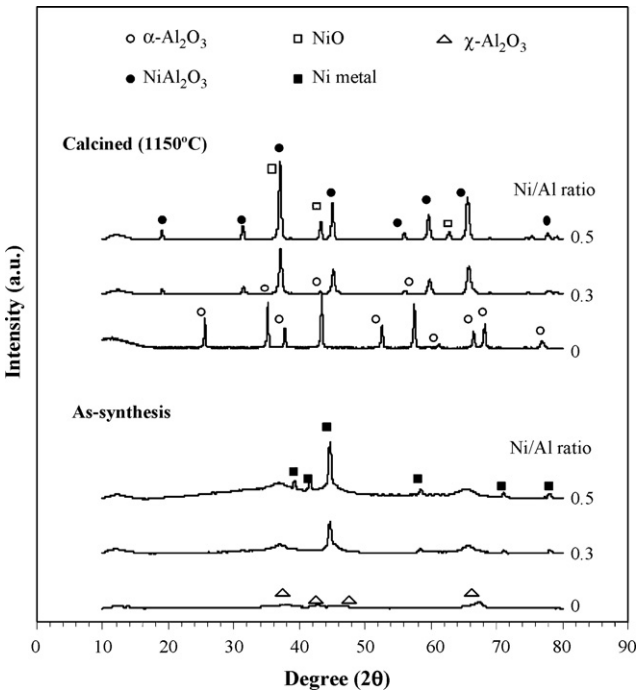

Fig. 1. XRD results of the as-synthesized and calcined α-Al_2O_3 and Ni-modified α-Al_2O_3 prepared by solvothermal method.

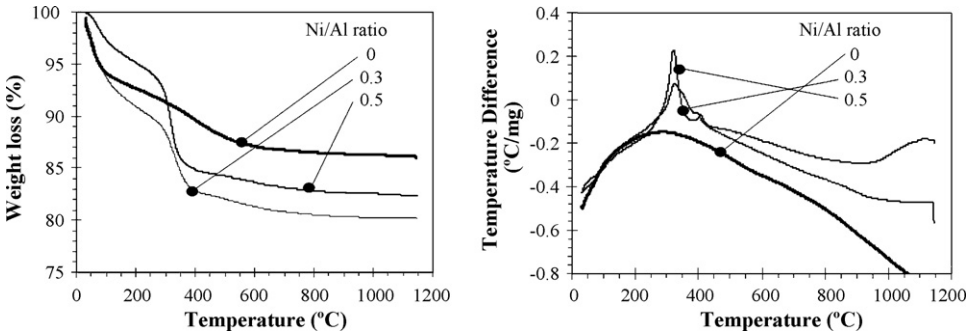

Fig. 2. TG/DTA results of the as-synthesized α-Al_2O_3 and Ni-modified α-Al_2O_3 prepared by solvothermal method.

Ni/Al ratio increased. These results suggest that the acetylacetonate groups from Ni precursor were not completely decomposed and remained on the surface of as-synthesized samples.

3.1.2. The sol–gel-made

The XRD patterns of sol–gel-made Al_2O_3 and Ni-modified Al_2O_3 with various Ni/Al ratios (0, 0.3, and 0.5) are shown in Fig. 3. The patterns in the lower half of the figure correspond to the powder calcined at 800 °C while the patterns in the upper part of the figure are for those which have been calcined at 1150 °C for 1 h in a post-synthesis treatment step. After calcination at 800 °C, γ-alumina was formed. It was then transformed to α-alumina by calcination at 1150 °C. The Ni-modifed Al_2O_3 samples which have been calcined at 800 °C exhibited XRD characteristic peaks of γ-Al_2O_3 and $NiAl_2O_4$. On the other hand, the samples calcined at 1150 °C with Ni/Al = 0.3 exhibited characteristic peaks of $NiAl_2O_4$ and α-Al_2O_3 while for Ni/Al = 0.5 only $NiAl_2O_4$ was found.

Results from thermal analysis of the obtained gel are shown in Fig. 4. Overall weight losses of all the gel samples were essentially similar at around 95%. Three weight-decrease processes were detected, which were accompanied by three endothermic peaks in DTA. The first peak observed below 100 °C was due to desorption of physisorbed water. The second and third weight decrease occurred at around 120–230 °C and 230–500 °C could be attributed to the elimination of chemisorption water and remaining nitrate species forming in the gel structure. The last exothermic DTA peaks without any weight loss were observed at around 520 °C and were assigned to crystallization of the $NiAl_2O_4$ from amorphous gel. This is confirmed by the crystallization of $NiAl_2O_4$ by calcination of gel at 800 °C.

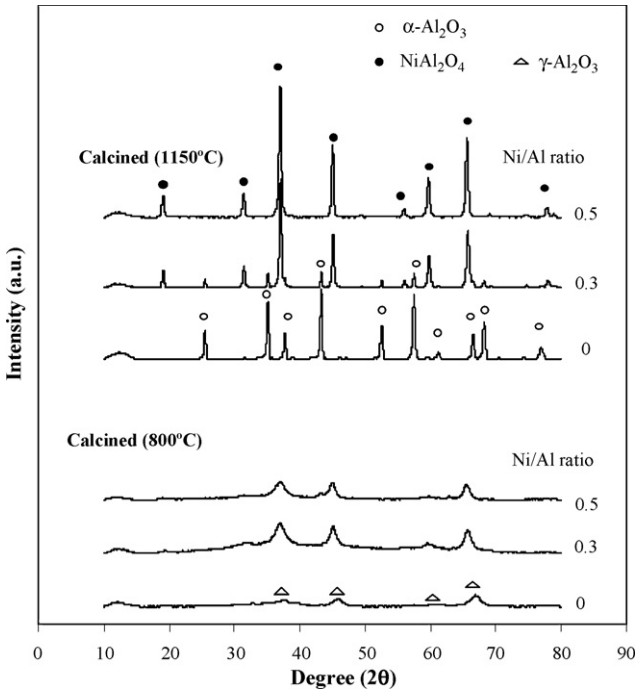

Fig. 3. XRD results of the sol–gel-derived α-Al_2O_3 and Ni-modified α-Al_2O_3 after calcination at 800 and 1150 °C.

3.1.3. Mechanism for $NiAl_2O_4$ formation of the sol–gel and solvothermal-made Ni-modified α-Al_2O_3

Many nanocrystalline materials with specific properties were successfully synthesized by thermal treatment of suitable precursors such as metal alkoxide, acetate and acetylacetonate in inert organic solvents. Crystallization mechanism of α-Al_2O_3 and Ni-modified α-Al_2O_3, however, was different for the two preparation methods used (sol–gel and solvothermal). While the solvothermal reaction of aluminum isopropoxide alone in toluene gave the nanocrystalline χ-alumina particles [23], the sol–gel method yielded a solid precipitate at relatively low temperature and crystallization occurred during the subsequent calcination step at high temperature. Addition of the nickel precursor solution during the sol–gel synthesis with Ni/Al = 0.3 resulted in the mixed phases of alpha Al_2O_3 and $NiAl_2O_4$ while increasing Ni/Al to 0.5 yielded formation of $NiAl_2O_4$ alone. Such results were expected based on the stoichiometric ratio of $NiAl_2O_4$ (Ni/Al = 0.5). However, the solvothermal synthesis of Ni-modifed α-Al_2O_3 with Ni/Al = 0.3 and 0.5 resulted in the formation of $NiAl_2O_4$ alone and the mixed phases between $NiAl_2O_4$ and NiO, respectively. The crystallization mechanism of Ni-modified Al_2O_3 probably started with the decomposition of aluminum isopropoxide, which yielded $Al–O^-$ and $(CH_3)_2CH^+$ and then the nucleophilic attack of $Al–O^-$ on nickel acetylacetonate or another AIP molecule took place yielding the Al–O–Ni or the Al–O–Al bond. This crystallization mechanism was similar to that of Si-doped Al_2O_3 prepared from aluminum isopropoxide and tetraethyl orthosilicate in toluene [24]. Based on XRD results of the as-synthesized and the calcined solvothermal-made Ni-modified Al_2O_3 samples, it is indicated that Ni metal was formed at the first place together with the crystallization of Al_2O_3. Calcination at high temperature then resulted in penetration of Ni atoms in Ni^0 metal phase to occupy the tetrahedral sites in $NiAl_2O_4$ matrix via a solid-state reaction. Because of the limitation of solid solution of Ni in $NiAl_2O_4$ phase, the excess NiO was shed from $NiAl_2O_4$ matrix at higher Ni/Al ratios (Ni/Al = 0.5).

3.2. Characteristics of the Pd/Ni-modified α-Al_2O_3 catalysts

The XRD patterns of the sol–gel- and the solvothermal-made Pd/α-Al_2O_3 and the Pd/Ni-modified α-Al_2O_3 catalysts after calci-

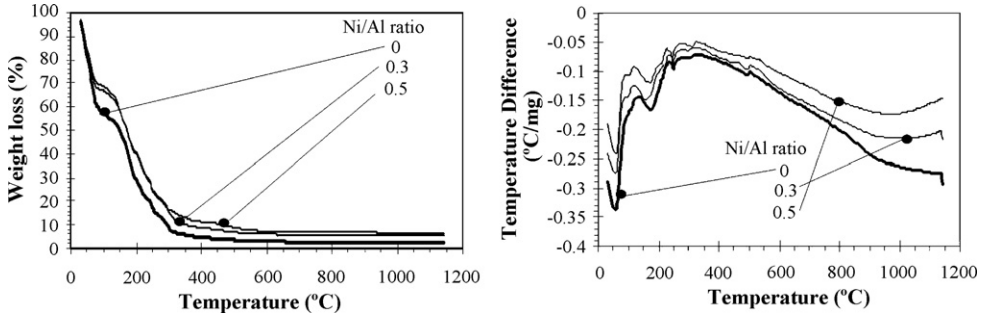

Fig. 4. TG/DTA results of the as-synthesized α-Al_2O_3 and Ni-modified α-Al_2O_3 prepared by sol–gel method.

nations at 1150 °C are shown in Fig. 5. The patterns in the lower half of the figure correspond to the sol–gel-made powder while the patterns in the upper part of the figure are for those prepared by solvothermal synthesis. Both the sol–gel- and solvothermal-made Pd/α-Al_2O_3 catalysts exhibited all the characteristic peaks of α-Al_2O_3 structure. While the diffraction lines for Pd/Ni-modified α-Al_2O_3 catalyst could be assigned to a spinel-type $NiAl_2O_4$ structure. Additional peaks corresponding to NiO were also presented at 43.3° and 62.9°2θ for the product obtained from solvothermal synthesis with Ni/Al = 0.5. The XRD characteristic peaks associated with Pd^0 or PdO phase were not observed for all the samples.

TEM micrographs were taken in order to physically measure the size of the palladium oxide particles and/or palladium clusters. For those prepared by solvothermal method, agglomeration of finger-like particles were observed for Pd/α-Al_2O_3 whereas spherical-shape particles were found for Pd/Ni-modified α-Al_2O_3 (Fig. 6a and b), respectively. The finger-like α-Al_2O_3 particles are normally obtained by calcination of the solvothermal-made α-Al_2O_3 powders at high temperature [22,23]. It can be seen that the sol–gel-made catalyst (Fig. 6c and d) was consisted of agglomerated particles with primarily irregular shape structure. Based on TEM analysis, palladium particles/clusters with average particle size ca. 5–10 nm were deposited on the alumina supports.

The physicochemical properties of Pd/α-Al_2O_3 and Pd/Ni-modified α-Al_2O_3 catalysts are summarized in Table 1. The average XRD crystallite size of each crystal phase was calculated from the Scherrer equation. The average crystallite sizes of the α-Al_2O_3 prepared by sol–gel and solvothermal method were 34 and 58 nm, respectively. Compared to the α-Al_2O_3, the crystallite sizes of $NiAl_2O_4$ formed in both cases were smaller suggesting that the presence of Ni atom in $NiAl_2O_4$ inhibited the growth of crystal. The surface areas of all the catalysts were not significantly different and still quite low, due probably to high agglomeration of these nanocrystalline particles during calcinations at high temperature. The amounts of CO chemisorption on the catalysts, the percentages of Pd dispersion, and the average Pd metal particle sizes determined from CO chemisorption are also given in Table 1. The pulse CO chemisorption technique was based on the assumption that one carbon monoxide molecule adsorbs on one palladium site [25–29]. It was found that the amounts of CO chemisorption slightly decreased as the Ni/Al ratio increased from 0 to 0.5 for all the Pd/Ni-modified α-Al_2O_3 catalysts. However, for Ni/Al ratio 0 and 0.3, there were no significantly differences of the percentages of Pd dispersion and calculated Pd^0 metal particle sizes for the catalysts prepared by two different techniques. For Ni/Al = 0.5, the solvothermal-made Pd/Ni-modified α-Al_2O_3 showed slightly higher amount of CO chemisorption than the sol–gel- made catalyst.

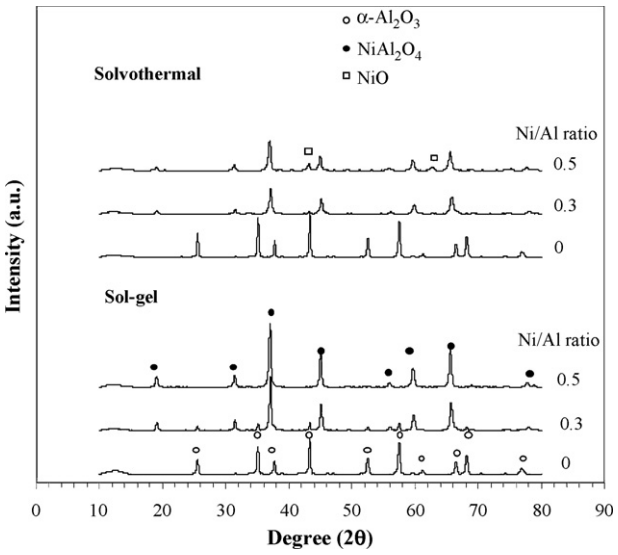

Fig. 5. XRD results of the various Pd/α-Al_2O_3 and Pd/Ni-modified α-Al_2O_3.

3.3. Catalyst performance in selective acetylene hydrogenation

The catalyst performance in selective hydrogenation of acetylene to ethylene was studied for all the catalyst samples using a fixed bed flow reactor. Changes in ethylene selectivity with acetylene conversion for Pd/α-Al_2O_3 and Pd/Ni-modified α-Al_2O_3 catalysts are shown in Fig. 7. In general, ethylene selectivity decreases with increasing acetylene conversion due to the fact that the ethylene is produced as an intermediate in acetylene hydrogenation reaction. In this study, it was found that Pd/Ni-modified α-Al_2O_3 exhibited better performances in selective acetylene hydrogenation Pd/α-Al_2O_3 and Pd/commercial α-Al_2O_3 regardless of the preparation method used. For a given method, ethylene selectivity was improved in the order of Pd/Ni–Al_2O_3-0.5 > Pd/Ni–Al_2O_3-0.3 > Pd/Ni–Al_2O_3-0 > Pd/α–Al_2O_3-commercial. When comparing the samples prepared by different techniques, the sol–gel-made samples showed higher ethylene selectivity than those of the solvothermal-derived ones.

During long-time investigation by many research groups, the catalytic activity and ethylene selectivity in the selective acetylene hydrogenation over Pd-based catalysts are found to be dependent on many factors such as metal dispersion (Pd metal particle size) [30–33], thermodynamic adsorption differences between acetylene and ethylene [34], and carbonaceous product formation [35,36], etc. Based on the reaction mechanisms for acetylene hydrogenation on Pd/Al_2O_3 catalysts reported in the literatures [37], there are three active sites on the Pd metal surface and one active site on the alumina support. The three sites on the palladium surface are responsible for selective hydrogenation of acetylene to ethylene,

Table 1
Characteristics of the various Pd/α-Al_2O_3 and Pd/Ni-modified α-Al_2O_3 catalysts

Sample	d_{XRD}[a] (nm)	BET surface area ($m^2\ g^{-1}$)	NH_3 uptake (μmol g-cat^{-1})	CO chemisorption ($\times 10^{17}$ sites g-cat^{-1})	Pd dispersion (%)	d_P[b] Pd^0 (nm)
Sol–gel						
Pd/Ni–Al_2O_3-0	34[c]	1.5	339.3	7.51	4.42	25
Pd/Ni–Al_2O_3-0.3	54[c], 31[d]	1.5	197.1	6.22	3.65	31
Pd/Ni–Al_2O_3-0.5	27[d]	1.9	127.1	5.37	3.16	35
Solvothermal						
Pd/Ni–Al_2O_3-0	54[c]	4.7	268.2	8.10	4.76	24
Pd/Ni–Al_2O_3-0.3	24[d]	1.8	175.6	6.28	3.69	30
Pd/Ni–Al_2O_3-0.5	23[d], 26[e]	1.4	380.7	7.35	4.32	26
Commercial						
Pd/α–Al_2O_3	391.6[c]	0.5	n.d.	5.91	3.48	32

[a] Crystallite size calculated by Scherrer equation.
[b] Average Pd metal particle sized calculated from CO chemisorption results. $d_P = 1.12\ D^{-1}$, where D = Pd dispersion [25].
[c] α-Al_2O_3.
[d] $NiAl_2O_4$.
[e] NiO.

direct ethane formation from acetylene and oligomer formation whereas ethylene hydrogenation is believed to take place on the support by means of a hydrogen transfer mechanism. It was claimed that the carbonaceous deposits present act as bridges for hydrogen spillover [38]. Sarkany et al. [39] discussed a mechanism of acetylene hydrogenation and suggested that the role of coke is primarily to promote hydrogen transfer from the metal surface to the adsorbed ethene. Moreover, acidity on alumina surface is known to promote formation of carbonaceous deposits on catalyst surface. Fig. 8 shows the NH_3 temperature program desorption profiles for the sol–gel and solvothermal-made α-Al_2O_3 and the Ni-modified α-Al_2O_3 supports. Typically, acidity of α-phase Al_2O_3 was much lower than γ-phase alumina so it is used in the commercial Pd/Al_2O_3 selective acetylene hydrogenation catalysts. In this work, desorption peak areas of the nanocrystalline powders obtained from both sol–gel and solvothermal syntheses were quite low, however, two desorption peaks corresponding to different acid sites were still observed at ca. 320 and 400–500 °C. For the sol–gel-made Ni-modified α-Al_2O_3, the desorption peaks decreased rapidly and the profiles became almost flat as the Ni/Al ratio increased from 0 to 0.5 suggesting that acidity of alumina significantly decreased with incorporation of Ni atoms and $NiAl_2O_4$ formation. A decrease of alumina acidity, however, was less pronounced for the solvothermal-made Ni-modified α-Al_2O_3. A broad desorption peak at ca. 250–500 °C was observed for the solvothermal-made Ni-modified α-Al_2O_3 with Ni/Al ratio = 0.5 due probably to the presence of NiO. According to the work reported by Areán et al. [40], a decrease in both Lewis and Brønsted acidity was observed for Ni-

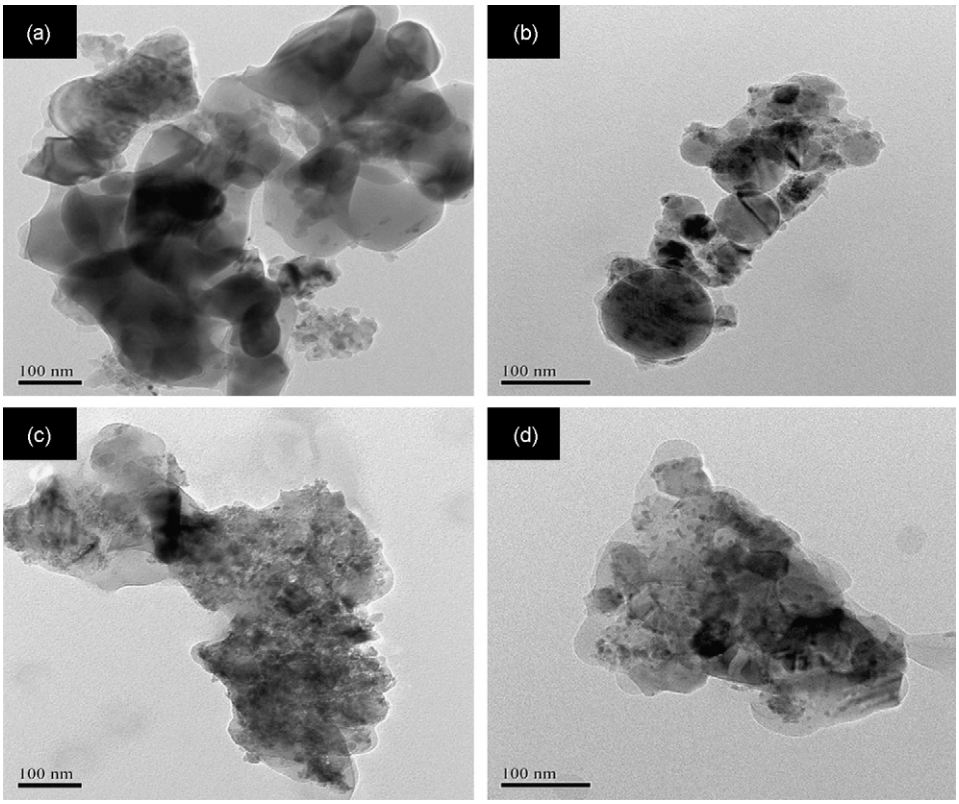

Fig. 6. TEM images of (a) Pd/α-Al_2O_3–solvothermal, (b) Pd/Ni-modified α-Al_2O_3–solvothermal, (c) Pd/α-Al_2O_3–sol–gel, and (d) Pd/Ni-modified α-Al_2O_3–sol–gel.

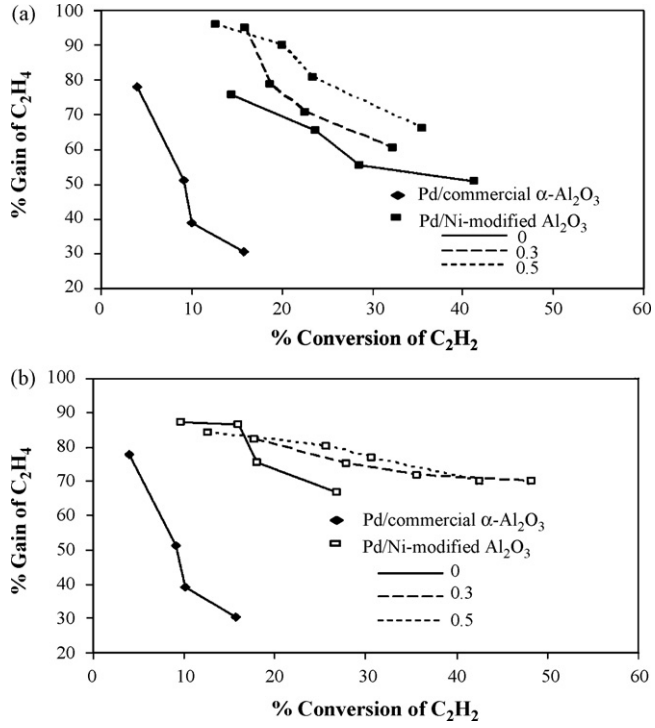

Fig. 7. Performances of the various Pd/α-Al_2O_3 and Pd/Ni-modified α-Al_2O_3 in selective hydrogenation of acetylene. (a) Solvothermal method; (b) sol–gel method.

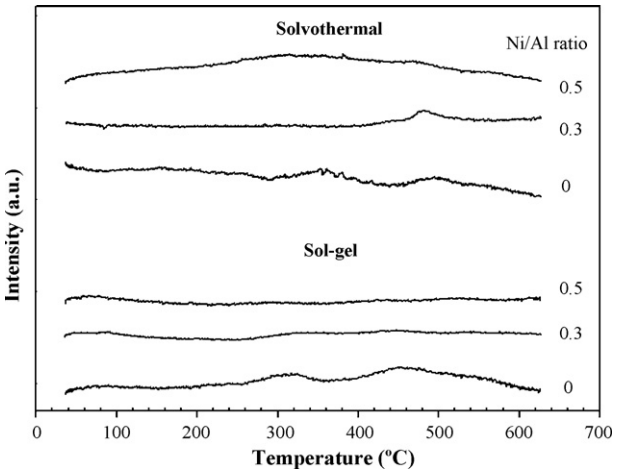

Fig. 8. NH_3-temperature program desorption profiles of the various Al_2O_3 and Ni-modified Al_2O_3 samples.

doped alumina as the Ni contents increased in the Ni-alumina solid solution as confirmed by IR spectroscopy of CO adsorbed at liquid nitrogen temperature. Moreover, the very low Brønsted acidity also appears to be typical for many oxide spinels as well as other aluminate spinels such as $MgAl_2O_4$ and $ZnAl_2O_4$ [41,42].

The amounts of coke formed on the spent catalysts were measured by TG–DTA technique and the results are shown in Fig. 9. All the catalysts were pretreated at 200 °C for 1 h in order to remove any adsorbed water remaining on the catalyst surface prior to TG/DTA experiments. Thus, one step weight loss observed with the maximum peak at ca. 250 °C can be attributed to the elimination of deposited "soft-type" coke by combustion reaction [43,44]. These also corresponded with the broad exothermic peaks observed in the plots of temperature difference versus temperature. The lower weight loss during temperature-programmed oxidation indicates a lower rate of coke deposition on the catalyst surface [45]. It was found that the use of sol–gel- and solvothermal-made Ni-modified α-Al_2O_3 supports (Ni/Al = 0.5) reduced the amounts of coke deposited by 44 and 38%, respectively.

The results of coke formation over the various α-Al_2O_3 and Ni-modified α-Al_2O_3 supported Pd catalysts were in accordance with acidity measurement. Formation of $NiAl_2O_4$ spinel during the preparation of Ni-modifed Al_2O_3 by sol–gel or solvothermal method resulted in a decreased acidity of α-Al_2O_3. As a consequence, the catalysts exhibited high ethylene selectivities at high acetylene conversions and lower amounts of coke deposited. For-

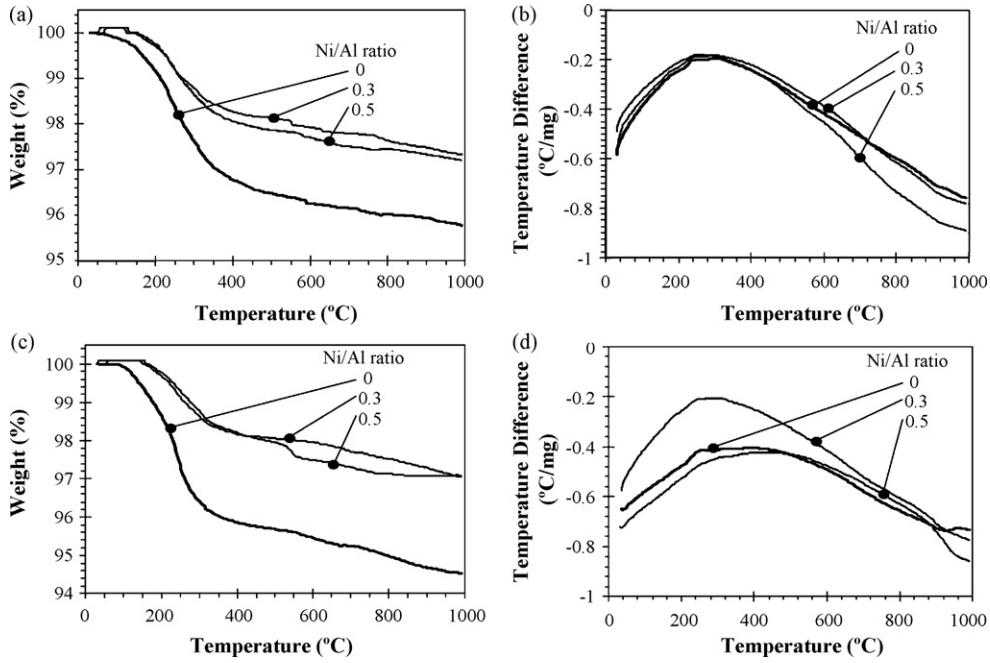

Fig. 9. TG/DTA results of the spent Pd/α-Al_2O_3 and Pd/Ni-modified α-Al_2O_3 catalysts, (a and b) solvothermal-made; (c and d) sol–gel-made.

mation of $NiAl_2O_4$ in Ni-based hydrogenation catalysts has also shown high resistance to deactivation by coke formation [46–48]. In addition, Bhattacharyya and Chang [47] have recently proposed that the use of a nickel aluminate spinel catalyst could reduce coke formation during CH_4/CO_2 reforming. Sueiras and co-workers reported that $Ni/NiAl_2O_4$ catalysts exhibited high conversion and selectivity towards benzene in 1,2,4-trichlorobenzene hydrodechlorination [49]. Unlike the conventional Ni/Al_2O_3, the most selective $Ni/NiAl_2O_4$ catalysts had the highest TOF values.

4. Conclusions

This study explored the effect of Ni-modified α-Al_2O_3 prepared by sol–gel and solvothermal methods on the properties of Pd/α-Al_2O_3 in gas-phase selective acetylene hydrogenation. While the sol–gel-made sample with Ni/Al = 0.5 showed formation of $NiAl_2O_4$ alone, the solvothermal-made resulted in the mixed phases between $NiAl_2O_4$ and NiO. The improved catalytic performances in terms of higher ethylene selectivity and lower amount of coke formation for the Pd/Ni-modified α-Al_2O_3 were attributed to the lower acidity of α-Al_2O_3 by incorporation of nickel into alumina matrix.

Acknowledgements

Financial supports from the Thailand Research Fund (TRF), the Commission on Higher Education, and the Research and Development Institute of Silpakorn University are gratefully acknowledged.

References

[1] G. Pajonk, S. Teichner, in: J. Fricke (Ed.), Aerogels, Spinger, Berlin, 1986.
[2] J.S. Church, N.W. Cant, D.L. Trimm, Appl. Catal. A 101 (1993) 105.
[3] C. Misra, Industrial Alumina Chemicals, vol. 184, ACS Monograph, Washington, 1986.
[4] H. Topsoe, B.S. Clausen, F.E. Massoth, Hydrotreating Catalysis, Springer, Berlin, 1996, p. 310.
[5] C.J. Brinker, G.W. Scherrer, Sol–Gel Science: The Physics and Chemistry of Sol–Gel Processing, Academic Press, San Diego, 1990.
[6] W.H. Dawson, Am. Ceram. Soc. Bull. 67 (1988) 1673.
[7] S.G. Deng, Y.S. Lin, J. Mater. Sci. Lett. 16 (1997) 1291.
[8] Y. Sarikaya, I. Sevinc, M. Akinc, Powder Technol. 116 (2001) 109.
[9] I. Sevinc, Y. Sarikaya, M. Akinc, Ceram. Int. 1 (1991) 17.
[10] W.B. Scott, E. Matijevic, J. Colloid Interface Sci. 66 (1978) 447.
[11] M. Inoue, H. Kominami, T. Inui, J. Am. Ceram. Soc. 75 (1996) 2597.
[12] M. Inoue, H. Otsu, H. Kominami, T. Inui, Ind. Eng. Chem. Res. 35 (1995) 295.
[13] M. Inoue, H. Kominami, T. Inui, J. Am. Ceram. Soc. 75 (1992) 2597.
[14] Y. Deng, X. Zhou, G. Wei, J. Liu, C.W. Nan, S. Zhao, J. Phys. Chem. Solids 63 (2002) 2119.
[15] Y. Deng, G.D. Wei, C.W. Nan, Chem. Phys. Lett. 368 (2003) 639.
[16] Y.-J. Huang, C.F. Shun, L.G. Daniel, E.L. Mohundro, J.E. Hartgerick, US Patent 5,332,705, Exxon Chemical Patents Inc., 1994.
[17] J. Cosyns, J.-P. Boitiaux, US Patent 4,571,442, Institut Francais du Petrole, 1984.
[18] M.H. Chen, W. Chu, X.Y. Dai, X.W. Zhang, Catal. Today 89 (2004) 201.
[19] W. Khaodee, B. Jongsomjit, P. Praserthdam, S. Goto, S. Assabumrungrat, J. Mol. Catal. A: Chem. 280 (2008) 35.
[20] O. Mekasuwandumrong, V. Pavarajarn, M. Inoue, P. Praserthdam, Mater. Chem. Phys. 100 (2006) 445.
[21] O. Mekasuwandumrong, P.L. Silveston, P. Praserthdam, M. Inoue, V. Pavarajarn, W. Tanakulrungsank, Inorg. Chem. Commun. 6 (2003) 930.
[22] A.R. West, Solid State Chemistry and its Application, John Wiley & Sons, New York, 1997.
[23] O. Mekasuwandumrong, H. Kominami, P. Praserthdam, M. Inoue, J. Am. Ceram. Soc. 87 (2004) 1543.
[24] P. Praserthdam, M. Inoue, O. Mekasuvandumrong, W. Thanakulrangsan, S. Phatanasri, Inorg. Chem. Commun. 3 (2000) 671.
[25] N. Mahata, V. Vishwanathan, J. Catal. 196 (2000) 262.
[26] S.H. Ali, J.G. Goodwin Jr., J. Catal. 176 (1998) 3.
[27] E.A. Sales, G. Bugli, A. Ensuque, M.J. Mendes, F. Bozon-Verduraz, Phys. Chem. Chem. Phys. 1 (1999) 491.
[28] A. Sarkany, Z. Zsoldos, B. Furlong, J.W. Hightower, L. Guczi, J. Catal. 141 (1993) 566.
[29] N.K. Nag, Catal. Lett. 24 (1994) 37.
[30] J. Panpranot, K. Kontapakdee, P. Praserthdam, Appl. Catal. A 314 (2006) 128.
[31] A. Sarkany, A.H. Weiss, L. Guczi, J. Catal. 98 (1986) 550.
[32] C.E. Gigola, H.R. Aduriz, P. Bodnariuk, Appl. Catal. 27 (1986) 133.
[33] Y.A. Ryndin, L.V. Nosova, A.I. Boronin, A.L. Chuvilin, Appl. Catal. 42 (1988) 131.
[34] G.C. Bond, Catalysis by Metals, Academic Press, London, 1962.
[35] A. Borodzinski, A. Cybulski, Langmuir 13 (1997) 883.
[36] A. Borodzinski, A. Cybulski, Appl. Catal. A 198 (2000) 51.
[37] R.N. Lamb, B. Ngamsom, D.L. Trimm, B. Gong, P.L. Silveston, P. Praserthdam, Appl. Catal. 268 (2004) 43.
[38] S. Asplund, J. Catal. 158 (1) (1996) 267–278.
[39] A. Sarkany, L. Guczi, A.H. Weiss, Appl. Catal. 10 (1984) 369.
[40] C.O. Areán, M. Penarroya Mentruit, A.J. Lopez Lopez, J.B. Parra, Colloids Surf. A 180 (2001) 253.
[41] C.O. Arean, C. Mas Carbonell, Vib. Spectrosc. 8 (1995) 411.
[42] C.O. Arean, B. Sintes Sintes, G. Turnes Palomino, C. Mas Carbonell, E. Escalona Platero, J.B. Parra Soto, Microporous Mater. 8 (1997) 187.
[43] Z. Xiangjing, W. Yan, X. Feng, Appl. Catal. A 307 (2006) 222.
[44] M.R. Jovanovic, P.S. Putanov, Appl. Catal. 159 (1997) 1.
[45] B. Pawelec, V. La Parola, R.M. Navarro, S. Murcia-Mascarós, J.L.G. Fierro, Carbon 44 (2006) 84.
[46] A. Al-Ubaid, E.E. Wolf, Appl. Catal. 40 (1988) 73.
[47] A. Bhattacharyya, V.W. Chang, Stud. Surf. Sci. Catal. 88 (1994) 207.
[48] J.A. Peña, J. Herguido, C. Guimon, A. Monzón, J. Santamaría, J. Catal. 159 (1996) 313.
[49] Y. Cesteros, P. Salagre, F. Medina, J.E. Sueiras, Appl. Catal. B 25 (2000) 213.